GEOPHYSICAL STUDIES OF THE LIMPOPO BELT

Wendy Helen Barker

A Dissertation Submitted to the Faculty of Science
University of the Witwatersrand, Johannesburg
for the Degree of Master of Science

Johannesburg 1991

ABSTRACT

The multiply deformed, metamorphic Limpopo Belt separates the granite-greenstone terranes of the Kaapvaal and Zimbabwe Cratons. The belt is divided into three zones, the Southern Marginal Zone (SMZ), the Central Zone (CZ) and the Northern Marginal Zone (NMZ), all consisting of high-grade metamorphic rocks.

Previous geophysical investigations, which included gravity (Coward and Fairhead, 1980) and electrical methods (Van Zijl, 1978), presented models in which the Kaapvaal Craton (KC) had been thrust over the Zimbabwe Craton (ZC). Recent geophysical studies (De Beer and Stettler, 1988) indicate a south dipping contact between the ZC and NMZ and a north dipping contact between the KC and SMZ, which suggests a pop-up structure (Van Reenen et al., 1990).

This study includes seismic reflection and refraction work as well as gravity modelling. The seismic reflection section is typical of Archean sections, i.e. a reflective upper crust overlying a seismically transparent lower crust. The SMZ and a block thought to be the NMZ are characterised by numerous short, dipping reflectors. The CZ is largely seismically transparent except for sedimentary rocks close to surface. The KC is characterised by sub-horizontal reflectors indicating thin skinned tectonics. The contact between the SMZ and KC is seen as a zone of discontinuous north dipping reflectors. No continuous reflector at mid-crustal levels is seen connecting the SMZ and NMZ which could represent the decollement as postulated by McCourt and Vearncombe (1987). Free-air gravity modelling results indicate that the positive anomaly over the SMZ is a result of dense rocks within the upper crust having a maximum thickness of 7 km. The lower regional value over the CZ can be accommodated by increasing the crustal thickness beneath the CZ by between 2 and 5 km. This is in agreement with the refraction data. The 0.6 s slowdown seen in the reduced travel-time refraction data near the boundary between the CZ and SMZ is modelled using a 3 to 4 km thick low velocity layer at a depth of 42 km rather than an increase in crustal thickness.

DECLARATION

I declare that this dissertation is my own, unaided work, except where it is acknowledged in the Preface. It is being submitted for the degree of Master of Science at the University of the Witwatersrand, Johannesburg. It has not been submitted before for any degree or examination in any other University.

28th day of October, 1991

K Barker

PREFACE

The origin and structure of the Limpopo Belt has been discussed for many years. Since the mid-1970's the Limpopo Belt has been the subject of many research projects in South Africa, Botswana and Zimbabwe. Results from this research have been published in several publications and conferences, including:

Van Biljon, W. J. and Legg, J. H., (Eds.), (1983). The Limpopo Belt. Geol. Soc. S. Afr. Spec. Publ., 8.

Van Reenen, D. D. and Roering, C., (Eds.) The Limpopo Belt - A field workshop on granulites and deep crustal tectonics. Johannesburg. (1990).

The aim of this project is to present a unified discussion of the several geophysical data sets available for the Limpopo Belt.

Dr. R. Durrheim (University of the Witwatersrand), Dr. R. Green (University of the Witwatersrand) and Prof. C. Roering (Rand Afrikaans University) supervised this project. I am grateful for their advice and practical assistance. Prof. D. van Reenen from Rand Afrikaans University provided many helpful discussions on the geology of the area.

The reflection seismic line was acquired by Rockplan Pty Ltd. of South Africa for the South African Geological Survey and the National Geophysics Programme. Most of the reprocessing was carried out at the Genmin Geophysics Data Processing Centre at Springs. I am grateful to Genmin for the use of the facilities and especially to Nick Wood for help with the processing.

The gravity modelling was carried out at the CSIR. I am grateful for the use of their facilities and the help of K. Geerthsen, M. Maher and B. Pitts.

G. Cooper assisted with the computer work at the University of the Witwatersrand and provided the signal detection algorithm. Carol Beadle from the Geophysics department provided assistance in the printing of the dissertation.

Financial support for the project was provided by the Foundation for Research and Development and Rand Afrikaans University.

The major findings of the study have been accepted for publication in *Precambrian Research* and have been presented at the South African Geophysical Association technical meeting.

Durrheim, R, Barker, W. H. and Green, R. W. E. (in press). Seismic studies of the Limpopo Belt. Precambrian Research.

Barker, W. H., Durrheim, R. J. and Green, R. W. E. (1991). Geophysical studies of the Limpopo Belt. Extended Abstracts SAGA: 11-14.

CONTENTS page

List of Illustrations

1. INTRODUCTION

The high-grade metamorphic Limpopo Belt (LB) separates the low-grade Kaapvaal and Zimbabwe Cratons. The LB can be subdivided into three zones, the Southern Marginal Zone (SMZ), the Northern Marginal Zone (NMZ) and the Central Zone (CZ). The zones are separated from each other and from the adjacent cratons by prominent terrane boundaries (Watkeys, 1983). The SMZ consists of highly attenuated granite-greenstone lithologies mostly at granulite grade (De Beer and Stettler, 1988). The NMZ, which lies largely in Zimbabwe, also comprises high-grade equivalents of granite-greenstone lithologies (Gwavava et al., in prep.). The CZ consists mainly of high grade epicontinental rocks (De Beer and Stettler, 1988).

Several tectonic models have been proposed to explain the evolution of the Limpopo Belt and geophysical studies can be used to verify and distinguish between them. In this study two seismic investigations and a gravity model are presented. The results are used to determine the present day structure of the LB and the nature of the boundary between the LB and KC, and to provide further evidence in order to determine the origins of the belt.

The 218 km long, 13 s two way time, reflection seismic line from Pietersburg to Pont Drift shot for the National Geophysics Programme and the Geological Survey in 1987 has been reprocessed and interpreted. Reprocessing concentrated on the deep data and achieved greater continuity of the reflections through extensive editing and residual statics calculations. Traveltimes of Witwatersrand mine tremors between Pietersburg and Harare have been modelled. Free-air gravity anomaly values taken from the Geological Survey Handbook 3 have been modelled using a model which included the isostatic root calculated from the topography values.

2. GEOLOGY

The Limpopo Belt is an east-northeast trending polymetamorphic, multiply deformed zone separating the Archean granite-greenstone terranes of the Kaapvaal Craton (in the south) and Zimbabwe Craton (in the north). It is located in Botswana, southern Zimbabwe and northern Transvaal (figure 2.1) and emerges from beneath the Kalahari Sands in the west and extends for about 600 km in length before disappearing beneath Phanerozoic cover at the eastern end. It has a maximum width of about 300 km.

The origins of the belt remain uncertain, and in the past it has been referred to as an orogeny (MacGregor, 1953), an orogenic belt (Cox et al., 1965), a mobile belt (Anhaeusser et al., 1969) and a metamorphic complex (Du Toit and Van Reenen, 1977). Although this study refers to the Limpopo Belt, the term 'belt' has no genetic implications. The present belt-like geometry (a belt type geometry is described by Tankard et al. (1982) as being one where the body has a high length to width ratio) is probably due to later strike-slip movement (in post-Bushveld times) along the Palala and Tuli-Sabi shear zones bounding the Central Zone. This movement exaggerated the lateral extent of the originally oval shaped structure (Van Reenen et al., 1987, 1990). In addition, ages reported by Barton et al. (1983b) indicate that the rocks of the Limpopo Belt have ages at least 200 Ma greater than those from the adjacent cratons. Therefore the term mobile belt is inaccurate since the term is used to describe 'younger, linear metamorphic belts surrounding adjacent cratons' (Anhaeusser et al., 1969). The whole belt was subjected to granulite facies metamorphism in response to the collision between the Kaapvaal and Zimbabwe Cratons during the Limpopo orogeny around 2700 Ma (Van Reenen et al., 1990). The belt was subjected to further deformational and metamorphic events until the deposition of the Karoo rocks at 200 Ma. As a result it is characterised by repeated shear deformation, igneous intrusion and extrusion. However, the CZ also shows evidence of metamorphic and deformation events predating the Limpopo orogeny (Barton, 1990).

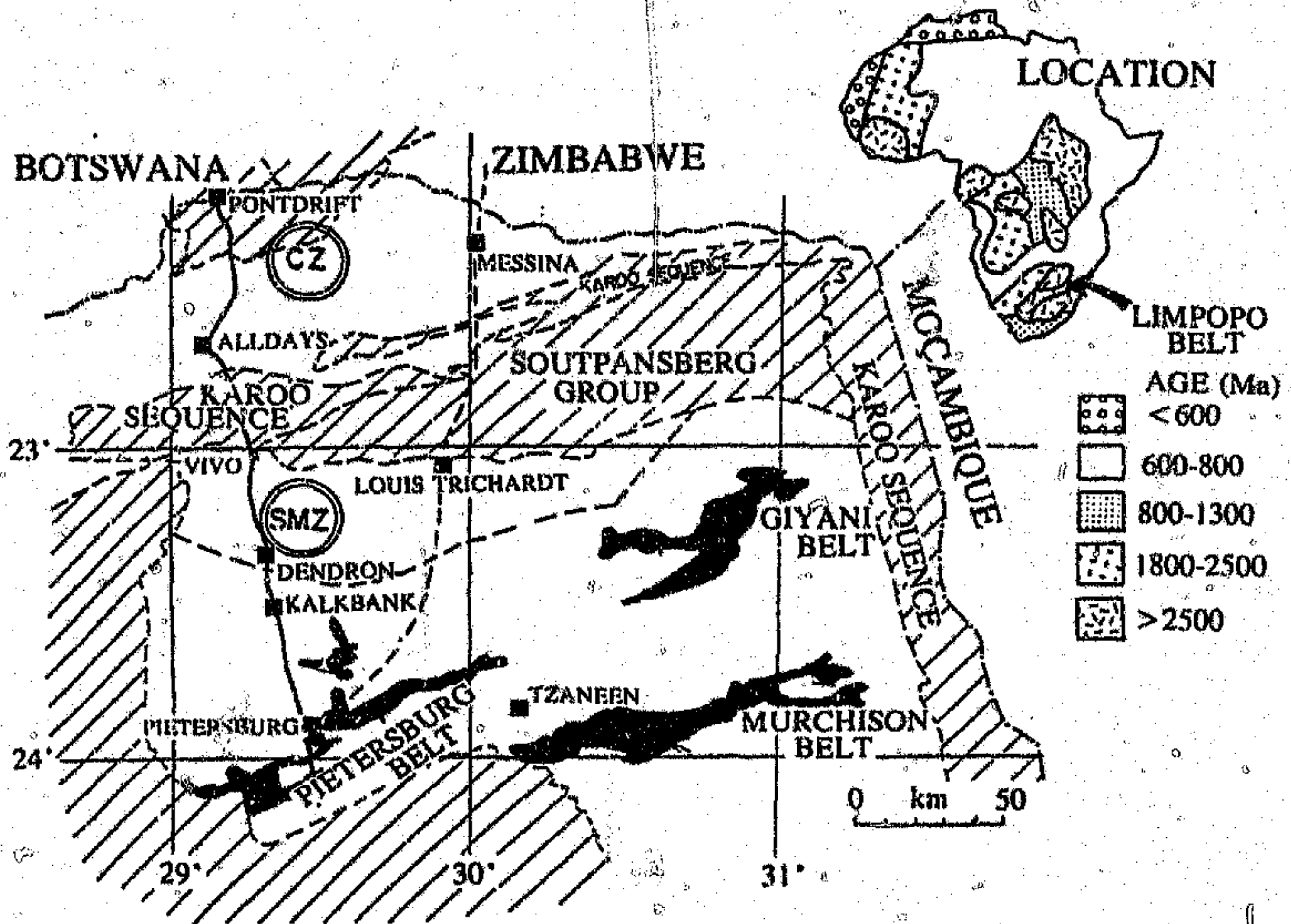

Figure 2.1 Geology of the Limpopo Belt and locations of the geophysical traverses. Cover strata are indicated by diagonal hatching and Archean greenstone belts are coloured black. - - - refraction and gravity line, -·-·- reflection line
SMZ - Southern Marginal Zone, CZ - Central Zone (from Durrheim et al., in press)

The belt can be divided into zones on the basis of lithology and structure. A three-fold division has been used by Cox et al. (1965) where a central east-northeast zone exhibiting nearly north-south trending folds is flanked on either side by marginal zones where the regional fold structural trend is east-northeast. The three zones also have distinct lithologies. The marginal zones consist largely of reworked granite-greenstone successions of the adjacent cratons and the CZ consists of high-grade metamorphosed epicratonic supracrustal rocks (Barton, 1983a). Van Reenen et al. (1987) consider that metamorphism and structural styles in the CZ and marginal zones are similar. All lithologies have undergone extreme deformation which is indicated by highly attenuated fragments caught up in complex fold patterns.

The CZ is separated from the adjacent marginal zones by broad shear zones, the Tuli-Sabi shear in the north along which movement is strike-slip and dextral and the Palala shear zone in the south along which movement is strike-slip and sinistral. Both boundaries are often mylonitic. Movement directions in the belt have been described by McCourt and Vearncombe (1987) as a westward movement of rocks in the CZ, a northward movement of rocks in the NMZ and a southward movement of rocks in the SMZ. The CZ was moved a further approximately 70 km to the west after the emplacement of the Bushveld Complex around 2060 Ma (Van Reenen et al., 1987).

2.1 CENTRAL ZONE

The Central Zone (CZ) is characterised by a supracrustal succession termed the Beit Bridge Complex (BBC) (SACS, 1980), which consists of metaquartzites, amphibolites, a variety of gneisses, calcsilicates and marble. It is suggested that these rocks are intensely deformed and metamorphosed equivalents of some elements of a modern ocean floor (Fripp, 1983). Several suites of grey gneisses (Sand River, Zanzibar and Alldays) have been identified within the BBC and they all have a similiar mineralogy and chemistry (Van Reenen et al., 1990).

The Sand River Gneisses which crop out in the CZ were previously thought to be the oldest rocks in the area with an approximate age of 3790 Ma and as such formed a basement to the BBC (Barton, 1983a, Fripp, 1983). Recent radiometric evidence however, yields a younger age around 3200 Ma (Harris et al., 1987) and no unambiguous structural evidence exists to support the basement-cover relationship in the field. The Alldays Gneiss exhibits an intrusive relationship with the BBC and has an age of approximately 3200 Ma. This suggests that the other grey gneisses could possibly be time equivalents of an igneous event around 3200 Ma (Van Reenen et al., 1990).

Rocks of the BBC throughout the CZ have been intruded by the anorthositic-gabbroic Messina Layered Intrusion which was emplaced at or before 3270 Ma (Barton, 1983a). Gabbroic dykes occurring mainly within the grey gneisses were emplaced about 3000 Ma and crosscut an earlier metamorphic fabric in both the Sand River and Alldays Gneisses, indicating that the CZ may have experienced an earlier orogenic event before the Limpopo orogeny around 2700 Ma (De Wit and Van Schalkwyk, 1990). All CZ lithologies underwent granulite facies metamorphism during the Limpopo orogeny. The Bulai Gneiss, emplaced in the supracrustal rocks at approximately 2700 Ma, is part of the Limpopo orogeny (Watkeys and Armstrong, 1985). The relative chronology of geological events in the Limpopo Belt is summarised in table 2.1.

Gneisses within the CZ are characterised by both amphibolite and granulite facies mineralogies. The close association between these two assemblages indicates that the amphibolites are possibly retrogressed equivalents of the mafic granulites. Three main metamorphic events affected the CZ after 3000 Ma. The first, M_1, was the Limpopo orogeny at approximately 2700 Ma and was a prograde event associated with the granulite facies metamorphism resulting from rocks being buried to depths around 35 km and reaching a peak pressure of 9.5 kbar. This was followed by the M_2 event, indicated by isothermal decompression with temperatures

Age in Ma	SMZ	CZ	NMZ	
3400 - 3500 Ma	Formation of granite-greenstone terrane of the Kaapvaal Craton. Relationship of the greenstone belts with the surrounding gneisses uncertain.	Deposition of platform-type sediments of the Beit Bridge Complex (> 3000 Ma?), probably overlying the Sand River Gneiss (3790 Ma ?).	Formation of the granite-greenstone terrane of the Zimbabwe Craton. Age uncertain, but probably similar to that of the SMZ.	Pre-Limpopo Fabrics
	—	Intrusion of the Alldays Gneiss.	—	
3250 Ma ?	—	Intrusion of the Messina Suite.	—	
	—	Metamorphic and deformational event of unknown intensity.	—	
3000 Ma ?	—	Intrusion of mafic dykes.	—	
> 2700 Ma	The Limpopo Orogeny: (D1) (i) peak metamorphism during continental collision (M1) superimposed on D1	The Limpopo Orogeny: (D1) (i) peak metamorphism during continental collision (M1) superimposed on D1	The Limpopo Orogeny: (D1) (i) peak metamorphism during continental collision? (2868 Ma ?) (M1)	
± 2700 Ma	(ii) Isothermal decompression (M2) (iii) Cooling and thrusting onto the Kaapvaal Craton (M3) during intrusion of the Matok porphyritic pluton (2670 Ma). Widespread rehydration. } D2	(ii) Isothermal decompression (M2) (iii) Cooling and further uplift (M3) during the intrusion of the Bulai Gneiss (± 2700 Ma). Widespread rehydration. } D2	(ii) Isothermal decompression? (iii) Cooling and thrusting onto the Zimbabwe Craton (M3) before the intrusion of the Great Dyke (± 2500 Ma). Widespread rehydration? Intrusion of late-tectonic porphyritic granite. } D2	
2650 Ma	—	Intrusion of post-tectonic lamprophyric dykes into the Bulai pluton.	—	
2500 Ma	—	—	Intrusion of satellite dykes of the Great Dyke.	
2450 Ma	Intrusion of post-tectonic Palmietfontein Pluton.	—	—	
1970 Ma	—	Intrusion of Palala Granite.	—	
> 1900 Ma	Strike-slip fault movements along the two shear zones bounding the CZ. The CZ was displaced about 70 km westwards relative to the two marginal zones.			

Table 2.1 Relative sequence of geological events in the Limpopo Belt based on field and petrographic evidence. (from Van Reenen et al., 1990)

greater than 750 °C and pressures between 6 and 7 kbar. The third metamorphic event, M_3, was a retrograde event during which cooling occurred and fluids entered the high grade rocks resulting in mineral replacement reactions. This event established the zones of retrogression in the CZ and SMZ as well as the retrograde orthoamphibole isograd in the SMZ (Van Reenen et al., 1990). The Limpopo orogeny ended in the CZ around 2650 Ma as indicated by the unmetamorphosed lamprophyric dykes which intruded the Bulai Gneiss (Watkeys and Armstrong, 1985).

On a regional scale the fold structures in the CZ are closed. Structural investigations indicate that these closed structures are macro sheath folds which plunge to the southwest. Similar closed structures are seen in the SMZ, as well as cross-cutting zones of straightening. These zones of straightening are steeply northward dipping reverse fault movement zones with southerly movement indicators (Roering and Smit, 1990).

2.2 SOUTHERN MARGINAL ZONE

The Southern Marginal Zone (SMZ) contains a significant proportion of high-grade metamorphic equivalents of rocks similar to the adjacent granite-greenstones of the Kaapvaal Craton (Mason, 1973). The main structural trend is east-northeast. Much of the SMZ is covered by sedimentary and volcanic rocks of the Karoo Sequence. The bulk of the SMZ is made up by the tonalitic and trondjhemitic gneisses of the 3500-3300 Ma Baviaanskloof Gneiss (Du Toit et al., 1983) in which greenstone slivers consisting of ultramafic, mafic and pelitic gneisses with banded iron formation occur (Van Reenen et al., 1990). The Baviaanskloof Gneiss is in tectonic contact with the supracrustal Bandelierkop Formation which consists of mafic, ultramafic and pelitic gneisses (Du Toit et al., 1983). The SMZ has been subjected to several phases of granite intrusion including the late tectonic Matok Granite around 2670 Ma (Du Toit et al., 1983) and the post tectonic Palmietfontein Granite at about 2450 Ma and the Schiel Alkaline Complex at about 2150 Ma (Barton et al., 1983a).

Van Reenen et al. (1990) divide the SMZ into two distinct metamorphic zones - a granulite zone in the north and a zone of hydration in the south. The two zones are separated by the retrograde orthoamphibole isograd. Granulite facies mineralogies are present in all lithologies in the granulite zone. The metapelitic granulite is the most common lithology in the granulite zone and is generally coarsely banded and often migmatitic. Mineral textures within the metapelitic granulites often indicate a complex metamorphic history. The mafic granulites are coarse foliated rocks, but do not show any textural evidence of a complex metamorphic history. Banded iron formations are found together with both types of granulites and occur as a banded or more massive type of rock. Ultramafic rocks have been serpentinised to varying degrees. The retrograde orthoamphibole isograd is well defined in the metapelitic granulites, seen in mineral replacement reactions. Metapelitic gneisses in the zone of hydration are completely recrystallised and well foliated and often contain little or no evidence of the previous high grade history. Mafic rocks in the zone of hydration are well foliated.

The metamorphic history of the SMZ after 3000 Ma is similar to that of the CZ i.e. prograde granulite facies metamorphism (M_1) followed by decompression (M_2) and retrogression (M_3). However, maximum pressures were slightly less, (8-9 kbar) and the retrogression event, during which the orthoamphibole isograd was established, was steeper i.e. temperatures decreased quicker for the same decrease in pressure.

2.3 NORTHERN MARGINAL ZONE

The 30 - 50 km wide Northern Marginal Zone (NMZ) lies in Zimbabwe and south-eastern Botswana. The NMZ is a granulite terrane similar to the SMZ, consisting mainly of reworked granite-greenstone lithologies of the adjacent Zimbabwe Craton (ZC). The grade of metamorphism decreases westwards into Botswana, but there is insufficient evidence to show whether this decrease is due to regional retrogression of original granulites, or whether the granulites were never developed at all (Robertson and Du Toit, 1981). Hickman (1978) obtained an age of 2930 ± 60 Ma for granulites from the Bangala Dam region. The boundary with the Zimbabwe Craton is marked by a series of southerly-dipping faults and mylonite zones (Gwavava et al., in prep.), with downdip lineation. The granulite facies rocks of the marginal zone were carried over the rocks of the ZC along these shear zones (Coward and Daly, 1984). At least 2 regional deformation events are recognised (Barton, 1983b).

2.4 KAAPVAAL CRATON

Much of the granite-greenstone terrane of the Kaapvaal Craton (KC) is covered by Proterozoic formations. Where exposed, it is characterised by variably sized greenstone belts surrounded by tonalitic and trondhjemitic gneiss (Roering and Smit, 1990). All the greenstone belts found on the KC are characterised by an east-northeast structural grain and have a depth extent of less than 7 km (De Beer and Stettler, 1988). Some high grade granulite bodies found on the KC are probably tectonic klippe since they have no gravity signature (De Beer and Stettler, in press). The low-grade terrane is characterised by prograde metamorphism.

2.5 ZIMBABWE CRATON

The southern part of the Zimbabwe Craton (ZC) is a granite-gneiss terrane associated with extensive greenstone belts. Hawkesworth et al. (1975) obtained two different ages for rocks from the ZC indicating two major events. The first event occurred around 3500-3600 Ma and was associated with the formation of the granitic crust. The second event with an age of between 2600 and 2700 Ma was related to the formation of the greenstone belts and associated granite intrusives. The Great Dyke emplaced at about 2500 Ma intrudes all these formations.

2.6 TECTONIC MODELS

Several tectonic models based on geological and geophysical data have been proposed for the evolution of the Limpopo Belt. Early models include those of Barton and Key (1981), Fripp (1983) and Light (1982), all of which are based on the assumption that plate tectonics was an active mechanism during the Archean. Coward and Fairhead (1980), on the basis of gravity data, proposed that the Limpopo Belt comprises lower crust exposed by the thrusting of the Kaapvaal Craton over the Zimbabwe Craton. Barton and Key (1981) proposed that the Limpopo Belt formed in an intracratonic environment which was then deformed by shearing and compression across a rift between the Kaapvaal and Zimbabwe Cratons. The compression tilted parts of the crust on edge which were later exposed by erosion. Light (1982) proposed that the Limpopo Belt formed as a result of a collision between the Kaapvaal and Zimbabwe Cratons with a southward dipping subduction zone beneath the Kaapvaal Craton. Fripp (1983) suggested that the Limpopo Belt is a remnant of a back-arc basin with an associated magmatic arc and subduction zone. Later deformation resulted from compression between the Zimbabwe and Kaapvaal Cratons. All the models involve compression across the belt during which lower crust granulite facies rocks were forced upwards and exposed by erosion. They also attempt to explain the history of the belt from about 3800 Ma, when a significant amount of crustal rock was present, until about 2500 Ma when compression ceased, with uplift and erosion continuing until 1950 Ma. Differences between the models are found in the age relationships between the Central Zone and the adjacent cratons, and the presence of volcanic rocks. Both Fripp (1983) and Light (1982) consider the Limpopo Belt to have formed as a result of interaction between the two cratons which were formed before 3800 Ma and should be associated with large quantities of volcanic rocks. Barton and Key (1981) consider the two cratons to be younger than the proto-craton onto which they accreted.

Current models of Van Reenen et al. (1987, 1990) and McCourt and Vearncombe (1987) also include continental collision. The model proposed by Van Reenen et al. (1990) attempts to explain the processes resulting in the juxtaposition of the high-grade terrane against the low-grade terrane rather than the processes involved in the early deep burial of the Limpopo Belt to depths at which granulite facies metamorphism occurred. Thus the present geometry of the belt is a result of response tectonics followed by lateral movement of the Central Zone. McCourt and Vearncombe (1987) propose that the LB formed as a result of a collision between a crustal block containing the Zimbabwe and Kaapvaal Cratons and another crustal block containing the CZ which collided from the east. Gwavava et al. (in prep.) suggest that the present crustal structure in the east is a result of the relatively recent process of crustal thinning during the Karoo period.

The models of Van Reenen et al. (1990) and McCourt and Vearncombe (1987) are discussed in more detail below.

2.6.1 East-to-west emplacement of the Central Zone (micro-)plate

McCourt and Vearncombe (1987) propose that a (micro-)plate bounded by the Tuli-Sabi and Palala shear zones, (now represented by the CZ), was emplaced from the east onto a single plate containing the Zimbabwe and Kaapvaal Cratons. Thus the marginal zone boundary thrusts are only secondary displacements resulting from the collision. Granulite facies metamorphism occurred due to crustal thickening resulting from the collision.

The following field observations are used to support their model -

- The Central Zone differs from the marginal zones in rock types, structural style and isotope signature.
- Both marginal zones exhibit steep downdip mineral elongation and north verging thrusts are associated with the NMZ.

- The Tuli-Sabi shear zone forming the boundary between the NMZ and CZ is a zone of gently dipping north directed thrusts. Movement on the shear zone is strike slip and dextral.
- The southern boundary of the CZ is marked by the Sunnyside-Palala shear zone system along which movement is strike-slip and sinistral.
- The gravity profile of Coward and Fairhead (1980) is interpreted as suggesting that the Tuli-Sabi and Palala shear zones are linked at depth to form a major decollement zone at the base of the CZ. A continuous shear zone linking the two lateral shear zones has not been recognised in the west due to limited exposure and a younger granitoid complex around 26° 30' E. Two phases of movement occurred along these shear zones, one between 2.7 and 2.6 Ga and the other between 2.0 and 1.8 Ga.
- The CZ is characterised by large scale shear zones and probable sheath folds, mineral elongation fabrics are upright to highly oblique and plunge along the length of the CZ.
- The pattern of kinematic movement indicators in the Limpopo Belt is arcuate, i.e. towards 350° in the NMZ, between 220° and 250° in the CZ and towards 200° in the SMZ, which constrains the plate motion during the collision to be between 260° and 290°.

2.6.2 Craton-craton collision followed by rebound

The model for tectonic evolution of the Limpopo Belt as proposed by Van Reenen et al. (1987, 1990) concentrates on the processes which brought about the juxtaposition of the high-grade terrane against the low-grade terrane rather than the processes which caused the initial deep burial of the Limpopo Belt to granulite facies metamorphism depths.

The following stages are included in the model -

- Initial possibly oblique continental collision around 2700 Ma which resulted in continental thickening.

- Readjustment of isotherms, which established at depth high-grade isograds on mixed lithologies.
- Rapid rebound of crust accompanied by diapirism and lateral spreading.
- Erosion and attainment of equilibrium with uniform crustal thickness over the area.
- Strike slip motion along the Palala and Tuli-Sabi shear zones in post-Bushveld time around 2060 Ma, where the CZ was displaced about 70 km to the west relative to the marginal zones.

Thus the Limpopo Belt was a unit at 2700 Ma when a major tectonic-metamorphic event occurred. The CZ lithologies had a unique pre-2700 Ma history indicated by geochronology and isotope values. The rocks were subjected to high-grade conditions at about 3150 Ma and again, together with the marginal zones at about 2700 Ma.

The model is based on several field observations -

- The clockwise P-T time evolution of the CZ and marginal zones records a single continuous loop.
- The boundaries of the Limpopo Belt separate undeformed granite-greenstone areas from ones in which it is intensely deformed and occurs as highly attenuated lenses in a mass of granitoid gneisses and migmatites.
- Low-grade crust of the cratons dips beneath the high-grade crust of the belt along the shear zones bounding the marginal zones. Compression across the belt forced the belt upwards along these dipping shear zones.
- A uniform grade of metamorphism exists over the whole Limpopo Belt i.e. no tectonic stacking occurred, however granulite facies conditions could have been superimposed on previously stacked assemblages.
- The ubiquitous presence of deformation textures throughout the SMZ, NMZ and CZ reveal that uplift was fairly uniform and continuous.

- Rapid isothermal uplift was aided by the presence of large volumes of anatectic melt.
- Apparently uniform orientation of movement vectors (NE-SW) within the SMZ and CZ indicates that the two areas experienced the same movement as well as metamorphic evolution. This movement trend is at an angle to the trend of the whole belt (ENE) which could indicate oblique collision between the Kaapvaal and Zimbabwe Cratons.
- Strike slip motion of 70-100 km along the Palala shear zone occurred in post-Bushveld time.

3. PREVIOUS GEOPHYSICAL INVESTIGATIONS

Several geophysical investigations have been carried out in the Limpopo Belt and adjoining cratons to determine the deep structure in these provinces. These methods have included the use of gravity, electrical methods, long offset transient EM (LOTEM) and refraction seismics.

3.1 ELECTRICAL METHODS

The results of deep and ultra-deep Schlumberger electrical soundings are reported by Van Zijl (1978) and De Beer et al. (1991). Van Zijl (1978) identified two kinds of terrane depending on the amount of fracturing. Massive terranes consist of strongly consolidated, unfractured, granitoid material characteristic of stable cratons. Fractured terranes consist of intensely deformed, fractured metamorphic rocks characteristic of mobile belts. Four electrical zones (excluding the surface weathered layer) are present in the low-grade cratonic terranes. The upper zone has a resistivity of 40000 - 100000 ohm.m with an average thickness of less than 10 km. The underlying zone is less resistive, with resistivity values ranging from 2000 - 10000 ohm.m with the average around 5000 ohm.m. This zone has a depth extent of 25 to 30 km so that its base occurs around the crust-mantle boundary. The third zone is conductive with a resistivity in the range [illegible] - 100 ohm.m. The deepest recognisable zone, which occurs in the uppermost lithospheric mantle, is resistive. In the Limpopo Belt, Van Zijl (1978) found the geo-electrical character of the upper crust in the high-grade area to be similar to that of the moderately resistive second zone in the adjacent low-grade Kaapvaal Craton. De Beer and Stettler (in press) suggested that high-grade areas in the CZ which have an upper resistive layer similar to that found in low-grade areas may be crustal remnants of a previous cratonic terrane and were probably not affected by the thrusting and shearing during the last Limpopo deformation event. From electrical models, Van Zijl (1978) concluded that the moderate resistivity rocks of the SMZ dip southwards beneath the high resistivity, low-grade rocks of the cratonic crust at the KC-SMZ boundary.

Further direct current (DC) resistivity results are presented by De Beer et al. (1991). Schlumberger sounding data were used to investigate the relationship between the low- and high-grade metamorphic rocks. They found the (DC) data to show conclusively that the high-grade rocks were thrust over the low-grade rocks which contradicts the findings of Van Zijl (1978), but agrees with the recent seismic reflection data (this study and Stettler et al., in press). The boundary between the high and low-grade rocks dips northward at an angle of about 20° to the horizontal. The position of the northern boundary of the Kaapvaal Craton with the SMZ was also shown to be further south than the orthoamphibole isograd suggested by Du Toit et al. (1983).

Long offset transient EM (LOTEM) was used to study the conductive zone observed near the base of the cratonic crust at the transition from the low-grade Kaapvaal Craton to the high-grade SMZ (De Beer et al., 1991). The depth to the top of the conductor which occurs near the base of the crust was modelled to occur at approximately the Moho - 35 km. Using the LOTEM method they traced the conductor from the Kaapvaal Craton into the SMZ and found it to shallow from about 30 to 22 km over a surface distance of 12 km. However this does not reflect the difference in metamorphic depth of about 30 km seen at surface, which indicates that the conductor is more likely a transient feature of the crust.

3.2 REFRACTION SEISMICS

Observations of mining induced tremors in the Witwatersrand basin were made by Gane et al. (1956) to determine the crustal structure in the Transvaal. The northern profile extended about 480 km from the source region to Messina using a large station spacing. The depth to the Moho was determined to be 36.6 $\pm$ 2.4 km in the northern Transvaal using a crustal velocity of 6.20 km/s and a mantle velocity of 8.21 km/s. The far offset records were erratic and weak and the S_n phase was almost completely eliminated. These effects were attributed to structural heterogeneity and a variable sub-Moho velocity. No conclusions could be reached regarding the structure beneath the Limpopo Belt.

Stuart and Zengeni (1987) reported on the seismic crustal structure of the Limpopo Belt in Zimbabwe. Their study was based on recorded events from the earthquakes around Kariba to the north, Witwatersrand mine tremors to the south and timed Buchwa iron-ore mine blasts to the north of the NMZ along a 145 km N-S seismic traverse in southern Zimbabwe. Crustal thickness was estimated to be 34 km beneath the NMZ at Rutenga, from a phase identified as a Moho reflection (PmP) on the timed Buchwa blast recordings. Based on this depth; they produced a model showing the depth to the Moho being 40 km within the Zimbabwe Craton, decreasing to 35 km in the NMZ, and shallowing further to 29 km in the CZ (figure 3.1). This crustal thinning occurs in association with a positive gravity anomaly centered over the late-Karoo Nuanetsi Igneous Province and Karoo Tuli syncline, implying that it was in response to extension during Karoo times and was controlled by the previous Precambrian structure in the Limpopo Belt, rather than being associated with the development of the belt (Stuart and Zengeni, 1987). The model shows the Zimbabwe Craton boundary to be a steeply southerly dipping zone associated with high-velocity material separating cratonic crust about 40 km thick from that typical of the mobile belt some 6 km thinner. Interpretation of travel time curves indicates an upper crustal interface in the Limpopo Belt at a depth of 5.8 $\pm$ 0.6 km separating material with a velocity of 5.8 km/s from that of about 6.4 km/s. On the craton this boundary occurs at 4.4 $\pm$ 0.5 km and separates 5.8 km/s crustal material from the underlying 6.5 km/s velocity crust. An apparent mantle velocity of 8.4 km/s is probably a maximum estimate of the sub-Moho velocity due to the distance of the events being such that diving waves from the upper mantle may have been

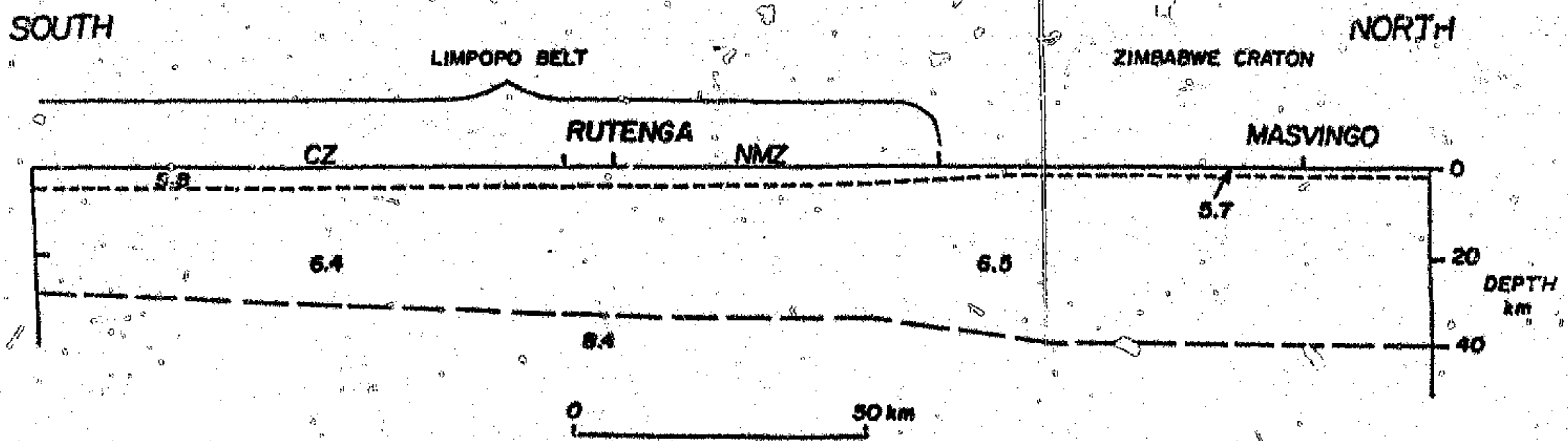

Figure 3.1 Seismic refraction crustal model from Stuart and Zengeni (1987). Velocities are in km/s.

recorded (Stuart and Zengeni, 1987). Teleseismic data show a significant contrast between the velocity structure of the Zimbabwean Craton and the Limpopo Belt down to depths of 80 km. Above 80 km the velocity of the cratonic lithosphere is some 4% faster, while below 80 km the mobile belt lithosphere appears to be faster.

3.3 GRAVITY

Gravity and density measurements have been used by several workers to describe the deep structure of the Limpopo Belt. The first regional gravity survey of South Africa by Smit et al. (1962) showed that the SMZ of the Limpopo Belt has positive Bouguer and isostatic anomalies. The CZ was found to be largely in isostatic equilibrium. The study by Coward and Fairhead (1980) found that positive Bouguer and isostatic anomalies exist over the SMZ and NMZ of the Limpopo Belt. They propose that the cause of the large positive Bouguer anomaly over the marginal zones of the Limpopo Belt is due to regional isostatic response. Their model is based on the Pratt mechanism of isostasy, i.e. high-grade granulitic rocks in the upper crust of the Limpopo Belt. In the model, the Limpopo Belt forms part of the Kaapvaal Craton which was thrust over the Zimbabwe Craton along a broad ductile shear zone outcropping along the northern edge of the NMZ. The granulites of both the SMZ and NMZ form part of the lower crust of the slab of the KC thrust onto the ZC. The granulites of the SMZ are uplifted as a result of a fault between the CZ and SMZ or a structurally necessary fold above a ramp connected to the southward dipping shear zone. Their model is shown in figure 3.2.a.

Emenike (1986) presented a model based on the averages of several north-south gravity profiles crossing the Limpopo Belt. The averaged profile showed values over the northern flank to be generally higher than those on the southern side. Based on the similarities between this profile and those used by Gibb and Thomas (1976) in modelling structural province boundaries

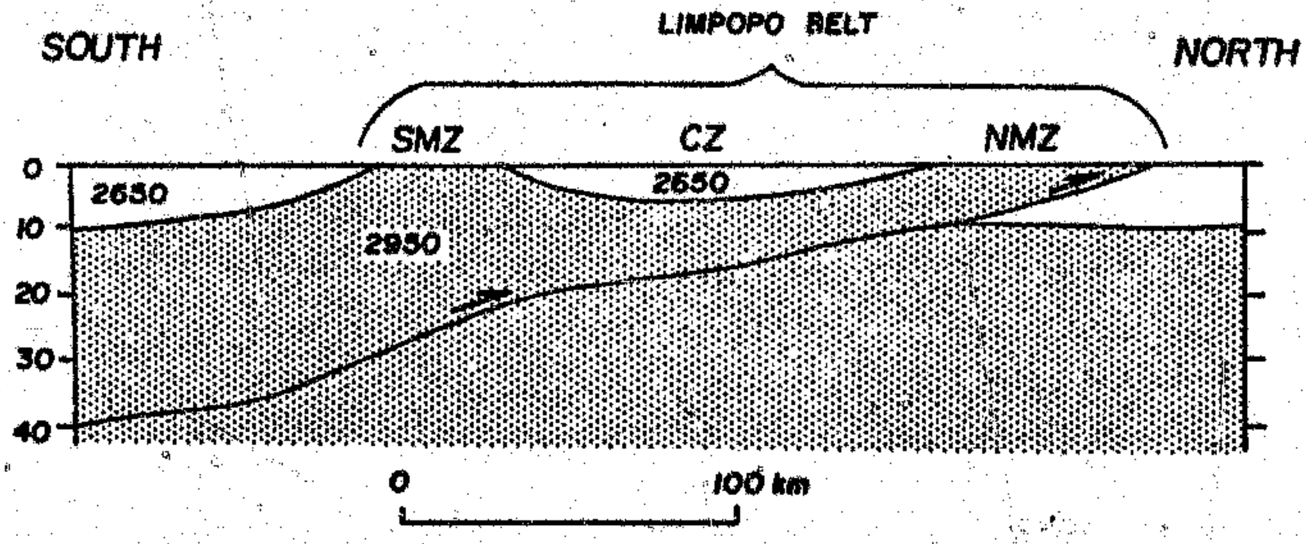

(a)

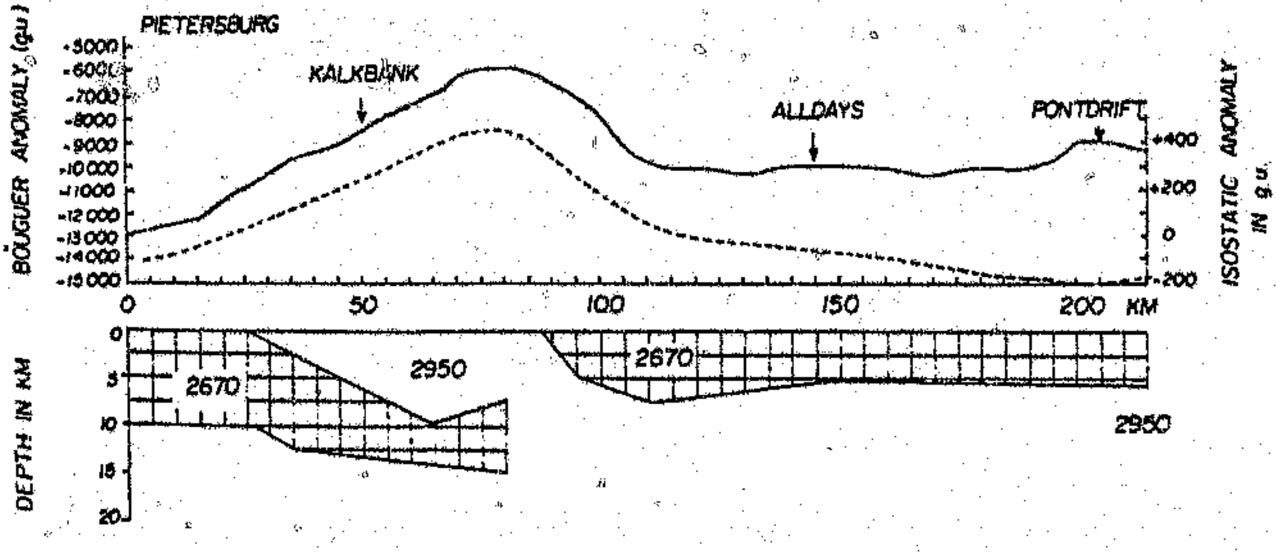

(b)

Figure 3.2 Gravity models of: (a) - Coward and Fairhead (1976) and (b) - De Beer and Stettler (in press). Densities are given in kg/m^3.

in the Canadian shield, he concluded that the Limpopo front gravity low probably represents the boundary between the Kaapvaal Craton and the Limpopo Belt. The positive anomaly over the northern edge would mark the edge of the younger Limpopo province. The difference in ambient gravity levels between the north and south is explained using a thicker, denser crust beneath the Limpopo Belt. He assumes a normal continental crustal thickness of 35 km beneath the Kaapvaal Craton, thickening to between 39 and 41 km beneath the Limpopo Belt. A density contrast of 250 to 450 kg/m^3 between the Kaapvaal and Limpopo provinces, deduced from surface rocks, is used. However, Kleywegt (1988) in a discussion of the earlier paper by Emenike (1986) found the density contrasts used were an order of magnitude too large. In an alternative model, the main positive anomaly over the high-grade SMZ is generated by a dense mass of lower crustal rocks which extend to the surface from an average depth of 9.5 km, while the large southern negative anomaly is attributed to a thickening of the crust by about 3 km in response to the rise in elevation towards the south.

Gwavava et al. (in prep.) used many new gravity measurements from Zimbabwe to supplement the existing data set from Botswana, Mozambique and South Africa in their study of crustal thickness in Zimbabwe and mechanisms for crustal thinning. The profiles crossing the Limpopo Belt show that the Bouguer anomaly is fairly flat over the Zimbabwe Craton, with a slight low over the NMZ, rising over the CZ to a peak over the Nuanetsi-Sabi intrusives. In this study, density measurements showed no density contrast between cratonic and Limpopo Belt rocks. The gravity high is therefore attributed to changes in crustal thickness. Their findings are that the Zimbabwe Craton is characterised by a horizontal Moho at a depth of 34 km. The linear gravity low between the southern boundary of the Zimbabwe Craton and the NMZ of the Limpopo Belt probably represents crustal thickening from the belt overthrusting the craton. The regional gravity high associated with the Nuanetsi-Sabi volcanic rocks is a result of crustal thinning caused by the breakup of Gondwana. As a result of this, the crust thins in a SSE direction to about 30 km in the CZ of the Limpopo Belt.

De Beer and Stettler (in press) modelled a gravity profile coincident with the reflection seismic line. The model shows the more than 400 g.u. isostatic anomaly over the SMZ of the Limpopo Belt to be a result of dense middle to lower crustal material in the upper 10 km of the crust. The granitoid rocks of the low-grade upper crust dip northward under the high-grade granulitic rocks of the SMZ. The model is shown in figure 3.2.b.

3.4 MAGNETICS

Stettler et al. (1989) extracted an aeromagnetic profile from the regional survey along the seismic reflection line. A strong low-pass filter was applied to the data and the results are shown in figure 3.3. Numerous high frequency anomalies in the unfiltered data are superimposed on a regional field which shows a laterally extensive magnetic low zone coinciding with the position of the high-grade rocks of the SMZ (Stettler et al., 1989). The regional aeromagnetic map of the region shows a large number of highly oriented magnetic lineations in the SMZ, whereas the KC is characterised by fewer lineations having random orientation. Stettler et al. (1989) identified 6 domains on the basis of the lineation directions. The lineations which are responsible for the short wavelength anomalies are due to magnetic dykes of various ages (Stettler et al., 1989). The parallelism of the directions within the Limpopo Belt led the authors to conclude that the dyke direction was determined by pre-existing fracture patterns rather than only the stress field operative at the time of intrusion. Examination of the data indicates that a 15° anticlockwise rotation of the CZ relative to the SMZ will bring the two directions in line with one another. De Beer and Stettler (in press) consider the greenstone belts on the KC to be of minor importance with regard to the present lithospheric structure since the lineation patterns of the domains cut across the trends of the greenstone belts. When only induced magnetism is considered, the regional field can be modelled using a three unit crustal structure (figure 3.3) similar to that indicated by the electrical, gravity and seismic models. The SMZ unit has a much lower magnetic susceptibility

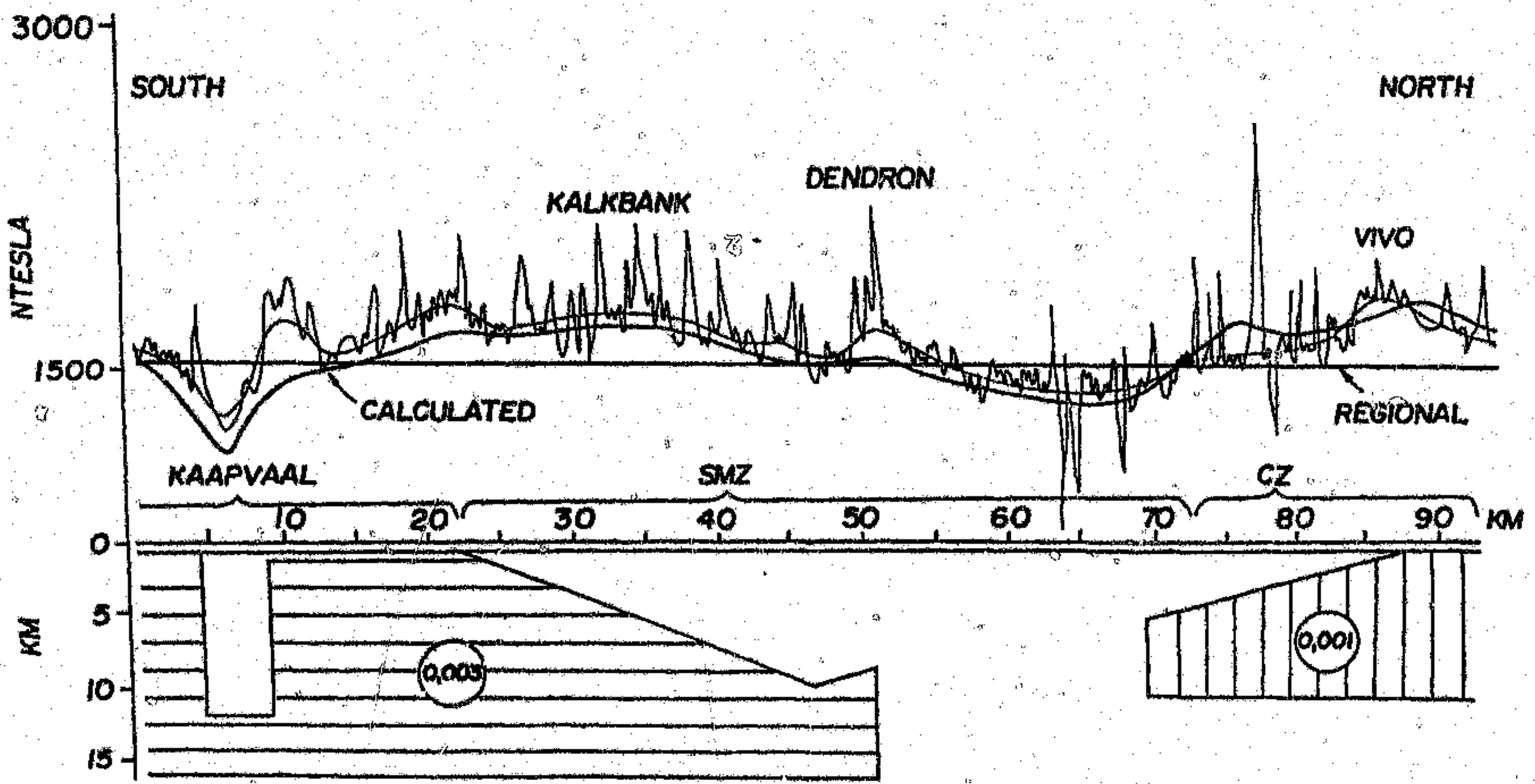

Figure 3.3 Aeromagnetic data along the seismic reflection line. The unfiltered data and a low-pass filtered data set are shown, as well as calculated values for the model. (from Stettler et al., 1989).

than that of the KC or CZ. Grant (1984a, 1984b) attributed the very low susceptibilities recorded for the high-grade rocks of the Canadian shield to the fact that magnetite-ilmenite solid solutions formed during granulite-grade metamorphism are accompanied by a marked reduction in magnetic susceptibility. An alternative model would have to include strong remnant magnetism in the SMZ, but this has not been verified in the field.

4. GRAVITY STUDIES

Gravity data can be used to determine variations in deep crustal structure (Free-air anomaly values) as well as locate anomalous values having a contrasting density to the surrounding rocks (Bouguer anomaly values). Gravity data has been interpreted along two seismic profiles crossing the Limpopo Belt. The positions of the survey lines are shown in figure 2.1. The first line follows the road from Pietersburg through Alldays to Pont Drift in the north. Gravity data was collected along this line by the Geological Survey to complement the reflection seismic survey. The second line running from Pietersburg to Beit Bridge was part of the Geological Survey's countrywide project (Smit et al., 1962).

Gravity data collected along the reflection seismic line has been modelled by De Beer and Stettler (in press). The results are presented in chapter 3. Gravity data values along the line from Pietersburg to Beit Bridge were taken from the Geological Survey Handbook 3 (Smit et al., 1962). The average station spacing was 4 km and the possible error in the relative data values is 10 g.u. A rectangular grid of data was computed using a minimum curvature algorithm (Briggs, 1974). A profile was extracted using the surface integral algorithm of Barnett (1976), and approximately follows a straight line between Pietersburg and Beit Bridge with a station spacing of 3 km.

Interpretation of field gravity data requires certain corrections to be made. The first involves the use of the International Gravity Formula whereby measured gravity values are reduced to values on a reference plane, in this case the geoid, which is the equipotential surface located at sea-level. The second, the Free-air correction, accounts for the effects of the station elevation above or below the reference plane. The third, the Bouguer correction, accounts for the effect of the mass located between the station and the reference plane. Bouguer anomaly values are used to indicate deviations of the actual earth density distribution from that of the assumed model.

The method of modelling follows the method used at the CSIR (Maher et al., 1991). Free-air anomaly (FAA) values were modelled since Free-air anomaly values calculated from the observed gravity values use the minimum approximations and corrections. Also the FAA value on the geoid is the same as that at the station elevation. Therefore there is less confusion as to the location of the anomalous density distributions if the gravity model incorporates the topography. However, Free-air anomaly values still contain some elevation effects. The inclusion of an isostatic root at the base of the crust can result in improved modelling results as it may approximate the regional field or bring attention to deviations from the assumed isostatic model for the crustal section.

The equation used to calculate the FAA at the surface of the earth is

$$g_{fa}=g_o-(g_t-h.dg/dr)$$

where -

g_{fa} = Free-air anomaly value

g_o = observed absolute gravity acceleration

g_t = theoretical gravity value given by the International Gravity Formula

h = station elevation above mean sea level

dg/dr = vertical gradient of gravity

The FAA values are then compared with the sum of the theoretical gravity effects from three models -

- Approximation of the actual Bouguer slab.
  This is an infinite slab located between the actual topography and sea level having a density of 2670 kg/m³.
- Approximation of the isostatic root.
  This is calculated from the surface topography using the Airy-Heiskanen hypothesis. The root is given a negative density

contrast equal to the difference between the bulk crust and mantle densities.

- Approximation of the density distribution within the earth's crust. Density values are chosen as contrasts to the Bouguer slab density of 2670 kg/m³. The blocks may have the surface of the earth as a boundary.

The formula used in calculating the root is

$$r = h.\rho_c / (\rho_s - \rho_c)$$

where

r = depth of root below compensation depth

h = height of topography

ρ_c = bulk density of crust

ρ_s = mantle density

In calculating the root a compensation depth of 30 km was used which gives an average crustal thickness of 38 km [illegible]h the KC. Average density values of 2840 kg/m³ and 3300 kg/m³ were used as densities of the bulk crust and mantle respectively.

4.1 THE GRAVITY MODEL

Input to the gravity modelling programme consists of a data file containing the surface topography block, the root topography block and any blocks with anomalous densities within the crust. Density values used were similar to those used by Coward and Fairhead (1980) and De Beer and Stettler (1988) i.e. 2930 kg/m³ for the SMZ granulites, 2670kg/m³ for rocks in the KC and CZ and 2550 kg/m³ for the sediments. To avoid edge effects both the surface and the root blocks are extended to three times the profile length on either side using the first and last elevation values. In areas of fairly constant elevation this assumption works well. However in this case, where the profile ended in the Limpopo valley at a low elevation compared to that of the

Zimbabwe plateau, true elevation values up to the Zimbabwe plateau had to be entered to achieve a better approximation.

The gravity profile shows a large positive anomaly of 600 g.u. over the SMZ. The background value over the Kaapvaal Craton is 100 g.u. and -100 g.u. over the CZ of the Limpopo Belt. Two models were produced. In the first model, the lower background value at the northern end of the profile can be modelled by increasing the thickness of the isostatic root by between 1 and 3 km below part of the CZ (figure 4.1.a), which achieves a slightly better fit than the second model where the root was calculated directly from the surface topography (figure 4.1.b). The other bodies and densities in the two models are identical. The positive anomaly over the SMZ is modelled using a block having a maximum depth extent of 7 km with a density of 2930 kg/m^3. The southern edge of the block dips northwards while the northern edge is almost vertical. The Soutpansberg trough in the southern marginal zone is modelled with a depth extent equal to the height of the topography and a density of 2550 kg/m^3.

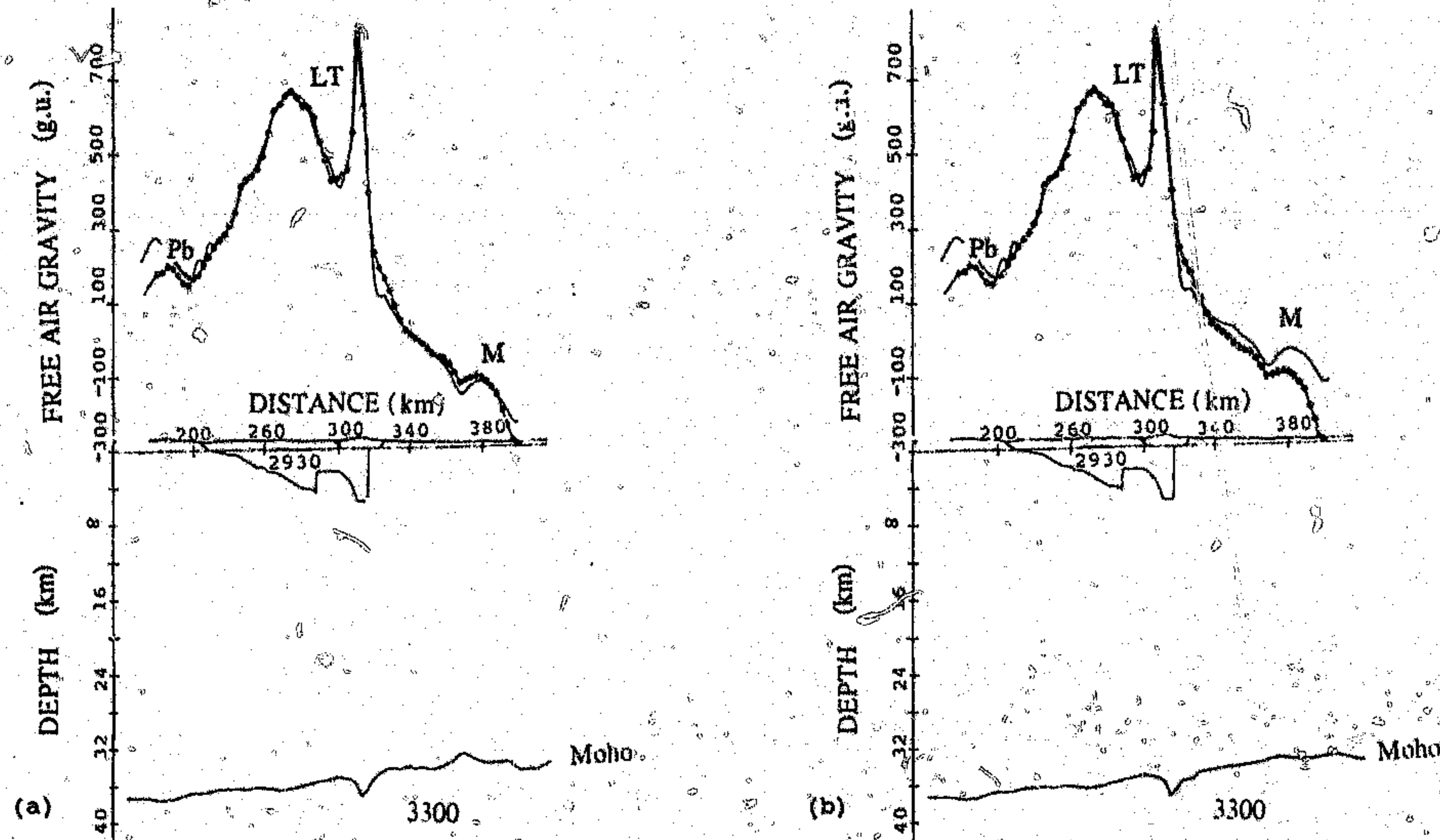

Figure 4.1 Gravity models along a line between Pietersburg and Beit Bridge. Densities are given in kg/m³. Models a and b are identical with the exception of the Moho topography.

■-■ measured profile, --- calculated profile Pb - Pietersburg, LT - Louis Trichard, M - Messina

5. REFRACTION SEISMIC STUDIES

Refraction seismic studies involve the measurement of arrival times of refracted waves where the ray path is mostly horizontal. Refraction of waves occurs across a boundary between two units having different acoustic properties, or waves may be bent due to the velocity gradient within a rock unit. Where the separation between source and receiver is of the order of hundreds of kilometers, the velocity structure of the upper mantle may also be investigated.

Various models have been postulated for the velocity-depth structure of the earth, based on refraction results. Most models include an overall positive velocity gradient in the crust. The Conrad discontinuity which occurs in the middle part of the continental crust is often included as a discontinuity in the velocity-depth function. It marks the transition from sialic to more mafic material, or material which is at a higher grade of metamorphism. The boundary between the crust and mantle, the 'Moho', is generally shown as a sharp discontinuity, however in reality it is more likely a complex transition zone, involving mineral phase transformation, which may be up to twelve kilometers thick (Bott, 1971). This may result in a layered structure with layers of alternating high and low velocity, or a zone having steep velocity gradients. Laboratory tests have shown that seismic velocity is a function of both pressure and temperature. Seismic velocities increase with increasing confining pressure and decrease with increasing temperature. Laboratory tests have shown that the known temperature gradients make it possible that velocities decrease with depth. This is a possible explanation for the low velocity layers which may exist in the crust and mantle.

The present study is based on unpublished measurements by R.W.E. Green, where Witwatersrand mine tremors were recorded at 12 stations along a line from Pietersburg through Harare to Lusaka during the 1960's. The method of data collection was similar to that used by Gane et al. (1956). The data set is rather limited. Only traveltimes of first arrivals were recorded and these times represent the average times of arrival for events over a range of distances from the recording station, since source locations and times could only be approximated. Also the station spacing is large (about 100 km north of Messina) and the profile is unreversed. Therefore the modelled results are only an average representation of the real subsurface structure. However the arrival times do provide an absolute time reference for the more detailed observations of Stuart and Zengeni (1987). The combined data sets are shown in figure 5.1. In the current data set the source-receiver distances are large, between 300 and 1000 km, which allowed the model to extend into the upper mantle. The results can be used to determine the velocity structure and crustal thickness of the northern Kaapvaal Craton and the Limpopo Belt, and to investigate possible differences in the gross crustal and upper mantle structure between the two terranes.

In this study, ray tracing was used to compute traveltimes for 2-D velocity models and the results were compared with the first arrivals, P_n (waves travelling in the uppermost mantle) and P_mP (waves reflected at the Moho). The programme RAYAMP-PC, written by D. Crossley of the Geophysics Laboratory, McGill University was used. It is an interactive microcomputer version of the program RAYAMP (Spence et al., 1984). The program is based on asymptotic ray theory and allows ray tracing and the calculation of synthetics through media where the velocity can vary both vertically and laterally. A model is constructed by assigning a velocity and a velocity gradient to all boundaries. The velocity value is constant along the length of the boundary and the gradient is normal to the boundary. Where the velocity varies laterally, adjacent boundaries of differing velocity must be separated by a vertical or near-vertical boundary with velocity and velocity gradient equal to zero. Two adjacent boundaries with the same velocity but different dips must also be separated by a vertical boundary with velocity equal zero so that the regions where the velocity gradients are different are separated. Ray tracing is done in groups and for each group the initial and the final angle of departure as well as the ray spacing must be given. In this way ray

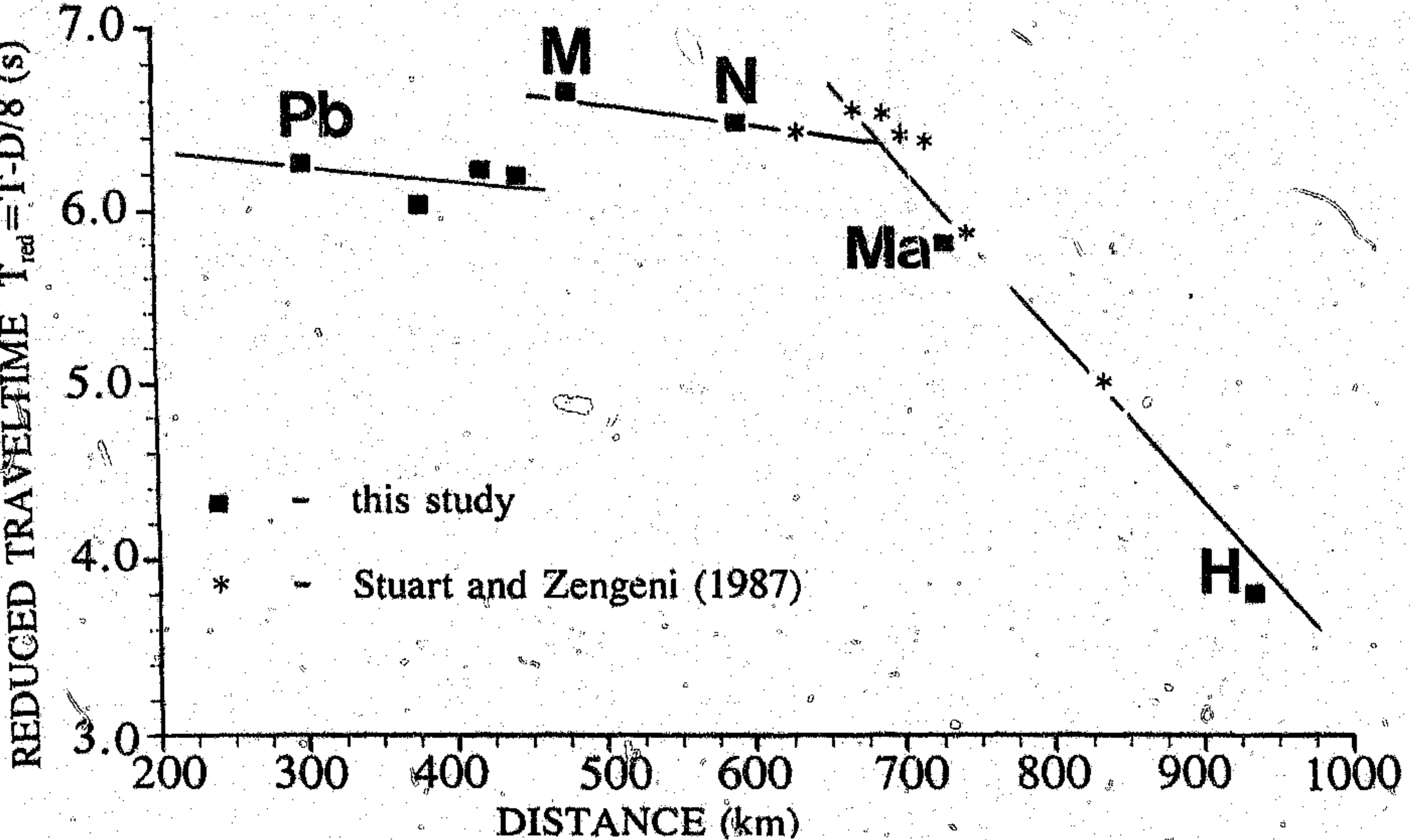

Figure 5.1 Reduced traveltimes of Witwatersrand mine tremors (this study) and the study by Stuart and Zengeni (1987). Pb - Pietersburg, M - Messina, N - Nuanetsi, Ma - Masvingo, H - Harare

groups may be chosen to penetrate selected parts of the crust or mantle. Synthetics are calculated in either real time or using the given reduction velocity.

Three branches are apparent on the traveltime data plotted using a reduction velocity of 8 km/s (figure 5.1). The branch between 300 and 450 km has a small downward dip, indicating a velocity of about 8.1 km/s, which is interpreted to represent energy travelling in the uppermost mantle. A 0.6 s offset separates this from the second branch between 475 and 600 km which has a similar dip to the first branch. The extinction of the first branch together with the 0.6 s offset is most simply explained using a low velocity layer in the upper mantle. The traveltime branch observed at offsets of 600 - 950 km has an apparent velocity of about 8.5 km/s.

Data from old Precambrian shield areas typically shows a rather continuous increase in velocity without low velocity layers or other prominent first order discontinuities. The division into upper and lower crust exists, but the transition is gradational and not as strong as that found in younger crusts (Meissner, 1986). The Moho does not generally produce strong P_mP arrivals in accordance with the more transitional nature of the crust/mantle boundary beneath Precambrian cratons (Jarchow and Thompson, 1989). This has been shown to be true for the central Kaapvaal Craton (Durrheim, 1989). Consequently the first arrivals observed at distances greater than 300 km are considered to be waves which have penetrated the upper mantle and have been turned by a positive velocity gradient, rather than true headwaves guided by a velocity discontinuity at the crust/mantle boundary. Therefore variations in arrival times need not be explained by variations in Moho topography.

The velocity models, ray trace diagrams and synthetic seismograms are shown in figure 5.2. The models are based on first arrival P_n data only. No P_mP (Moho) reflections were documented, so the crustal thickness is based on the previous seismic work of Stuart and Zengeni (1987) and Gane et al.

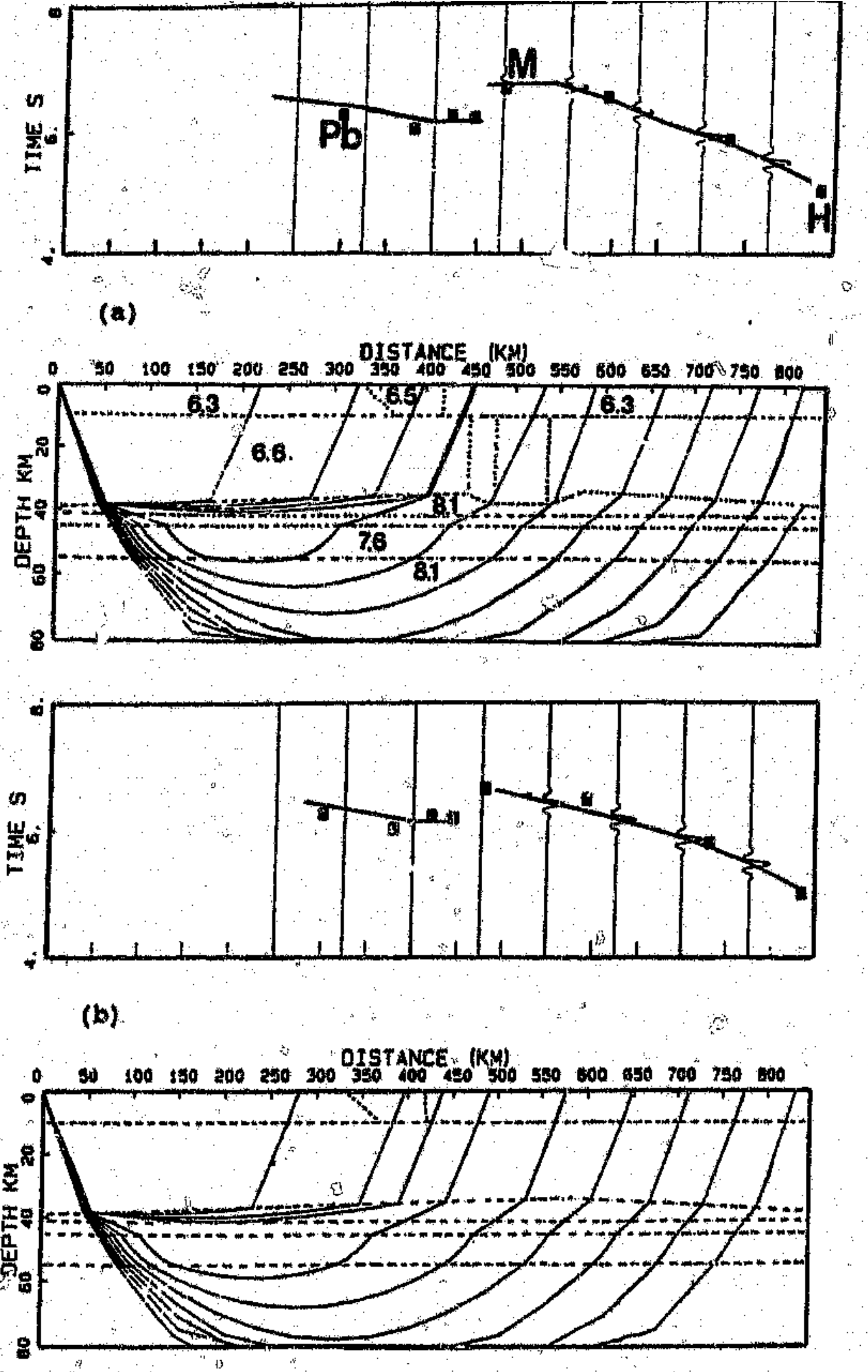

Figure 5.2 Seismic velocity models, ray trace diagrams and synthetic record sections. Seismic velocity is given in km/s. Reduced traveltimes were calculated using a reduction velocity of 8 km/s. Models a and b are identical with the exception of the Moho topography.

■ - observed travel times, Pb - Pietersburg, M - Messina, H - Harare

(1956) as well as gravity studies. Crustal models of the Limpopo Belt have been produced based on gravity studies of the positive Bouguer anomaly which is observed over the SMZ of the belt. Emenike (1986) based his model on a Pratt-type isostatic mechanism whereby the crust is slightly thicker and denser beneath the SMZ. Kleywegt (1988) and De Beer and Stettler (in press) assume an Airy-type isostatic mechanism whereby the crust is thinner beneath the SMZ and the excess mass is confined to the upper crust. The two refraction models based on the different isostatic mechanisms are shown in figures 5.2.a and 5.2.b respectively.

The upper crust beneath the craton and the CZ was assigned a velocity of 6.3 km/s and the dense granulites in the SMZ, 6.5 km/s. A velocity of 6.6 km/s was used for the lower crustal material. These values are within the range of values determined by Durrheim (1989) i.e. velocities between 6.0 and 6.3 km/s for the upper crust and 6.5 to 6.7 km/s for the lower crust within the Kaapvaal Craton. The position of the interface between the upper and lower crust could not be accurately modelled because of the limited data set. Therefore a boundary was included at 10 km depth to be compatible with the electrical and gravity data. An abrupt boundary was used because the data could not be used to distinguish between an abrupt or gradational boundary and Durrheim (1989) reported both abrupt and gradational boundaries between upper and lower crust within the central Kaapvaal Craton. This crustal structure, along with a sub-Moho velocity of 8.07 km/s and a slight thinning of the crust northwards, fits the first branch on the traveltime plot. The distance travelled through the faster SMZ material is short in relation to the overall travel path and therefore has no effect on the overall traveltimes. The crust thins from about 39 km beneath Johannesburg to about 35 km around Messina in association with the decrease in surface elevation.

The exact nature of the 0.6 s delay in traveltimes between 450 and 475 km is uncertain. A traveltime delay may be brought about by either an increase in crustal thickness or variations in the upper mantle velocity e.g. a low velocity layer. A thickening of the crust by 8 km would result in a delay of

0.6 s, however such an abrupt increase in crustal thickness seems unlikely when other geophysical evidence is considered. An 8 km increase in crustal thickness of a body the size of the CZ would result in a negative anomaly of around 800 g.u., whereas the CZ is characterised by a negative anomaly of only 100 g.u. In this case the delay was modelled by including a low velocity layer (LVL) between 41.5 and 45 km with a velocity of 8.087 km/s at the top and a negative velocity gradient of 0.003 km/s/km. No constraints could be placed on the thickness or velocity of the LVL and a thicker layer with a smaller reduction in velocity would produce a similar delay.

The final branch on the traveltime curve was produced using a velocity of 8.1 km/s, with a gradient of 0.0085 km/s/km, with the velocity reaching 8.5 km/s at a depth of 110 km, where the gradient was reduced to 0.002 km/s/km. This is in accordance with the model of Durrheim (1989) who suggested the presence of a slight positive gradient of about 0.01 km/s/km in the upper mantle. However this structure does not fit the second slightly dipping branch between 475 and 600 km very well. Therefore a thickening of the crust of about 5 km beneath the CZ was introduced. This is broadly compatible with the gravity model where the crust was thickened by between 1 and 3 km to obtain the best fit.

The observations of Stuart and Zengeni (1987) are in general agreement with the first model involving only a LVL, although short sections of their profile (offsets of 630-680 km and 730-760 km) show phase velocities of only 7.8 km/s which they attribute to a northward dip of the Moho. Also the 0.45 s offset between arrivals on the ZC and Limpopo Belt is attributed to anomalous faster material associated with the Buchwa greenstone belt or the boundary between the ZC and LB. Both effects probably represent local perturbations of the velocity structure, either in the crust or upper mantle.

Green and Bloch (1969) reported unusually early arrivals of P_n waves between 300 and 500 km north of Johannesburg. However, no other seismic refraction study in southern Africa has made detailed observations of events at distances exceeding 320 km, so it is unknown whether the LVL layer beneath the LB and northern KC in the upper mantle exists elsewhere. Bloch et al. (1969) using multi-mode surface wave dispersion methods, modelled the crustal shear velocity distribution. They found two low velocity channels beginning at depths of 12 and 24 km. The major increase to mantle velocities was found to take place at 45 km.

The formation of low velocity layers has been discussed by Meissner (1986). Areas of high heat flow have high temperature gradients, which may result in LVL's. These LVL's are most apparent in the crustal shear velocity distribution. Overthrusting which occurs in compressional zones may result in high velocity material being thrust over normal velocity material. This may result in LVL's in the crust and upper mantle.

Thus the refraction data do not provide any new geological knowledge in so far as separating between cratonic and upper mantle composition and structure in the Limpopo Belt and adjacent Kaapvaal Craton. The LVL is present beneath both the craton and belt, indicating that either it is controlled by recent conditions or was unaffected by the Limpopo orogeny.

6. SEISMIC REFLECTION STUDIES

6.1 DATA PROCESSING

The 218 km long Limpopo profile was shot for the South African Geological Survey and the National Geophysics Programme by Rockplan (Pty) Ltd of South Africa in 1987. The acquisition parameters are listed in table 6.1. The profile was recorded from just south of Pont Drift in the Central Zone, across the Southern Marginal Zone, ending south of Pietersburg on the Kaapvaal Craton.

This study involved the reprocessing of the data as well as migration for the first time. The field source and recording parameters (number and power of vibrators, number and length of sweeps, station interval, fold of coverage) were somewhat less than that usually used by other deep seismic reflection programmes such as COCORP, DEKORP and ECORS. Therefore much attention was given to the editing of noisy traces, definition of CMP bins and weighting of the stack during the reprocessing. Careful attention was also given to the estimation of residual statics in order to improve the continuity of the data.

In general the data from the Limpopo ~~line~~ is characterised by poor signal to noise ratio. The nature of the noise also varies considerably from one shot record to another. Therefore in the processing sequence, there is no one process which is the key to a final good section. Rather it is the correct application of all processes.

Parameter tests were run on a sample section of the data in order to determine the overall processing sequence and the parameters to use. The processing sequence followed is shown in figure 6.1 and the parameters used in each of the processors in table 6.2. A sample field file is shown in figure 6.2 where each panel shows a further step in the processing sequence.

Table 6.1: Acquisition parameters for the Limpopo reflection seismic profile.

Geophone station interval:	**50m**
Geophone pattern:	**Four rows of six geophones per station forming two parallel rows of twelve geophones with a 4.5 m separation between geophones, a 2.25 m stagger between rows, and a 0.25 m lateral separation.**
Vibrator station interval:	**200 m**
Vibrator pattern:	**Four vibrators in-line, 20 m pad separation and 5 m move-up after each sweep. Centre of gravity of pattern equidistant between the two adjacent geophone stations.**
Spread geometry:	**2525-175-0-175-2525 m**
Sweeps/vibration point:	**10**
Sweep frequency:	**15-63 Hz**
Sweep length:	**19 s**
Listening time:	**32 s**
Sample interval:	**4 ms**
Multiplicity:	**12 fold**

Table 6.2. Processing parameters for the Limpopo reflection seismic profile

The processing was carried out using the SierraSeis seismic processing package at the Genmin Geophysics Data Processing centre in Springs.

Gain recovery

Spherical divergence with a velocity of 6000 m/s.
Exponential gain of 10 dB/s from 4-1500 ms.
Trace-to-trace equalisation using a sliding 1000 ms window over the whole trace.

Geometry

Crooked line geometry with a bin width of 150 metres.
Field and elevation statics applied to move data to a 800 m datum using a datum velocity of 5700 m/s.

FK filter

20-80 Hz at the alias wave number, fan filter with a linear taper of 5 samples.

Sort

Sort into CMP gathers using a 25 m bin size.

Deconvolution

Predictive deconvolution with a 240 ms operator length, 24 ms gap and 3% pre-whitening was applied to all the data.

NMO correction

Final stacking velocities used are listed in Appendix A.

Table 6.2 (continued)

Initial mute

Initial mutes used are listed in Appendix B.

A taper of 40 ms was used.

Residual statics

Residuals statics were calculated using a window between 500 ms and 4500 ms with a correlation length output of 80 ms. Residual values were picked from the maximum peak of the correlation output.

Stack

A ROOTN stack was used where normalisation was by the square root of the fold.

Time variant frequency filtering

15-65 Hz at 1000 ms

15-60 Hz at 2000 ms

15-50 Hz at 4000 ms

Slopes used were 80 dB/octave on the low side and 120 dB/octave on the high side.

Migration

FK migration using 80% of the smoothed stacking velocities.

Display

Trace amplitudes were scaled using a 1000 ms window and 60% application.

Data values were displayed using an exponential power of 2.5.

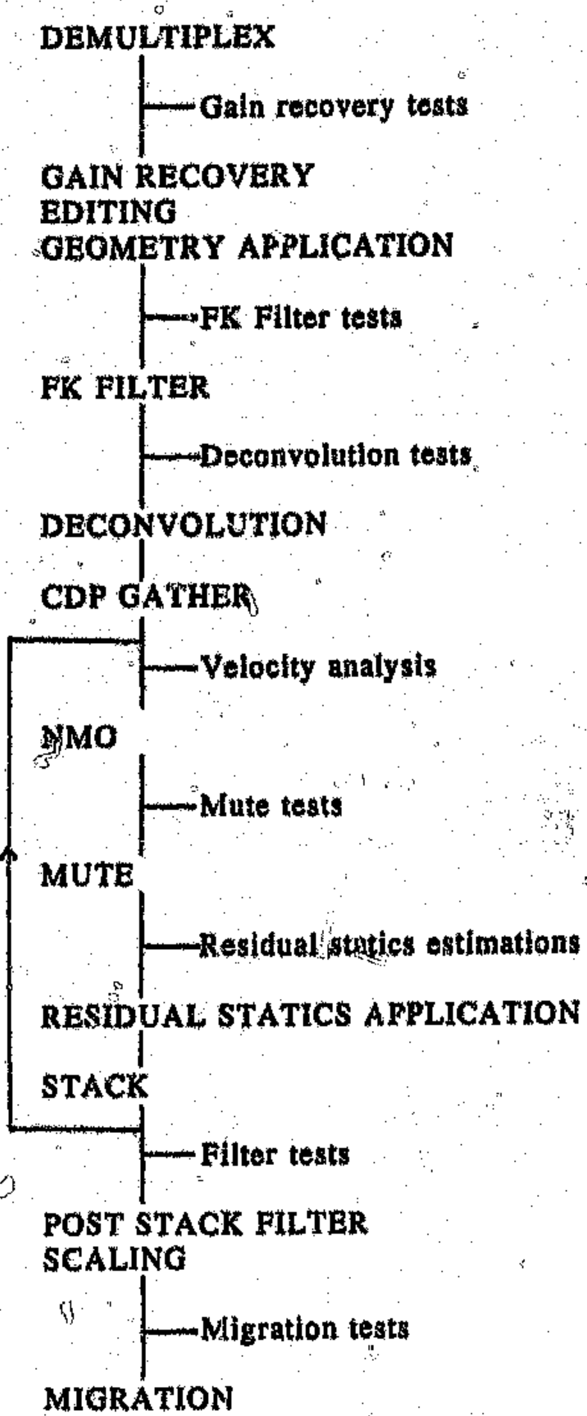

Figure 6.1 Processing sequence for the Limpopo seismic line.

Figure 6.2 A sample processed field file. Each panel shows a further step in the processing sequence.

1. No processing. 2. Field statics applied. 3. Gain corrections applied. 4. FK filtered. 5. After deconvolution. 6. Time variant filter applied. 7. NMO corrections applied. 8. Front-end mute applied. 9. Post stack scaling.

DATA EDITING

Data editing removes records, traces or parts of traces containing no useful signal. Data editing must be done early in the processing sequence (immediately after gain recovery) so that future processes are not affected by bad records or traces. Further editing can be carried out throughout the processing.

The first step in the data processing sequence was to examine all the shot records, with no gain correction applied, for editing purposes. A selection of raw field files are shown in figure 6.3. Figure 6.4 shows field files after gain corrections have been applied. The raw field files are dominated by high amplitude refractions in the first second. The velocity of the refractions is approximately 6000 m/s. Arrival times for the refractions are variable due to variations in travel time through the overburden since static corrections have not been applied. A low velocity airwave with an approximate velocity of 330 m/s is visible on field file 598 from trace 55 beginning at 2500 ms. Also visible on the raw field records are traces dominated by 50 Hz noise from powerlines - file 598 trace 30, noise bursts on near traces and high amplitude spikes - file 875 trace, [illegible] and 71. The signal to noise ratio on traces with gain corrections applied is low. The same noise problems are still apparent i.e. noise bursts on near traces between 7 and 9 s - file 750 traces 46 to 56, 50 Hz powerline signal, high amplitude spikes and groundroll.

Field records consisting entirely of noise were discarded from the processing sequence. Mono-frequency signal, in this case 50 Hz noise resulting from powerlines was removed before stacking using a notch filter. The frequency spectrum of a trace dominated by 50 Hz noise, before and after the application of a notch filter, is shown in figure 6.5. Spikes were removed using an autoedit routine where an entire trace was discarded if the amplitude within a moving time window exceeded a value calculated from the adjacent 4 traces within the same window. Noise bursts on the near traces

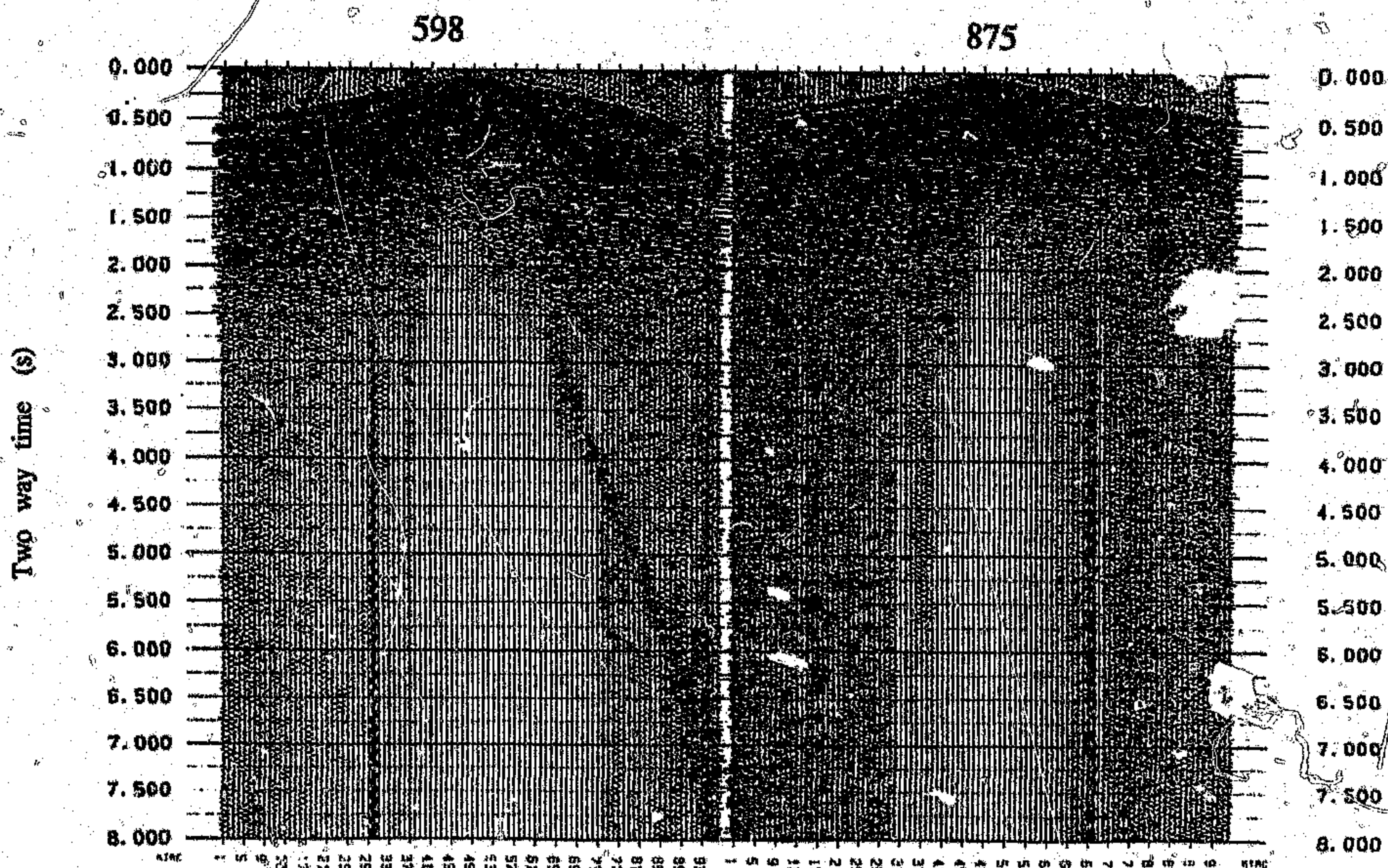

Figure 6.3 Sample field files - no processing.

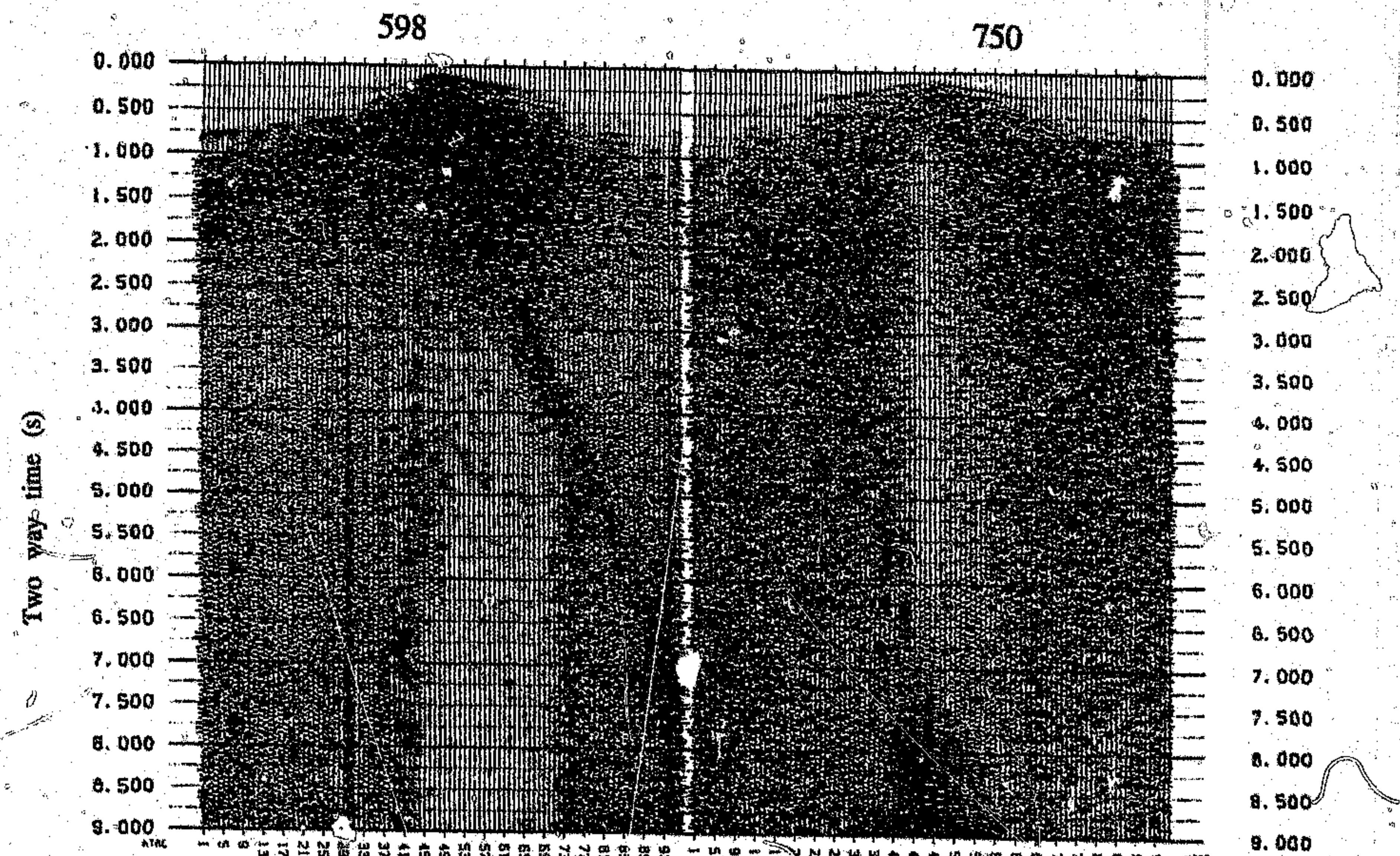

Figure 6.4 Sample field files - with amplitude recovery.

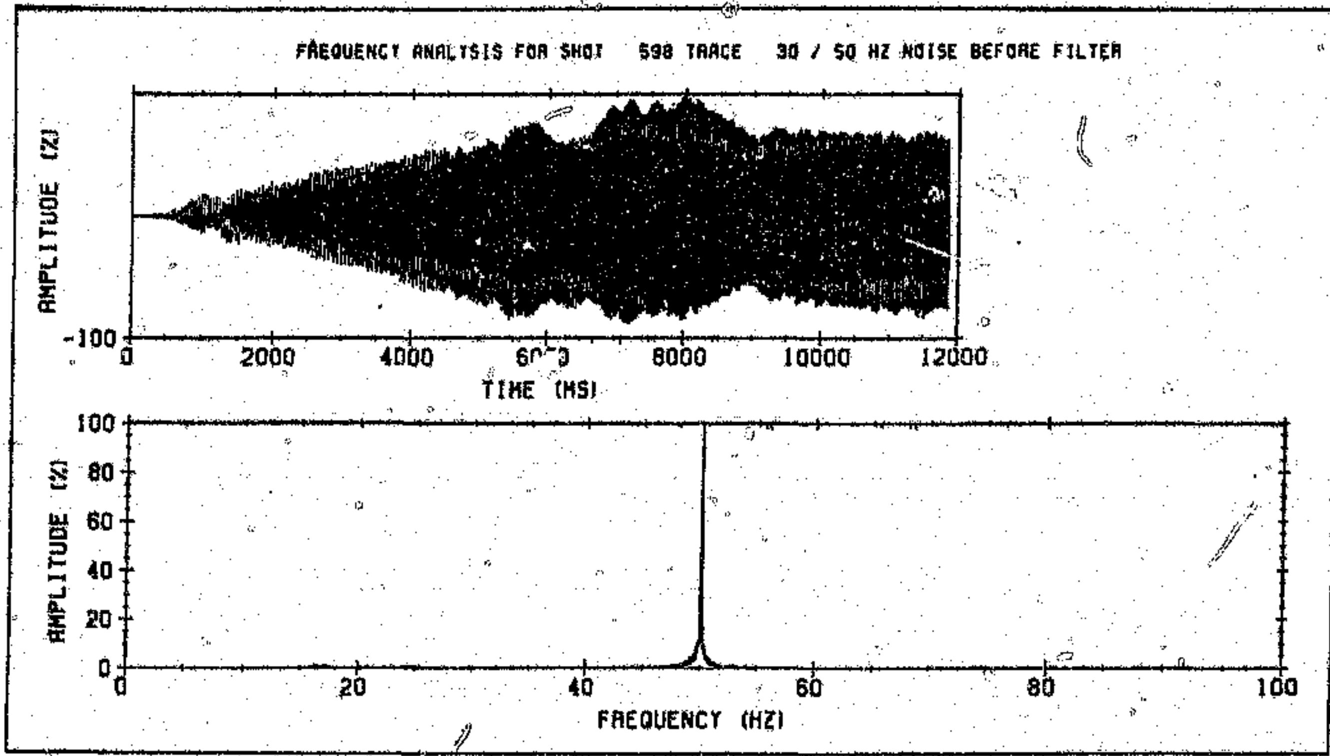

(a)

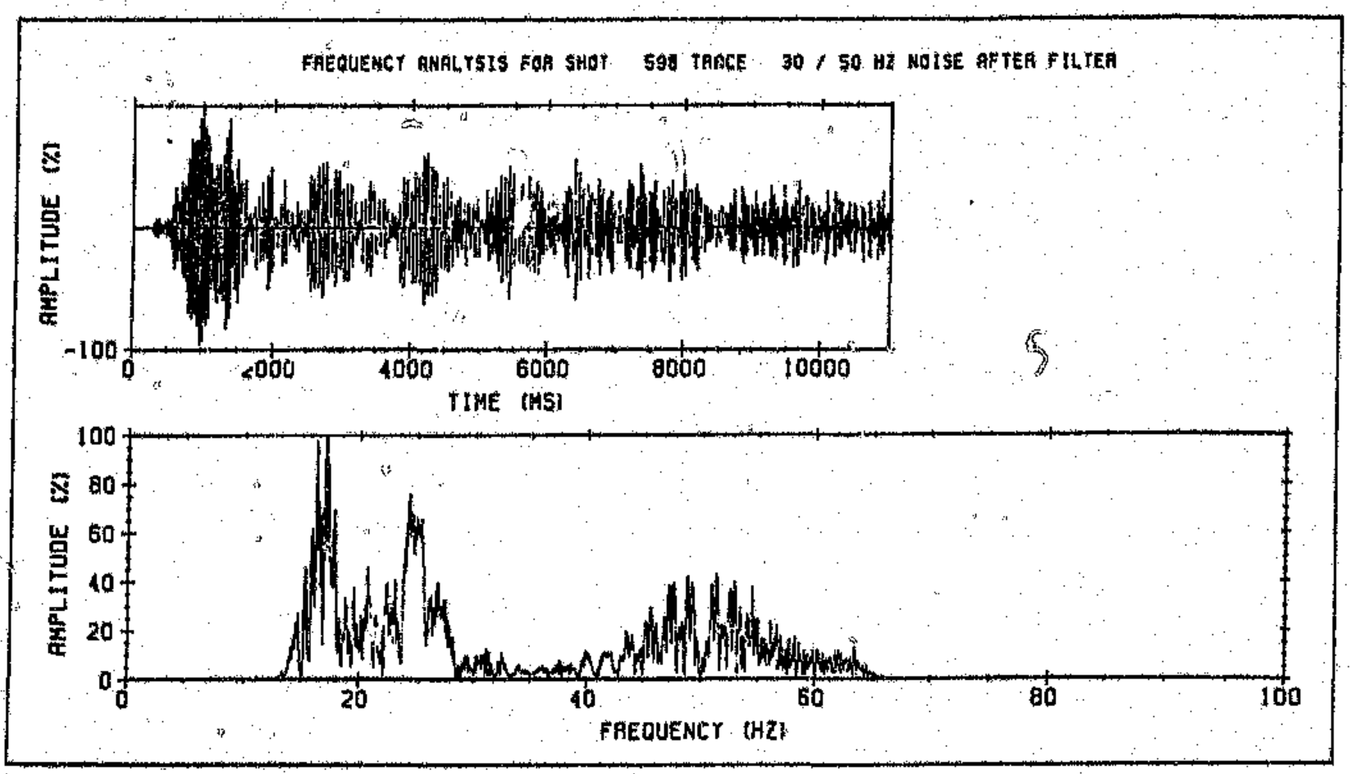

(b)

Figure 6.5 Frequency spectrum and amplitude plots. (a) before and (b) after application of a 50 Hz notch filter.

were more difficult to remove since they did not occur on all field records, and where they did occur, signal was also present on the traces. Also the frequency content of the noise was in the same range as the signal, so it could not be removed by filtering (figure 6.6). On the amplitude/time plot, the high amplitude noise is seen between 7 and 10 s. However, it is not distinguishable on the frequency spectrum plot. The same trace with a filter applied is seen in figure 6.6.b and although the amplitude of the noise is slightly reduced and the low frequency content of the trace has been reduced, the noise is still there. Therefore a surgical mute was applied to selected records where high amplitude noise bursts were a problem. A surgical mute can be used to zero samples in a selected time and offset range. Alternatively a percentage scaling processor can be used to reduce amplitudes by a given percentage. In this way traces 44 to 56 over times 6 to 10 s were zeroed on the selected field records. However, when a stacked section with the surgical mute applied was compared to one with no surgical mute, there was no obvious difference. Therefore it appears that noise bursts are eliminated during the stacking process.

Removal of high amplitude refractions visible in the first 1 s on the records will be discussed later in the section on FK filtering.

GAIN RECOVERY

Gain recovery, whereby the amplitudes of deep events are boosted, is achieved using time variant scaling functions. These processes are applied to correct for the decay of seismic energy with depth penetration and the resulting loss in amplitude with time.

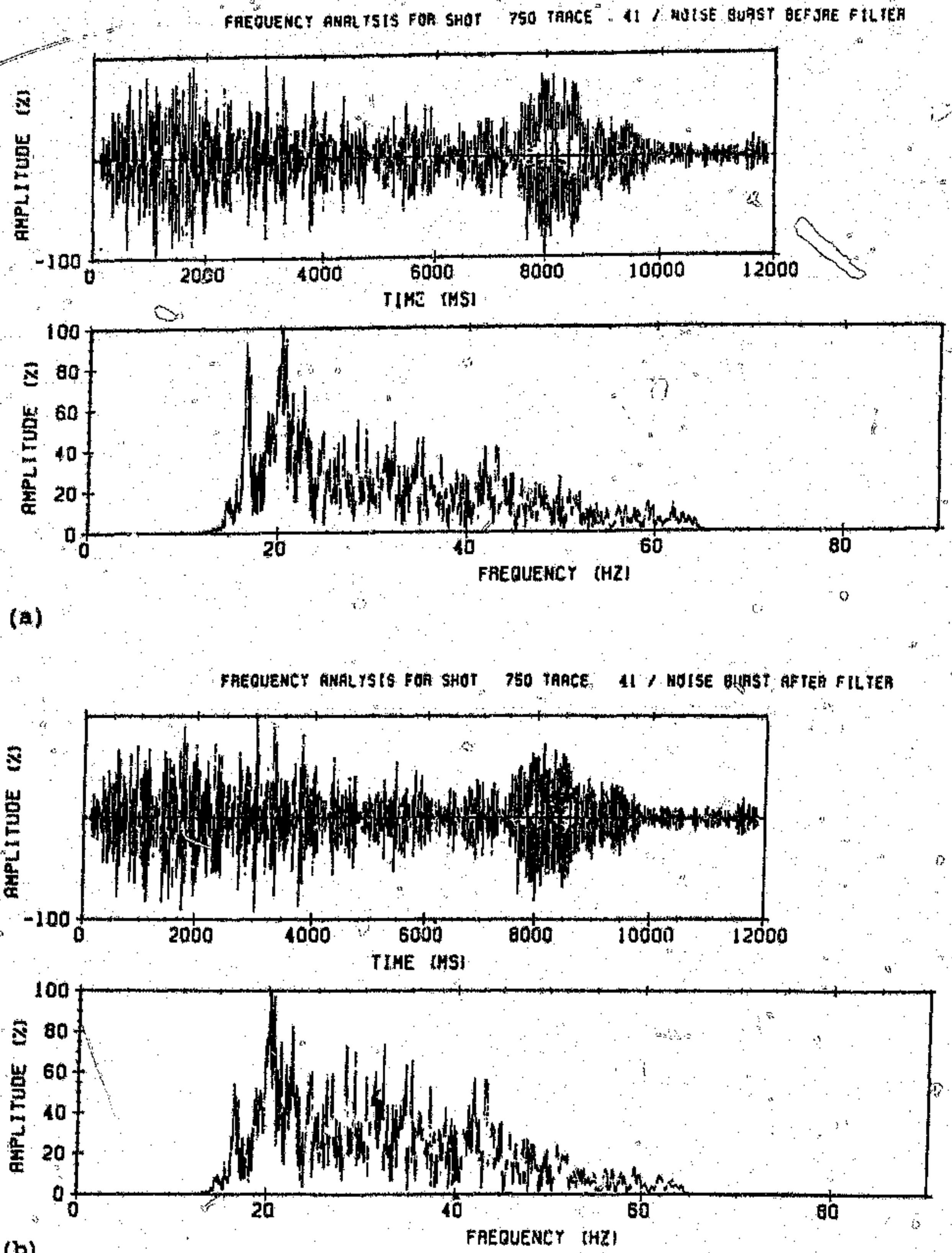

Figure 6.6 Frequency spectrum and amplitude plots of a trace dominated by a high amplitude noise blast between 7 and 10 s (a) before and (b) after the application of a time variant filter.

Considering the seismic energy source as a point source generating a spherical wave field, two effects due to propagation through the earth are apparent, namely

- a decay in energy amplitude with depth
- a change in frequency content with depth

The four main factors contributing to the decay of seismic energy with time/(or depth) are -

- Scattering and reflection at every discontinuity, where the amount transmitted can be approximated by the factor

$$(1-r)^{(bt)}$$

  r = average reflection coefficient
  b = number of reflections between 0 and t

- Spherical divergence,, which is the loss in energy per unit volume due to the expansion of the wavelet with time. The decay factor is approximated by $1/t$.

- Attenuation loss which is the loss of energy due to friction and is proportional to

$$e^{-aft}$$

  a is a constant
  f = frequency

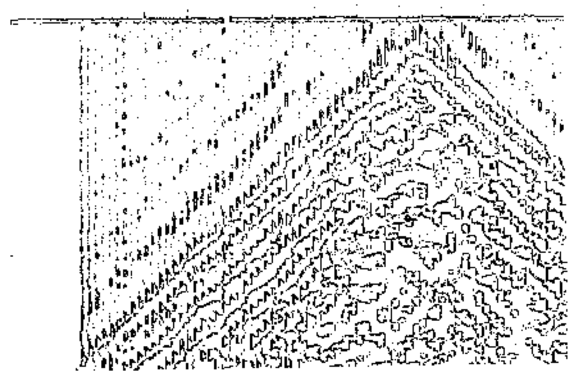

SIERRA RASTER IMAGE FILE: SS900.RAS
CREATION DATE/TIME: 22-JUL-91 15:52:21
SEQUENCE: 9 DESC:

Amplitude distortion due to frequency loss which is caused by dispersion, internal reflections and destructive interference. High frequencies are more rapidly absorbed than low frequencies, so spherical divergence corrections do not restore amplitudes of high frequencies as much as those of low frequencies. The amplitude spectrum can be broadened using spectral whitening or deconvolution.

All the above effects have nearly the same decay curve. In a homogenous medium, wavefronts emanating from a point source are spherical with amplitudes proportional to 1/t, but with velocity variations, refraction effects result in a wavefront which is no longer spherical.

Therefore in a layered earth the amplitude decay is approximated by

$$\frac{1}{(v(t))^2 \times t}$$

t = two way time

v(t) = RMS velocity of the primary reflections

Compensation for geometric spreading is achieved by applying a time varying scalar computed and applied to every sample of the trace using the formula

$$t\left(\frac{v(t)}{v(0)}\right)^2$$

t = time in seconds

v(t) = RMS velocity at time t

v(0) = RMS velocity at time 0

After a specified time, a constant scalar may be applied to the rest of the data. This time is estimated to be the time of the last meaningful amplitude data visible on a raw field record.

Amplitudes also vary with recording distance away from the energy source. Therefore a trace balancing processor is applied to balance amplitudes between traces in a field record so that all traces have the same average amplitude. This is necessary for F-K filtering.

Amplitude analysis of a field record after correction for spherical divergence and amplitude balancing between traces still shows a decrease in amplitude with time. The final process in gain recovery is an exponential gain function given by

$$e^{k(T-t)}$$

T = time

t = start time of gain application

k = exponent in decibels per second

Values for the start time (before which no gain is applied to the samples), and an end time (after which a constant gain is applied), and the exponent are determined from amplitude decay curves of field records. The amplitude variation with time after spherical divergence, amplitude balancing and exponential correction is nearly flat. However, amplitude recovery was done on noise as well as signal, so noise amplitudes have been boosted as well. Maximum and average amplitude decay curves before and after gain recovery for different traces within a field record are shown in figures 6.7 (a-c). Where the amplitude range at any one time is small (near or far traces only), the average and maximum amplitude curves overlap. Amplitudes are highest on near traces so the decay in amplitude with time is large (figure 6.7.a). On far traces amplitudes are low and so is the decay in amplitude with time (figure 6.7.b). In order not to bias the data toward either near or far traces a gain function was selected from the decay curve of amplitudes averaged from all traces within a record (figure 6.7.c).

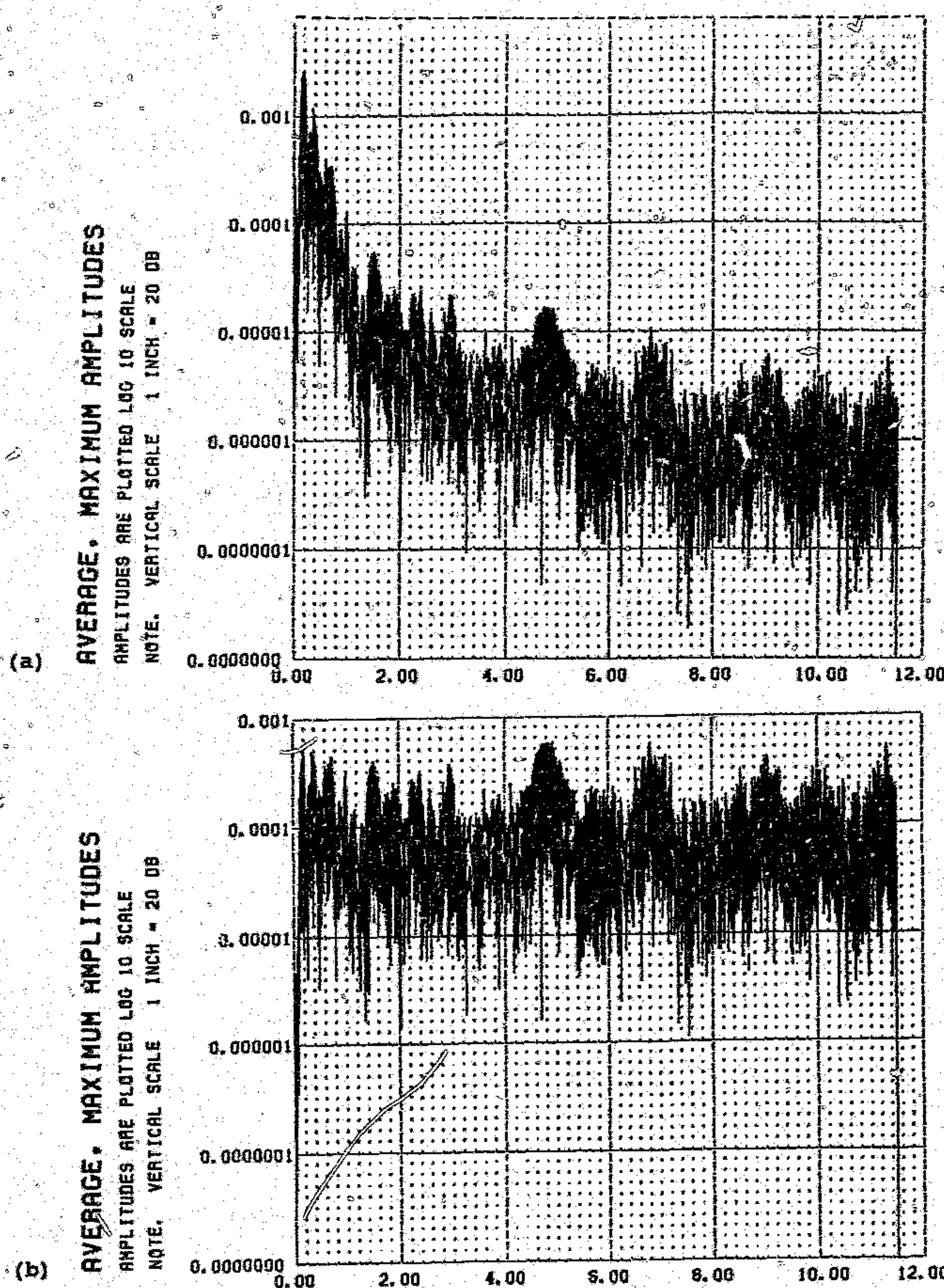

Figure 5.7.a Average and maximum amplitude decay curves for near traces (a) before and (b) after gain recovery.

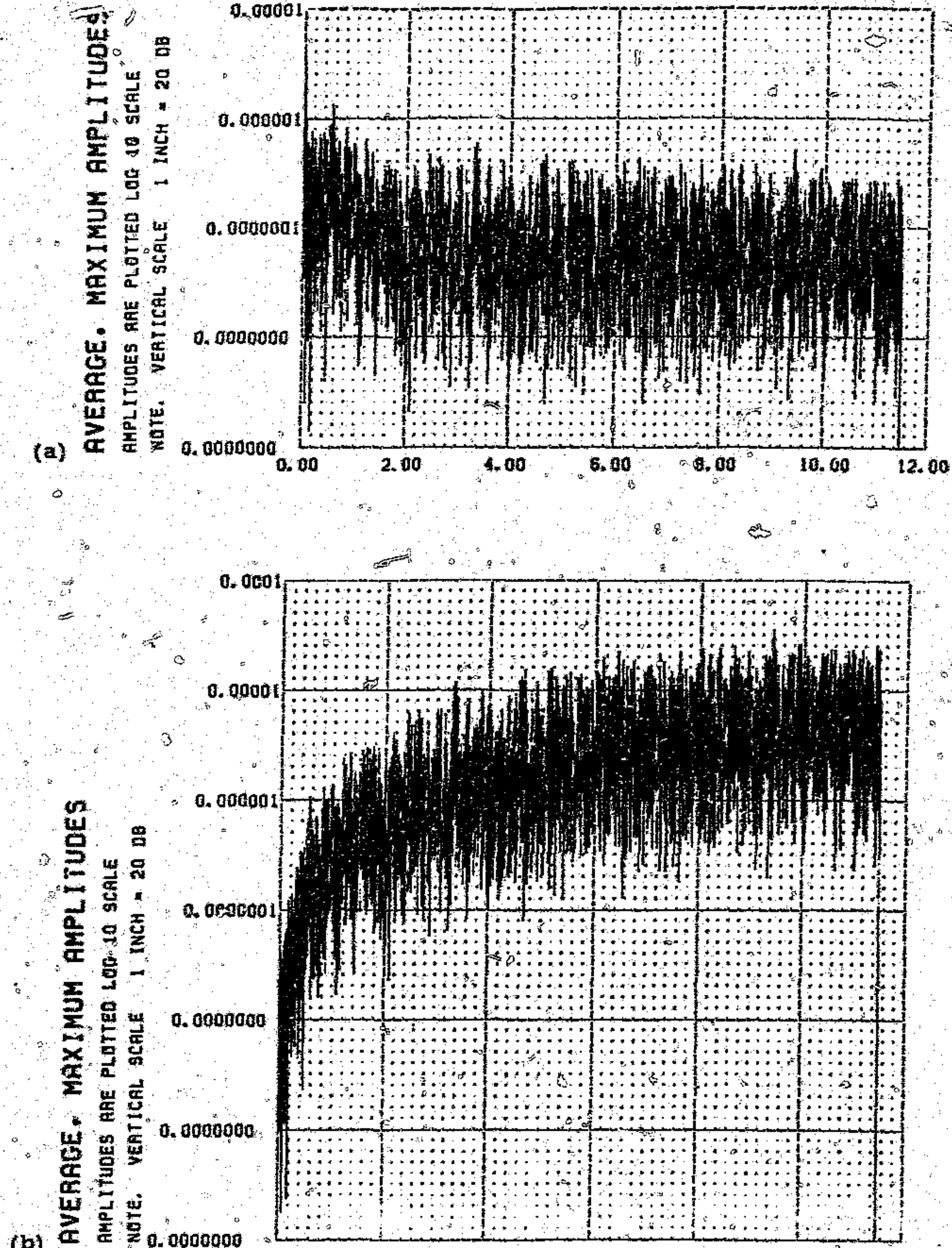

Figure 6.7.b Average and maximum amplitude decay curves for far traces (a) before and (b) after gain recovery.

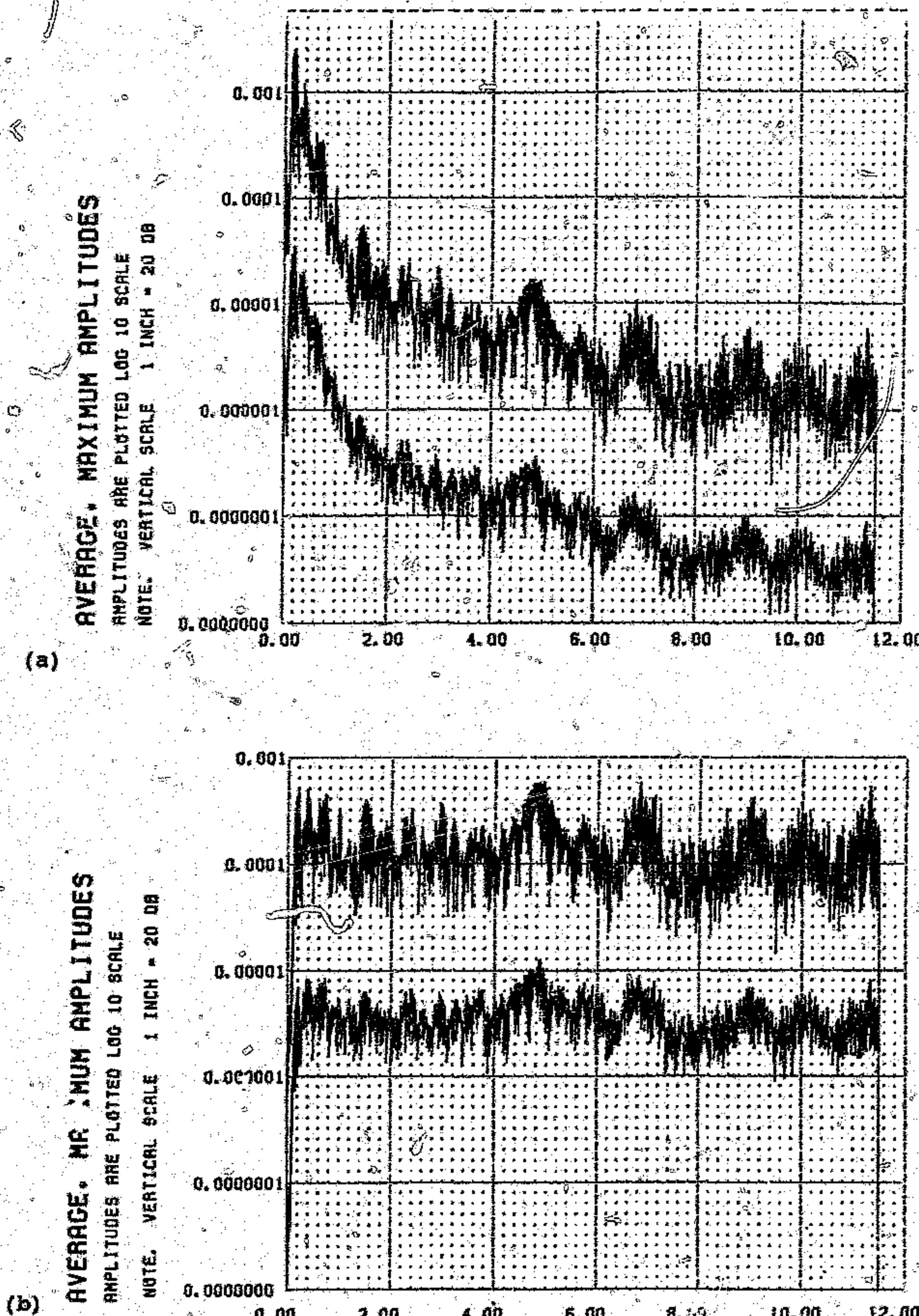

Figure 6.7.c. Average and maximum amplitude decay curves for a whole record (a) before and (b) after gain recovery.

FIELD STATICS AND GEOMETRY

The effect of applying static corrections is to remove the apparent negative correlation between subsurface structure and the ground surface elevation (figure 6.8.a) i.e. long wavelength static variations (Yilmaz, 1987), as well as to remove the effect of weathered layers, where the static correction shows no correlation with elevation (figure 6.8.c). Each trace in a CMP gather has its source and receiver located at different elevations resulting in a misalignment of reflections. Therefore before stacking a geometric correction is applied to place all source and receivers on the same horizontal plane. This is effectively a timeshift where the entire trace is shifted up or down depending on the position of the datum plane relative to the shot and receiver planes. This correction has two components

- elevation static calculated from elevation differences
- weathering static calculated from the thickness of the weathering layers

Source and receiver elevations within a CMP gather should not differ by more than ~100 m from the datum elevation, otherwise a floating datum should be used first, to prevent distortion of subsurface velocities (SSL course notes). The weathering layer static is calculated from a low velocity layer refraction survey carried out in the field.

The purpose of setting up the line geometry is to define the following -

- the vibrator point elevations, coordinates and offsets
- geophone elevations, coordinates and offsets
- the datum velocity and elevation
- parameters used in calculating the CMP line
- spread for each vibrator point

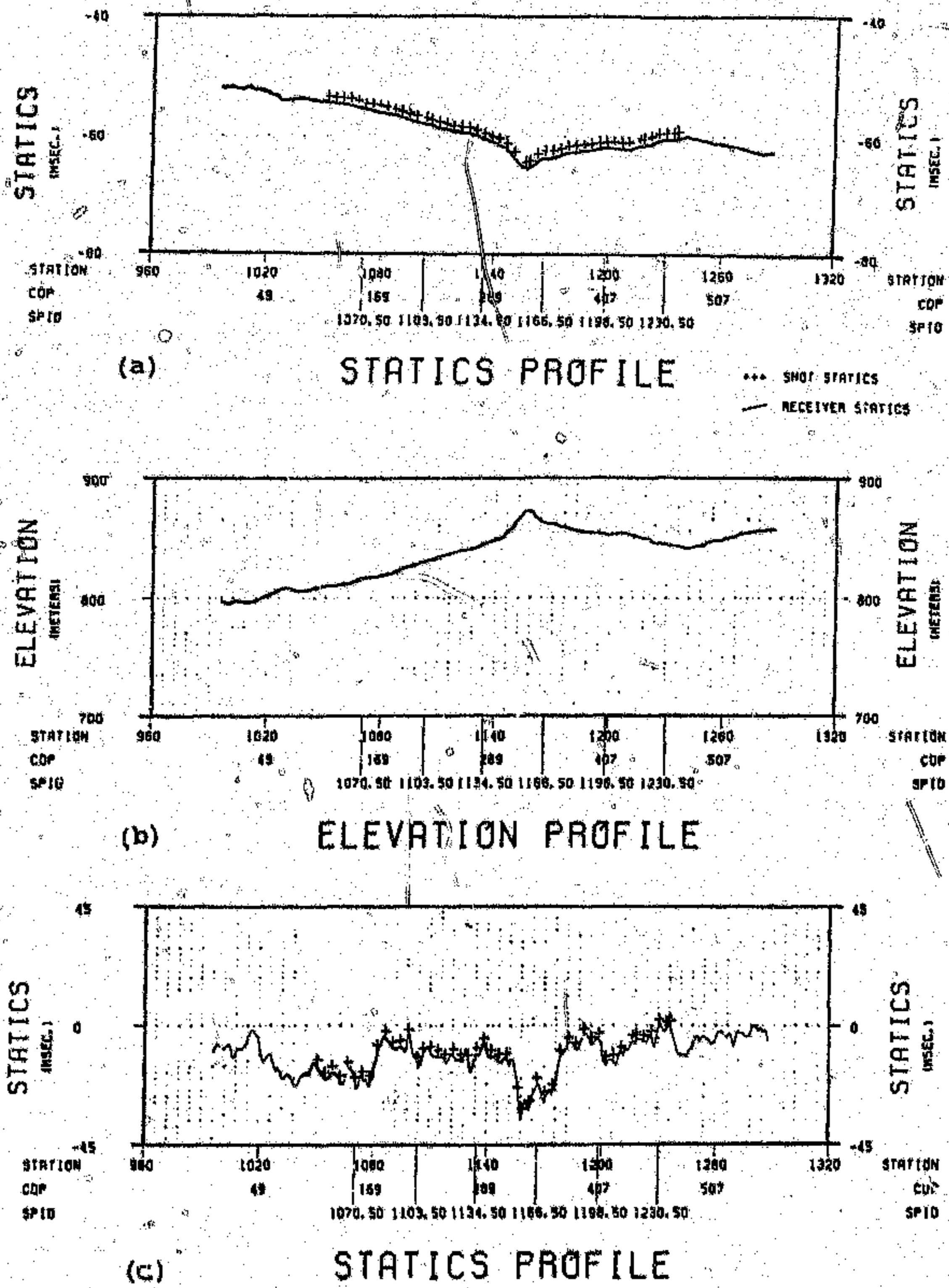

Figure 6.8 Field statics for a part of the Limpopo line calculated using a 500 m datum.

(a) Elevation statics profile. (b) Elevation profile.

(c) Weathering statics profile.

Since the elevation differences within a CMP gather were small, and therefore so were the static corrections, data was corrected from the surface to a constant 800 m datum rather than going through an intermediate floating datum. The elevation static correction applied to all the traces moved them to an 800 m datum using a velocity of 5700 m/s calculated from the first breaks from the low velocity layer survey. The shot elevation static correction was calculated as follows -

$$\textit{shot static} = \frac{\textit{datum} - \textit{shot elevation}}{\textit{datum velocity}}$$

Field calculated weathering statics were also applied to remove the effects of variable thickness and velocity within the weathering layers.

The CMP line was calculated using wavy line processing and a bin size of 25 m. There are several bends along the line involving changes in the direction of the line of up to 30°. One of these is shown in figure 6.9 where the position of the CMP line and the midpoint locations of each trace are shown. All traces occurring within three bin widths were included (one bin width equalled 150 m). A test stack plot around a bend where traces had a wide scatter showed no difference at late times whether traces in one or three bin widths were included (figure 6.10). However there is a loss of data in the first 500 ms when only including traces within one bin width, therefore in the final stack all traces were included.

FK FILTERING

FK filtering is a kind of dip filtering since events that dip in the t-x domain can be separated in the FK domain. It is effective in removing strong coherent linear noise trains and refractions. Removal of this energy is important before applying data dependent processes such as deconvolution,

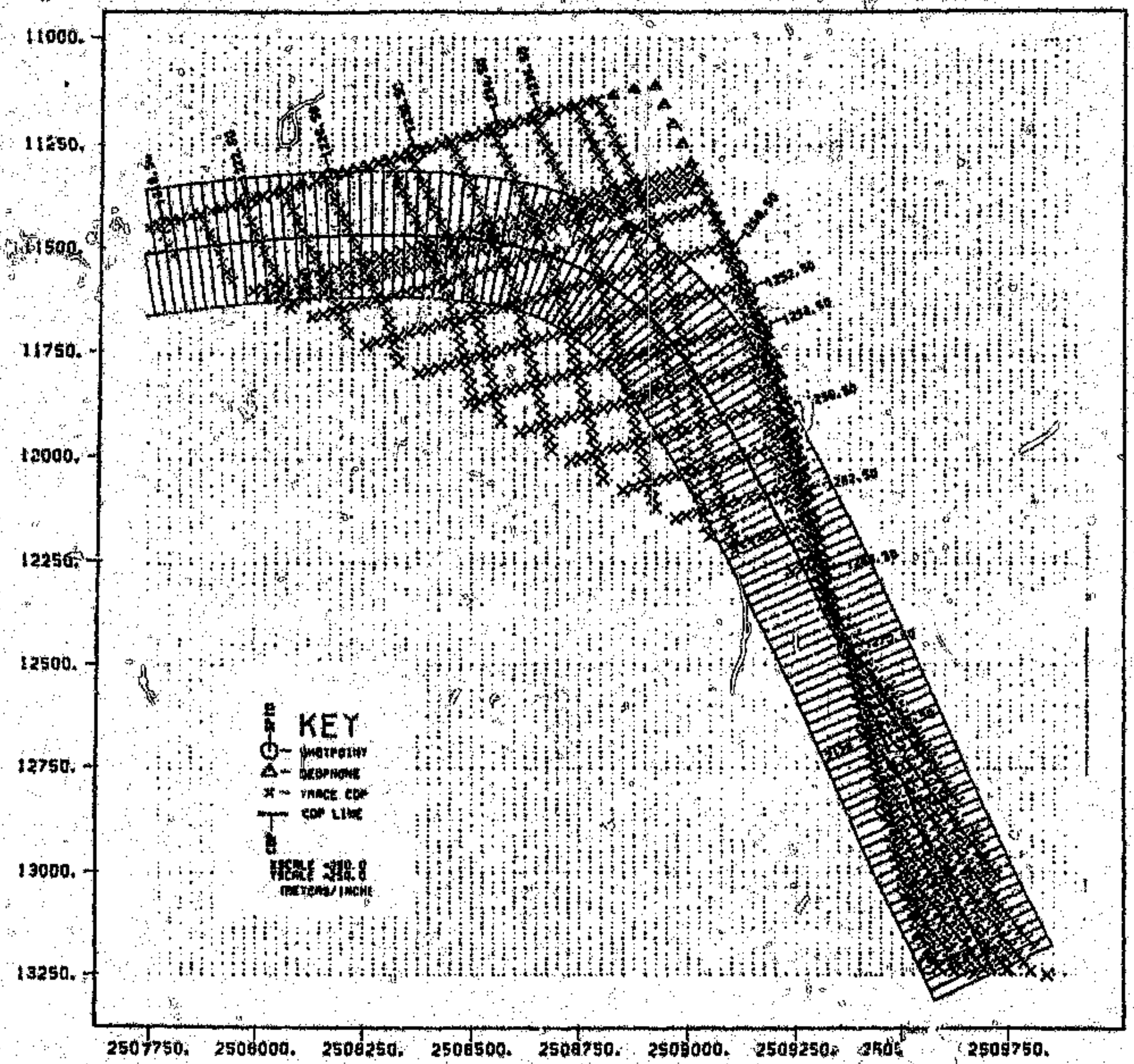

Figure 6.9 Scatter of trace midpoints and CMP line definition around a bend.

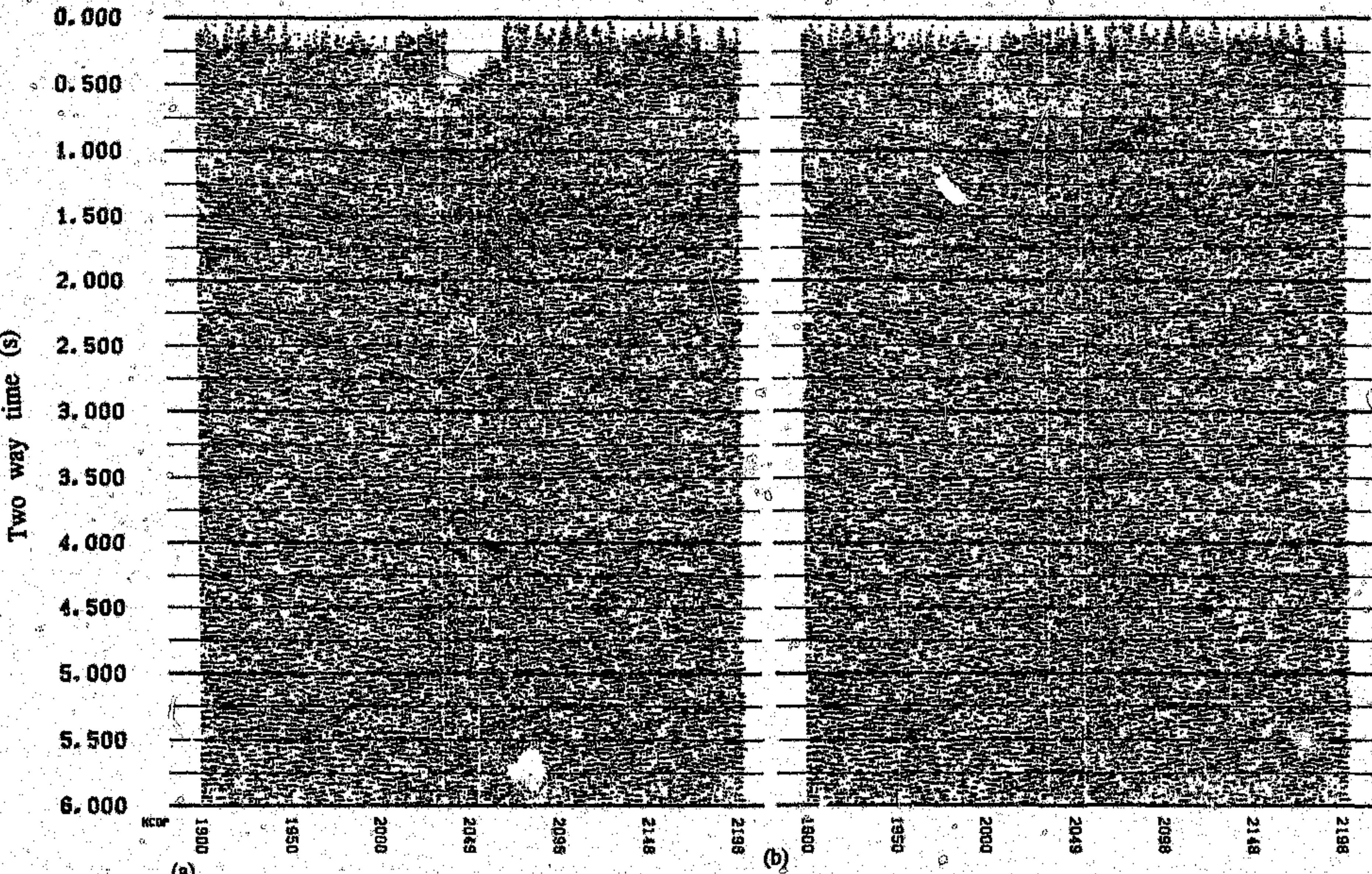

Figure 6.10 Stacked sections - (a) including traces within one bin width only and (b) all traces.

velocity analysis and residual statics (Seismograph Services course notes). Filtering in the frequency-wavenumber domain is useful for separating dipping events that cross in the time-distance domain i.e. refractions and groundroll (Sierra Geophysics, 1988).

The FK coordinates of the filter are calculated by -

$$K = \frac{F}{V} \times \textit{trace spacing}$$

where K = normalised wave number
F = frequency in Hz
V = noise velocity in m/s

In general true reflectors are concentrated around the frequency axis in the FK domain. The FK filter works by zeroing all energy in a selected zone in the FK plane and then transforming back to the t-x plane. Points considered when applying the FK filter were -

- The zone to be removed must not be too broad otherwise signal is removed as well.
- The boundaries of the filter zone must be tapered.
- Spatial aliasing occurs when the wavenumber exceeds the Nyquist wavenumber equal to 0.5 times the trace interval.
- Strong FK filtering can cause smearing of reflectors.

A field record in the FK domain before and after FK filtering is shown in figure 6.11, where the position of the refractions (with a velocity of ~6000 m/s) is clearly visible. A range of FK filter values and taper values were tested from which the final values given in table 6.2 were chosen. Parameters were chosen to pass all signal rather than suppress all noise.

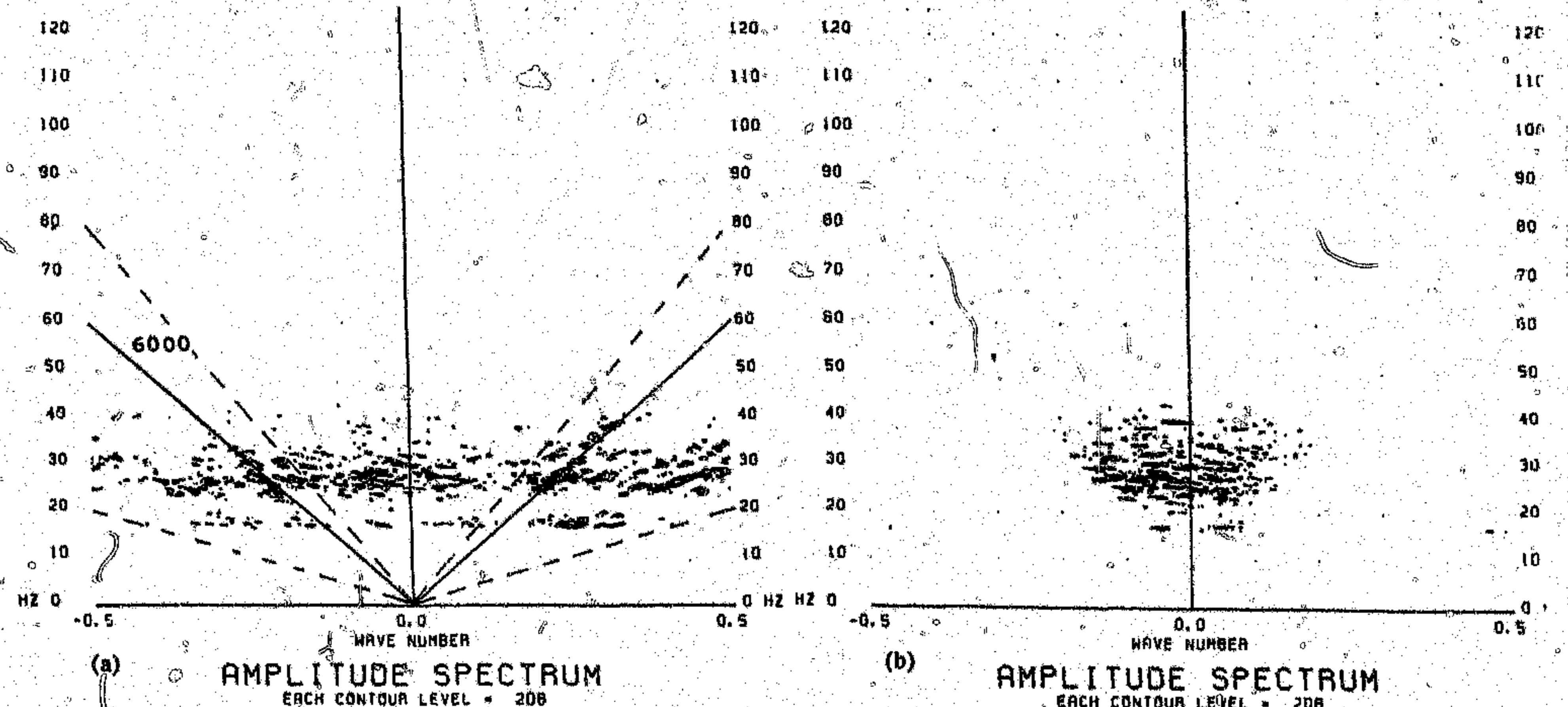

Figure 6.11 2-D Fourier transform of data (a) before and (b) after FK filtering. The position of the filtered area is shown as well as 6000 m/s refractions.

DECONVOLUTION

Deconvolution is a process applied to seismic data to improve temporal resolution and remove multiples. This is achieved by reshaping the wave form by removing the unwanted periodic parts and compressing the basic seismic wavelet. It also equalises the frequency content of the data.

Basic deconvolution theory is based on several assumptions - (Yilmaz, 1987)

- The earth is made up of horizontal layers of constant velocity.
- The source generates a compressional plane wave that impinges on layer boundaries at normal incidence so that no shear waves are generated.
- The source wave form is stationary i.e. it does not change with time.
- ~~The noise component is zero.~~
- The seismic wavelet is minimum phase and therefore so is its inverse.
- Earth reflectivity is random, therefore the seismic trace has seismic wavelet characteristics since their autocorrelations and amplitude spectra are similar. Therefore the autocorrelation of the wavelet can be estimated by computing the autocorrelation of a portion of the trace.

A vibroseis generated seismic trace can be modelled as

$$x(t) = s(t) * w(t) * e(t)$$

where $x(t)$ = recorded seismic trace

$s(t)$ = sweep signal

$w(t)$ = seismic wavelet

$e(t)$ = earth's impulse response

The basic assumptions of a minimum phase wavelet and a stationary source wavelet are violated for Vibroseis data. The problem of non-stationarity, due to wavefront divergence and frequency attenuation with time, is partially corrected for by applying a geometric spreading function, but frequency attenuation remains a problem so that spectral flattening is more effective in the shallow part of the record than in the deeper part.

There are two basic types of deconvolution, spiking and predictive. Spiking deconvolution strives to reduce the seismic wavelet to a spike whereas in predictive deconvolution the initial part of the seismic wavelet, defined by the prediction lag, is retained. Both methods of deconvolution level the amplitudes of all frequencies in the spectrum (figure 6.12). However, this is not always desirable since signal frequencies are concentrated in the lower part of the spectrum. After deconvolution the noise at the upper end is raised so the signal to noise ratio is decreased. This can be improved by post deconvolution filtering.

Three main parameters are necessary when applying deconvolution. These are generally chosen visually by keeping two constant and varying the third. The parameters are -

(a) operator length
(b) prediction lag and
(c) percentage pre-whitening.

(a) Operator length
The operator length is selected from the autocorrelation of the unknown wavelet. Assuming a stationary wavelet and an infinite random reflection series, this is the same as the autocorrelation of the seismic trace. The autocorrelation of the wavelet is estimated from the autocorrelation of a portion of the seismic trace. The part of the trace chosen should be at least 8 times the predictive lag and contain good reflections. For suppressing reverberations the operator length must be greater than the period of

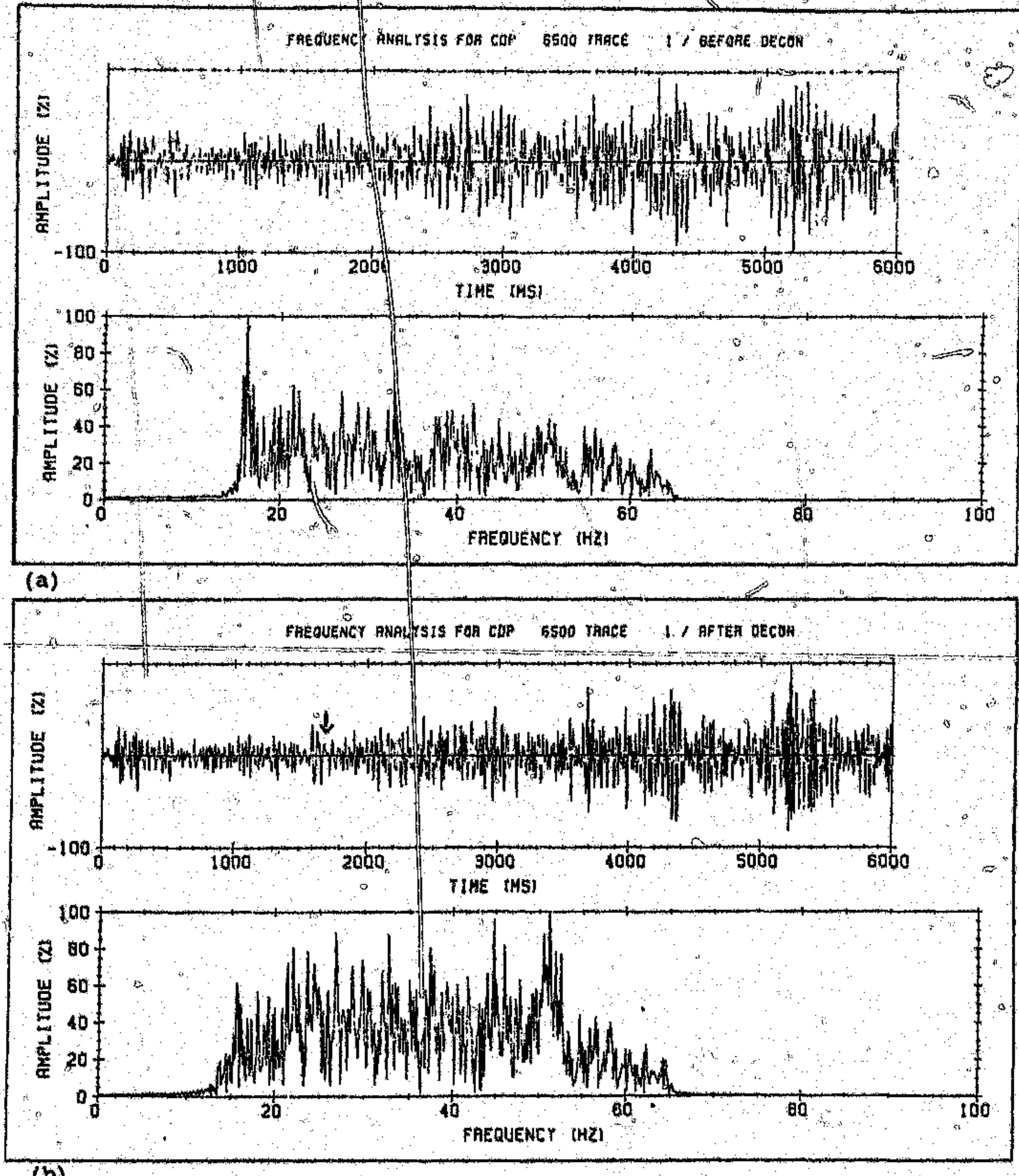

Figure 6.12 Frequency spectrum and amplitude plot (a) before and (b) after deconvolution.

repetition and for compressing the wave form it should be at least two zero crossings of the autocorrelation.

(b) Prediction lag
Spiking deconvolution is achieved using a prediction lag equal to the sampling rate. Using a prediction lag greater than the sampling rate yields a wavelet of finite length. Increasing the prediction lag limits the frequency bandwidth of the output spectra as well as decreasing resolution. Ideally it should be one or two zero crossings of the autocorrelation of the seismic wavelet, because if longer, it limits the low frequency end of the spectrum as well as the high frequency end.

(c) Percentage pre-whitening
White noise is added to the spectra to ensure stability when the matrix is inverted in the time domain for the autocorrelation. In the frequency domain this is the equivalent of adding a constant to each frequency so division by zero does not occur. The effect of increasing the percentage pre-whitening is similar to increasing the prediction lag i.e. the frequency spectrum becomes less broad band with increased pre-whitening. Therefore it is preferable to vary prediction lag and use only a small percentage pre-whitening to ensure matrix stability.

In figure 6.12 it can be seen from the frequency spectrum plot that after deconvolution the amplitude of all frequencies has been raised. In the amplitude/time plot, the wavelet at 1700 ms can be seen to have been sharpened after deconvolution.

NORMAL MOVEOUT CORRECTION AND MUTING

The traveltime curve as a function of offset for horizontal constant velocity layers approximates a hyperbola. The time difference between offsets is known as normal moveout (NMO). Before NMO correction, reflections in a CMP gather are misaligned because each trace has a different shot-receiver distance. These reflections must be correctly aligned before stacking. The general form of the NMO correction equation is -

$$T_x = (T_0^2 + \frac{x^2}{V^2})^{\frac{1}{2}}$$

where T_x is the time at offset x

T_0 is the time at zero offset

X is the offset of the trace

V is the RMS velocity at time T

The velocity used is referred to as the RMS velocity, but is really the velocity which gives the best data correction and stack, and does not necessarily have a precise physical meaning. The velocities used in the NMO equation are chosen from separate analyses performed at regular intervals along the line. Velocity analyses were performed using a multi-velocity stack processor where repeated stacks of the same 40 CMP's are displayed using a range of stacking velocities varying from 4000 to 8000 m/s. From the display, time-velocity pairs are chosen which give the best stack i.e. high amplitude, sharply resolved reflectors. Velocity analyses were done at 5 km intervals and at 2 km intervals in areas of complex structure and good data. A sample velocity analysis plot is shown in figure 6.13 with the velocity picks shown. Finally a velocity contour plot was produced to check whether the velocity-time functions chosen were reasonable.

The NMO correction is an upward shift of the trace which decreases with increasing time. This results in data stretching which is most severe at shallow times and large shot-receiver offsets. This distortion of the data is removed using a front-end mute. A front-end mute zeroes the shallow data on

Figure 6.13 Constant velocity stacks using velocities ranging from 4000 m/s 8000 m/s incrementing by 100 m/s.

each trace in a selected time window which varies with offset. In this way refractions can be excluded as well as stretch produced by the NMO correction. The end of the mute zone is tapered into the data zone to minimise edge effects that would be produced by a sharp cutoff.

The mute function is chosen by displaying a selection of CMP data stacked from single fold through full fold. Then the offsets can be identified at which stretching becomes apparent. An example of a mute test is shown in figure 6.14. The first panel includes traces with offsets up to 325 m. On the second panel traces with offsets 175 to 525 m are summed etc., until the last panel which is the sum of all traces with offsets 175 to 2525 m. Stretching becomes apparent in the first 100 ms at offsets greater than 525 m. The reflection at 170 ms becomes indistinct at offsets greater than 725 m so offsets greater than this were zeroed at times less than 170 ms. Similarly the reflector at 420 ms deteriorates at offsets greater than 1725 m. By 700 ms all offsets contribute meaningful data so muting ceased after 700 ms in this instance.

Mute tests were done at 1000 CMP intervals for the Limpopo data set. The severity of the mute applied depends on the signal to noise ratio. Where this is poor it is preferable to let some of the stretch zone in to maximise the data, since a filter will remove the low frequency stretch. After muting traces at long offsets and shallow depths, the fold of stack varies down the record. A trace amplitude balancing operator is applied to correct for variations in amplitude caused by variations in fold down the record.

RESIDUAL STATICS

Residual statics are the time variations remaining in the data due to near surface irregularities not accounted for by the weathering layer(s) and elevation statics. The Limpopo line is characterised by short, discontinuous reflections. Therefore it was hoped that careful calculation and application of residual statics would improve the continuity of the data. With this aim in

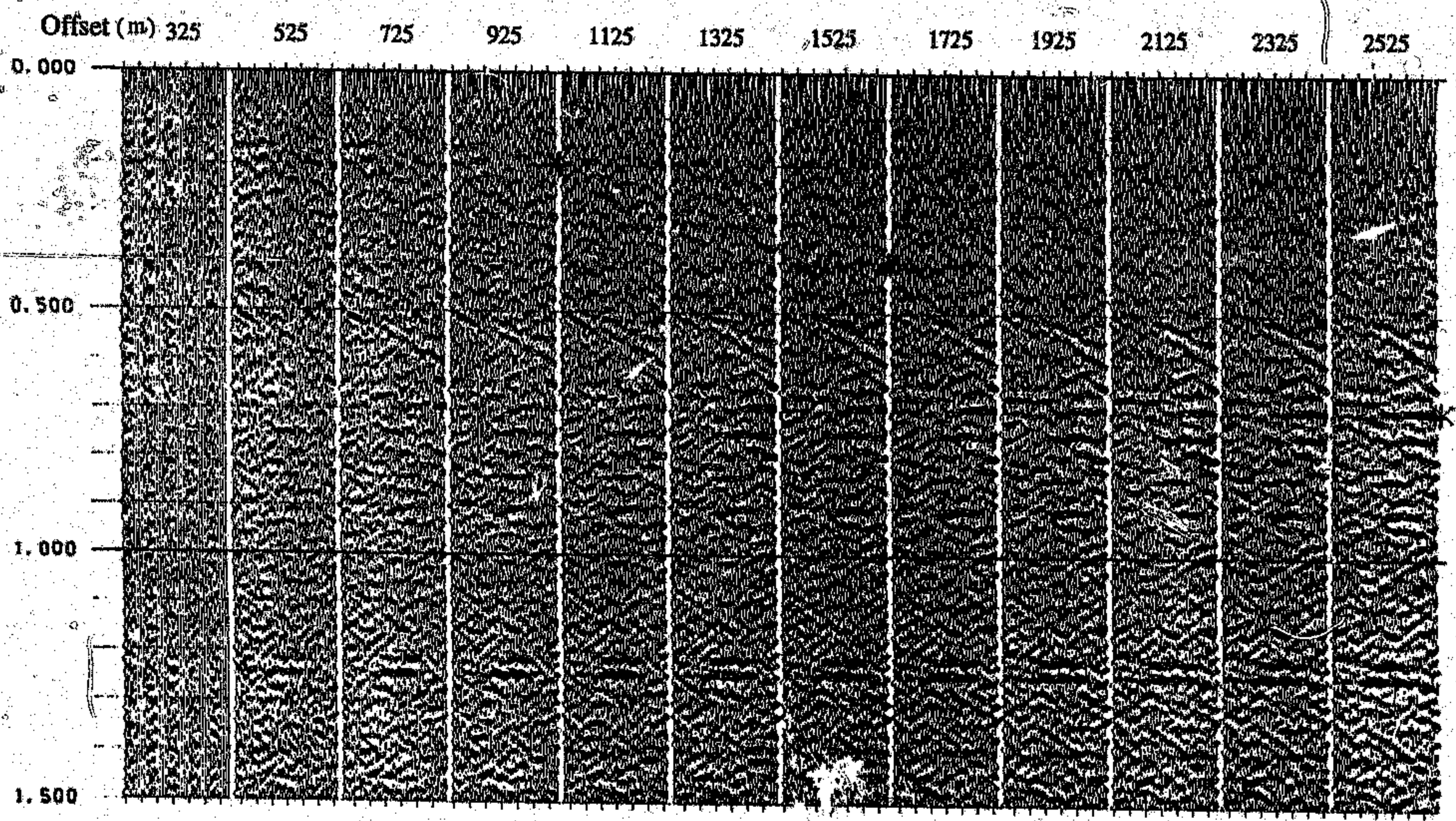

Figure 6.14 Stacked mute test for CMP's 6624 - 6663. Panels displayed are 1 fold through 12 fold stacked data.

mind, numerous different parameters values and combinations were tested. The results, however were disappointing.

The calculation of residual static corrections is performed in three parts -

(a) picking non-surface consistent residuals
(b) decomposition of these values into source, receiver, residual NMO and CMP components
(c) application of residuals

(a) Picking non-surface consistent residuals

The picking of these statics is entirely automatic. A reference stacked section is produced using the best current parameters. Then each trace in a CMP gather is correlated with the corresponding pilot trace in the reference section to determine a time shift for each trace. Parameters involved in the estimation are -

(i) normalisation of the amplitudes of the input trace
(ii) correlation window, position and length
(iii) correlation length output (maximum static)
(iv) basis of cross-correlation pick i.e. maximum peak or peak closest to zero lag

(i) Normalisation of amplitudes

Cross-correlations were calculated using true amplitudes.

(ii) Correlation window

The choice of correlation window is important where the signal to noise ratio is poor. Tests were done using different lengths and positions for the window. Ideally the window should begin below the mute zone and be long enough to include sufficient worthwhile data. The position of the window may be varied to include a strong reflection and follow structure.

(iii) Correlation length

The length of the cross-correlation output limits the value for the maximum allowable static shift. The value should be small enough so that cycle skips do not occur. This is more important where a long correlation window is used. It should also be large enough to be able to correct for the sum of shot, receiver, NMO and CMP statics.

(iv) Pick point

Tests were done using the maximum peak and the peak closest to zero lag. There was no apparent difference in the quality of the stack.

Several tests were done using different combinations of the above parameters. There seemed to be no real difference between the resultant stacks, indicating that either the signal to noise ratio of the data was too poor or the residuals program used was not optimum for the data. Figure 6.15 shows the same stack with and without the application of residuals. Reflections A (1200 ms) and B (1250 ms) have been enhanced by the application of residuals, as has the quality of reflections in the first 1000 ms, however the quality of reflections C (2250 ms) and D (4500 ms) has deteriorated. This illustrates the difficulty in choosing parameters for picking residuals when looking at a lot (12 s) of data. So as not to bias the residuals towards either the shallow or deep data, a wide window (4000 ms) was used which included most of the good quality data, but began below the mute zone (500 ms).

(b) Decomposition into individual components

The non-surface consistent residuals are decomposed into shot static, receiver static, CMP static and NMO static and an error term using the least squares method. An iterative procedure is used to solve for the individual components. The number of iterations was chosen to be 15 and the source and receiver components were calculated separately.

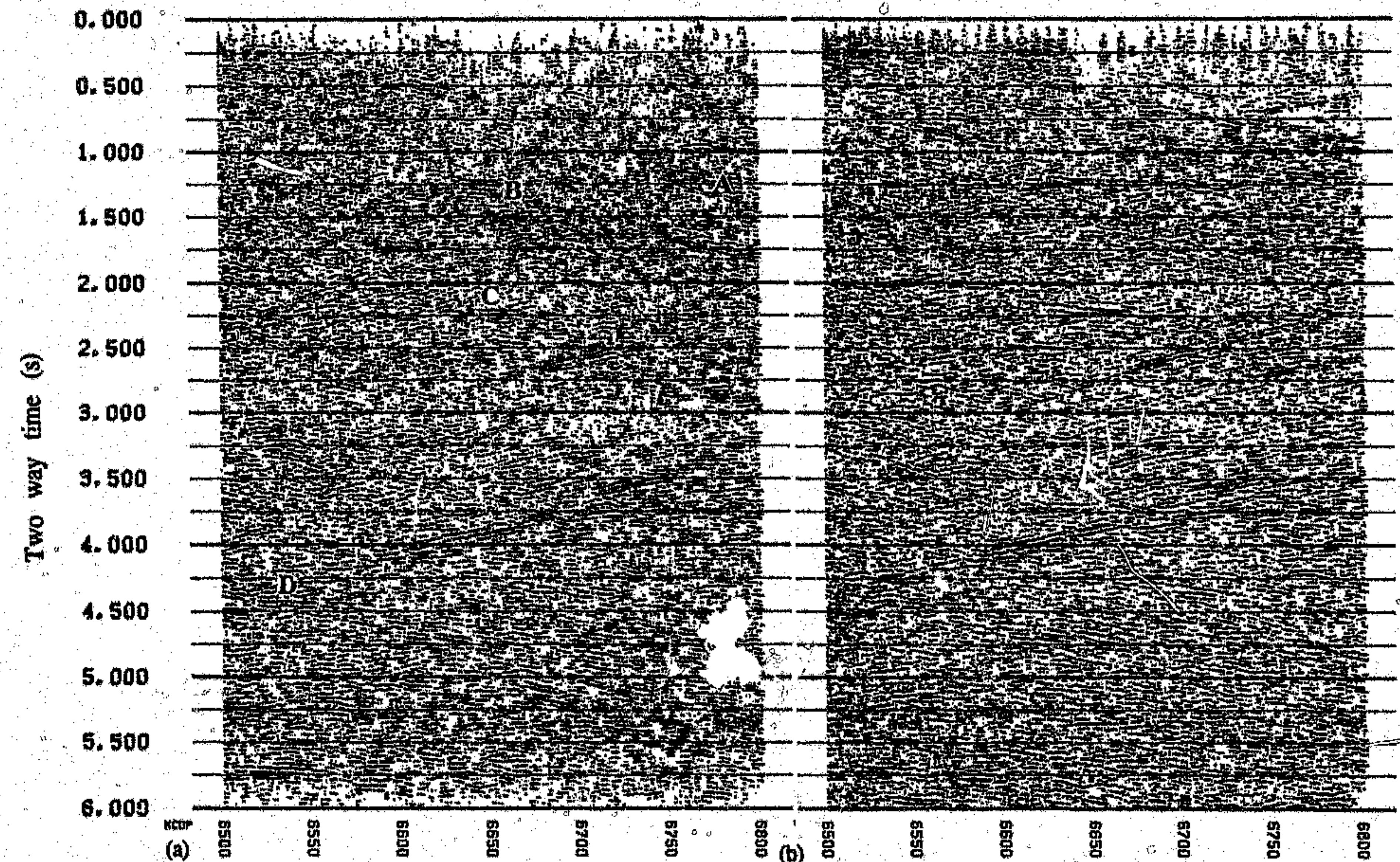

Figure 6.15 Stacked sections (a) before and (b) after the application of residual static corrections. Letters A - D are discussed in the text.

(c) Application of statics

A single pass of statics was applied to the traces. The quality of the velocity analyses depend on the quality of the statics. Removal of residual statics improves the quality of the velocity analyses, but good data are required to produce good residual estimations. Therefore the estimation of residuals and velocity analyses is an iterative process. Where data quality is poor, as is the case with the Limpopo data, further iterations did not make much improvement. Therefore residual statics were only calculated once; but two runs of velocity analyses were done.

STACKING

Common midpoint (CMP) stacking, where traces which have a common midpoint between source and receiver locations are combined after correcting for normal moveout, is the most effective method of improving the signal to noise ratio of seismic data. The effectiveness of the CMP stack depends on having approximately flat lying reflectors, since smearing occurs if reflection surfaces depart significantly from the horizontal. The stacked section is also degraded by near-surface complexities which generate residual static problems. Goleby et al. (1990) used various stacking techniques to emphasise different attributes of the data. Following their example a test section of the Limpopo line was stacked using a variety of stacking techniques, including normal CMP stacking using different normalising scalar values and a median stack.

Median Stacking

In the median stacking routine, the central population of the data is stacked, so completely removing portions of a trace or an entire trace where the amplitudes vary significantly from the rest of the amplitudes of the same CMP gather. In this way it can be used to eliminate high amplitude noise from a stacked seismic section. The user chooses the percentage of the maximum fold to use in the stack. The final fold of the stack is reduced, and the improvement in the data quality was not great, possibly due to extensive editing earlier in the processing sequence. Also the normalisation of amplitudes after stacking was not always effective resulting in an unbalanced section, so this processor was not used to produce the final section.

Conventional Stacking

Samples for all traces in a CMP gather are summed at each sample position. In order to restore the correct amplitude to the trace after summation, especially in the mute zone, each sample is normalised by a scalar. The value of the scalar is calculated as n, the number of live traces at the sample position, raised to a power p, where p is less than or equal to 1. In areas of good signal a value of $p=1$ can be used. But in areas where the signal to noise ratio is low, a value of $p=0.5$ or less should be used. For the test section the signal to noise ratio was low so a value of 0.5 was used. A stacked section using $p=1$ is dominated by high frequency noise. Two nth root stacking routines were tested-

ROOTN where the normalising scalar at each sample was $n^{-0.5}$.

RTWON stack calculated the normalising scalar by $(2n-1)^{-0.5}$.

Goleby et al. (1990) reported a decrease in background noise and suppression of noise spikes when an nth root stack was used. However no significant difference was noted between ROOTN and RTWON stacks, the final stack used was ROOTN. Figure 6.16 illustrates the RTWON and median stacks and the ROOTN stack is shown in figure 6.15.a.

TIME VARIANT FREQUENCY FILTERING

The frequency range of seismic reflected energy generally decreases with time. Certain processes such as deconvolution introduce high frequency noise. For this reason a time variant bandpass filter is applied to the data late in the processing sequence.

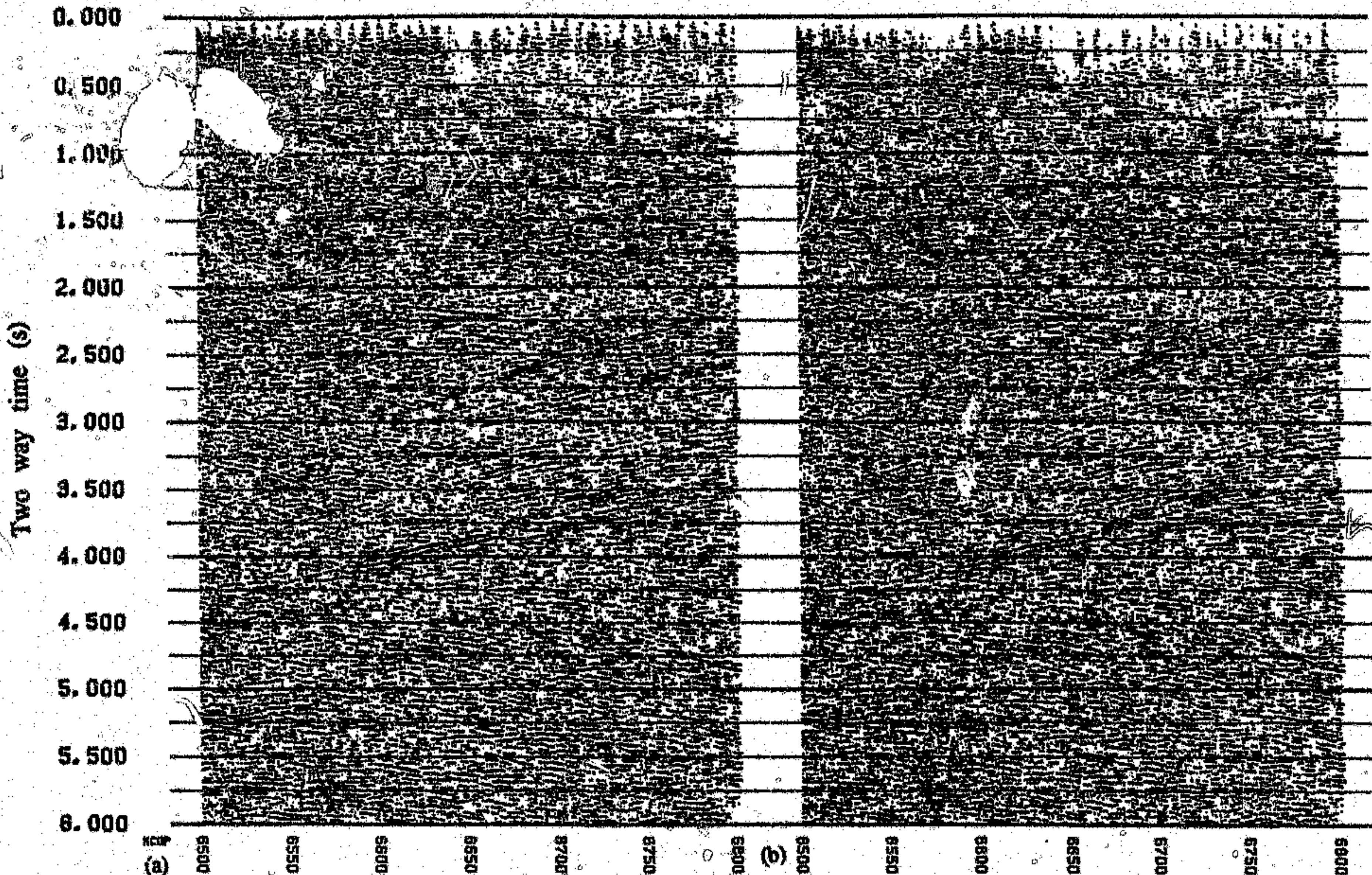

Figure 6.16 (a) RTWON stack. (b) Median stack.

The filter was designed with at least two octaves between the upper and lower bandpass limits and at least half an octave between the bandpass point and its corresponding cutoff point. Filter parameters were chosen by applying a number of bandpass filters to a stacked section. In the first test the low cutoff was kept constant at 15 Hz and the high cutoff varied from 65 Hz to 35 Hz in steps of 5 Hz. In the second test the high cutoff was kept constant and the low cutoff varied from 10 to 30 Hz in steps of 5 Hz. From the tests it is possible to identify the approximate frequency content of the reflections of interest. The filter parameters can be chosen to include as much as possible of the frequency range of the desired reflections while excluding frequencies which contain mainly noise. The final filter chosen from these tests is given in table 6.2.

POST STACK SCALING

An exponential gain function of 2.5 was applied to the data in order to further enhance the high amplitude events. A trace amplitude balancing processor calculated over a window of 1000 ms and 60 % application was also applied.

MIGRATION

Migration is a process whereby dipping reflections are moved to their 'correct' subsurface positions. Reflections are moved in an updip direction and the angle of dip is increased. The length of the reflection is decreased. A deeper event is displaced more than a shallow reflection by migration. Diffractions are collapsed back to points when correctly migrated. Steep synclines appear as 'bowties' on an unmigrated section, after migration the structure is broadened. Anticlines are compressed during migration.

The quality of a migrated section depends on -

- the migration algorithm
- how closely the stacked section approximates a zero offset section
- the signal to noise ratio
- migration velocity
- whether events come from only within the plane of the section

After migration the noise is reduced and changed in character. Random noise is suppressed whereas coherent noise is migrated as though it were data. This is the cause of 'smiles' at the bottom of the section. The amount of movement, i.e. change in x, t and θ, after migration is a function of velocity squared. Therefore the percentage error in velocity results in twice the percentage error in displacement (Yilmaz, 1987). Therefore the choice of velocity is very important. There is no difference between stacking and migration velocities in a horizontally layered medium, but for dipping reflections, migration velocity is independent of dip and stacking velocity is sensitive to dip (Yilmaz and Chambers, 1984). The velocity used for migration is therefore some function of the stacking velocity. One indication of when the correct velocity is chosen is when diffractions are migrated back to foci.

The migration algorithms are based on the scalar wave equation and treat all energy (noise, multiples and primary reflections) on the seismic section in the same manner. Two different migration algorithms were used, a finite-difference method and the FK method. Results from the two were very similar, however the finite-difference method takes six times longer to run. Therefore the data was migrated using the FK method.

The FK method involves a two dimensional double Fourier transformation of the t-x data. To prevent edge effects the data is padded in time and space using zero traces and adding zeroes to the end of the traces. The algorithm is based on a constant velocity field. This is achieved by stretching the time axis by applying a stretch factor of between 0 and 2. A value of 1 keeps the velocity constant and best results come from using a value of 0.5 (Yilmaz, 1987). The practical use of the FK migration involves a time to depth conversion which results in the frequency content of the data being altered and improper migration from incorrect lateral velocity variations (Stolt, 1978).

Warner (1987) reported on the difficulty of migrating deep data and in selecting the correct migration velocity. Results indicated that deep data appeared to be migrated best at velocities up to 50 % less than stacking velocities. A panel of data was migrated using percentages ranging from 70 to 90 % of stacking velocities. The final line was migrated using 80 % of the smoothed stacking velocities.

SEISMIC SIGNAL DETECTION FILTERING

Due to the low signal to noise ratio of the data, it was decided to pass a panel of the reflection section through a seismic signal detection filter, in order to aid interpretation. A programme to do the filtering was written by G. Cooper of the University of the Witwatersrand based on the work by Hansen et al. (1988).

The signal detection filter is based on statistical hypothesis testing (the sign test statistic) and the performance of the filter can be quantified i.e. it is possible to calculate the number of noise-only segments it will pass, depending on the filter parameters. The filter is designed to detect spatially linear signals of allowable slowness (dips) in noisy stacked seismic data. The effect is to suppress spatially incoherent events (noise) so that events visible on the input section become more obvious.

Filter parameters are set to determine what is designated signal. The parameters include -

- w - the window length, which is the number of traces over which the signals must exhibit phase coherence.
- t - threshold of significance, a window containing t or more positive amplitudes is designated signal.

Noise is assumed to be identically and symmetrically distributed about zero. The filter is applied along various slowness/dip lines in the stacked section using various window lengths.

The signal detector is passed over the stacked seismic section and another 2D array (the multiplier array) is produced. This array contains a one if a signal was detected at the same point on the seismic section and a zero if no signal was detected. The final step is the production of a final filtered section by the multiplication of the input stack with the multiplier array. Therefore the filtered section contains amplitude and signal information.

Application of the seismic signal detector to the Limpopo reflection seismic line removed much of the noise and passed most signal visible on the input section. But the signal remains very limited and the end result could not improve the interpretation. A test section of the line after the application of the signal detection filter is shown in figure 6.17.

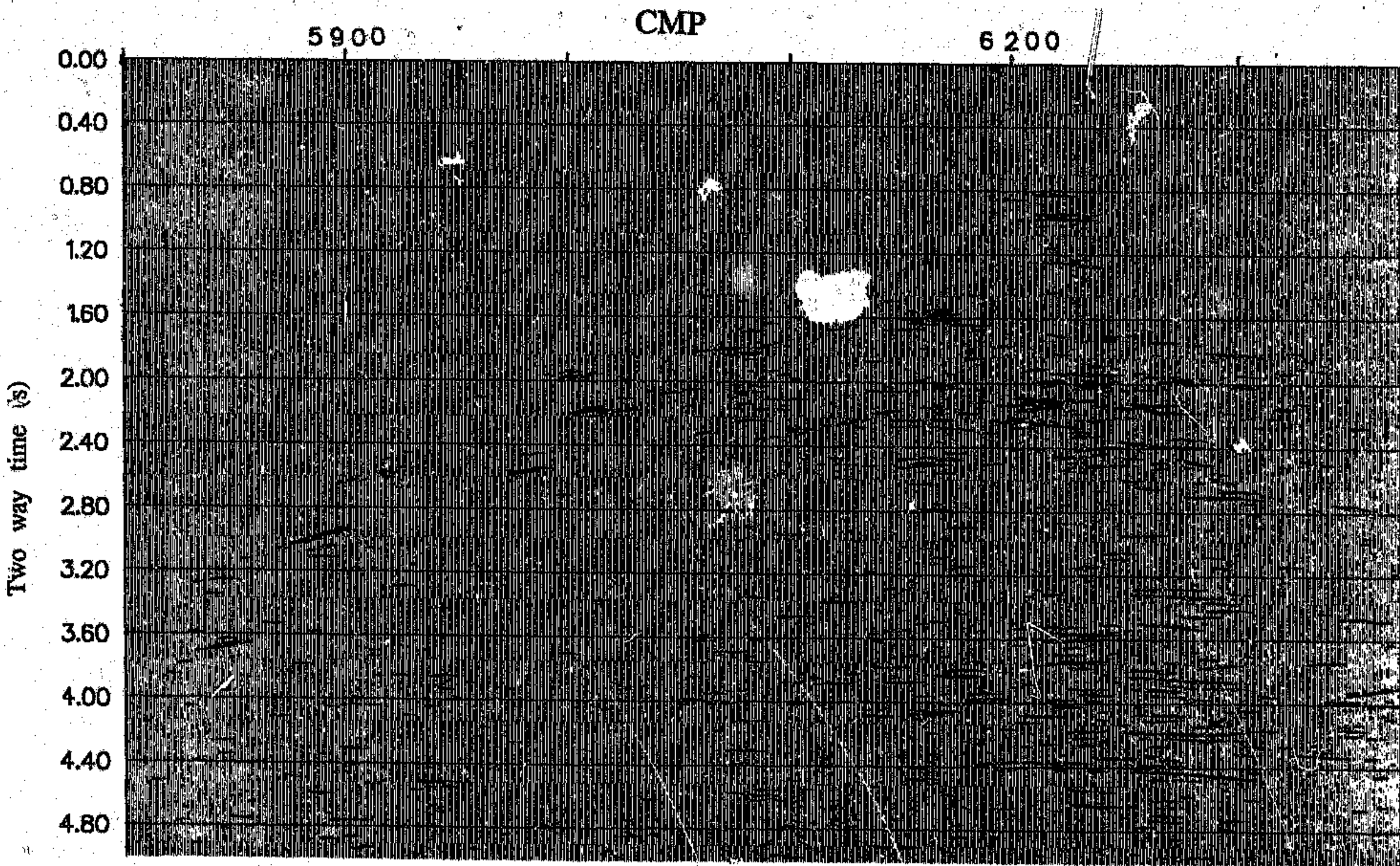

Figure 6.17 Unmigrated reflection seismic section after the applicati.. of the signal detection filter. CMP 5800-6400.

6.2 Seismic Interpretation

Origin of reflections

Seismic reflection occurs at an interface, structural or compositional, between two media having contrasting acoustic impedances. Acoustic impedance is calculated as the product of density and seismic velocity and is dependent on rock properties, such as mineral composition, porosity, fluid content etc. Whether a particular terrane appears reflective depends on a number of factors, including - surface recording conditions, presence of compositionally varying layers or fault zones, the attitude of the reflecting interfaces and complexity of the structure (Green et al., 1990). The amplitude of the reflection depends on the difference in acoustic impedance across the boundary, the geometry of the wave path and attenuation effects along the wave path (Brewer and Oliver, 1980).

Geologic possibilities for crustal reflections include primary lithological layering, metamorphic layering, tectonically imposed layering including unconformities and shear zones, physical properties of the rocks e.g. fluid content or fluid rich horizons not controlled by rock type or structure (Hatcher, 1986; Green et al., 1990; Klemperer et al., 1987). Compositional variations must be of a scale large enough to produce reflections. Migmatites which form a major portion of the middle crust are layered on too small a scale to produce reflections. Large amplitude reflections can be produced by layers of alternating high and low velocity material as found in metamorphic rocks (Hurich and Smithson, 1987). Reflections from fault zones are only observed directly if the fault plane dips at a low enough angle ($<30°$) and a sufficient impedance contrast exists across the boundary, or if the fabric created within the fault plane (e.g. mylonite), has an impedance contrast (Blundell, 1990). Reflections from known faults are generally complex and discontinuous, indicating that faults are not generally seen as a single layer. Most faults seem to be confined to the upper crust.

Deep seismic sections can be characterised by recurring reflection patterns, each possibly related to a particular geology (Hatcher, 1986; Gibbs, 1986).

(i) Layered subhorizontal reflections

These may be produced by alternating layers of silicic and gabbroic igneous rocks. They also identify sedimentary basins. Stratified relatively continuous upper crustal reflections are typical of Precambrian continental sedimentary basins. Single continuous reflections may result from large crystalline thrust sheets. Subhorizontal reflections are also produced by detachment faults. Broad deformation zones produce laminated reflections.

(ii) Zones of inclined and curved reflections and diffractions

A single zone of inclined reflections can result from a planar dipping fault. Gneiss terranes are characterised by complex reflections and diffractions as are the basements to continental sedimentary basins. Stacked and overlapping curved reflections identify large refolded isoclinal folds and intrusive complexes.

(iii) Seismically transparent zones

These are difficult to interpret since they may represent structurally complex or simple zones or rocks that contain no acoustic impedance. They may be associated with granitoid rocks, anorthosites and gneisses. Rocks may be rendered acoustically homogeneous in structurally complex zones. Also the scale of repetition by folding may be so small that acoustic energy is dispersed or the layering is thin compared to the seismic wavelength.

The upper crust is not usually reflective, which may be because it is dominated by brittle tectonics which produce short structures having steep dips (Matthews and Cheadle, 1986; Mooney and Brocher, 1987). Prominent reflections probably result from low angle faults or mylonite zones, highly extended terranes within core complexes and the base of exposed plutons (Klemperer et al., 1987). The deep crust is in general uniformly reflective and the many reflections result from compositionally layered gneissic rock, or may originate at lithologic boundaries and zones of mylonite (Green et al., 1990), or may originate within units from the juxtaposition of layers of different rock types, rather than originating from contacts between units (Christensen, 1989).

Problems in identifying true reflections

Complex middle and lower crustal stacked sections are characterised by numerous short reflection segments and poor signal to noise ratio - this may be a function of the complex target, or the response may be distorted by propagation effects, source generated and ambient noise and processing procedures. Results of modelling indicate that even a single undulating surface can produce a multiplicity of reflections on the record section because of reflections from out of the vertical plane of section (Blundell and Raynaud, 1986).

Clowes et al. (1983) observed that below 6 s (within the lower crust), many seismic sections show a multitude of short, coherent reflections. However not all reflections on a seismic section have geological origins, some may be true reflections, others multiples and others artifacts of the processing sequence. Most reflections on seismic sections arise from superposition of individual reflecting segments from a number of closely spaced interfaces, resulting in enhancement by constructive interference and loss by destructive interference (Blundell, 1990). Constructive interference associated with geological layering is at least as important as the magnitude of the reflection coefficient for producing reflections. Similarly, reflection amplitudes larger than those predicted by reflection coefficients are the result of constructive interference.

The lateral extent of coherent reflections in the lower crust is generally between 1 and 25 km, with most being about 4 km long, which is barely

longer than the Fresnel zone (Matthews and Cheadle, 1986). The length of phase correlatable reflections is affected by residual statics, noise and degradation due to scattering in the upper crust. Crystalline rocks of the continental crust are often characterised by compositional variations or lens-shaped bodies of limited size that may act as reflectors or small-body diffractors. Discontinuous reflections could result from interference between these adjacent reflectors (Hurich and Smithson, 1987). It is important to determine the real length of a reflector on a seismic section before it can be considered a geological reality. This is determined by the first Fresnel zone defined by Yilmaz (1987) as

$$r = (v/2)(t/f)^{0.5}$$

where r = radius
v = velocity at time t
f = dominant frequency at time t

Two points falling within the first Fresnel zone are indistinguishable. Similarly r is the segment length that would result from a point reflector at depth z (equivalent to time t). Therefore a reflective lower crust may result from numerous bodies smaller than the Fresnel zone. This is illustrated by a model where events on the section do not map one-to-one with reflectors of the model, demonstrating the importance of spatial interference in generating reflective wavefields in complex terranes (Hurich and Smithson, 1987).

A further problem is where stacked images appear layered because of enhanced lateral continuity attributed to the well known dip filter inherent in the stacking process (Yilmaz, 1987). CMP stacking is applied to improve the signal to noise ratio and approximate a zero offset section. Its limits in achieving this are seen in the attenuation of dipping features and the limited horizontal resolving power of the CMP stack, since the CMP stack shows stacking smear. The dip filter effect of the stacking process is most severe for early times and large offsets (Gibson and Levander, 1990). Poststack migration cannot remove the dip filtering effects of stacking, this can only be done by prestack migration or DMO.

Results from typical crustal sections

It is impossible to describe the geometry and significance of each individual reflection on a seismic section since most reflections do not project to the surface and therefore cannot be uniquely identified. Also, as explained above, not every reflection has geological significance. Instead zones with generally similar fabric are identified. Allmendinger et al. (1987) recognised that characteristics of deep seismic reflection data across mountain belts vary in a relatively systematic way. They produced a generic seismic section for Phanerozoic orogenic belts, in which the continental crust is divided into four zones, based on seismic reflection data from the US. The Limpopo Belt seismic section exhibits several similarities with this generic section, indicating that it may be a 'fossil' mountain belt. The four zones in the generic section are :-

(i) The little deformed Precambrian craton with few real reflections in the upper third to one half of crust except for thin bands of layered reflections from Phanerozoic strata on the surface. The middle and lower crust is dominated by diffractions and various oriented dipping reflections. No high amplitude reflections mark the Moho, instead there is a gradational or marked downward decrease in reflections and diffractions at Moho traveltimes.

(ii) The orogenic foreland deformed by thin skinned thrust belt tectonics which is characterised by numerous complex reflections from deformed sedimentary strata in the upper crust, but sparse deep reflections, possibly due to poor signal penetration through complex near surface structure.

(iii) The third zone relates to compressional tectonics and is characterised by a unidirectional dipping fabric where the reflective zone extends from near surface into the lower crust, although few individual reflections can be traced that far. There are generally some reflections and diffractions dipping in the opposite direction to the general fabric.

(iv) The fourth zone is found in the foreland or hinterland of the craton in regions of magmatism, elevated geotherms or extension. The upper crust is largely transparent but the middle and lower crust consist of numerous horizontal and gently dipping reflections. A reflection Moho is commonly seen as prominent laminated and laterally discontinuous reflections with an overall thickness of 0.2 to 1 s.

Zones 1 to 3 are found in mountain belts whereas zone 4 seems more likely to occur in a rift environment. Zone 4 is not found in sections across Precambrian terranes. Thus there is an apparent difference between cratonic and orogenic fabrics where the layering in orogenic environments may be a result of time dependent processes which are no longer active on ancient cratons. Terrane boundary zones with deeply penetrating moderately dipping and imbricate reflection zones can be interpreted as collisional orogens (Gibbs, 1986). Convergent zones are characterised by a typically reflective lower crust with discrete reflections. In extensional terranes the lower crust appears highly reflective with a strongly laminated character (Mooney and Brocher, 1987).

Surface geology in Precambrian shield areas indicates a high degree of structural complexity and lithological heterogeneity, which are not ideal conditions for generating reflections (Brewer and Oliver, 1980). Several seismic surveys across Archean terranes have been carried out, including Abitibi greenstone belt (Jackson et al., 1990), COCORP Minnesota profile (Gibbs et al., 1984) in the Superior Province, the COCORP Wind River (Smithson et al., 1980) and the Montana plains (Latham et al., 1988) profiles in the Wyoming province.

Reflections on the southern Abitibi profile are attributed to Archean igneous layering and tectonic high strain. The reflection profile reveals subhorizontal reflection zones in the upper 15 km, which is contrary to the steeply dipping surface structures. The shallowest subhorizontal zone at a depth of 6 - 12 km is interpreted as the base of the greenstone supracrustal assemblage. Some steeply dipping faults present on the profile penetrate to 5-6 s, but none extend into the lower crust. This suggests that the faults are either listric and root in the subhorizontal middle crustal shear zone or may have extended deeper, but have been overprinted by later events that produced the subhorizontal fabric.

Abundant deep reflections on the Wyoming profile emphasise the heterogeneous and complex nature of the Precambrian crystalline crust. These numerous deep events of marked curvature may represent complex fold structures in the middle and lower crust. The Wind River Thrust appears as a more or less continuous reflection which can be traced to depths of 24 km with an average dip of 30° - 35°. The continuous nature of the Wind River Thrust indicates that a sufficient impedance contrast exists across the fault zone which could be caused by bands of mylonitised rocks and/or the juxtaposition of different rock types in a heterogeneous crust.

Reflections on the Minnesota profile, which crosses late Archean granite-greenstone and older Archean gneiss and granulite, are sparse and more concordant in the gneiss and granulite than in the greenstone. The profile shows numerous north to northwest dipping reflections throughout the crust, with a particularly prominent and continuous series of such events projecting to the surface near the trace of the fault zone identified as the boundary between the two zones. The presence of the numerous north dipping reflections unconnected with the main fault zone suggests that collision may have produced imbricate underthrusts. The complex disrupted seismic pattern within late Archean terranes is consistent with the conventional view of such terranes. Lower crustal reflections are also complex and laterally discontinuous. Reflections between 13 - 15 s identified as originating from the Moho are laterally discontinuous with a moderate dip.

In general regions of stable continental crust have unreflective lower crust. There seems to be a correlation between lower crustal reflectivity and the age at which the last orogenic event occurred. Wever (in Meissner, 1986) shows a general histogram for the occurrence of reflections per 1 s two way time interval, which seems to be typical for old shield areas with little recent crustal deformation. The histogram shows that the upper 2-6 s are considerably more reflective than the lower 6-20 s.

The refraction definition of the Moho is generally shown by a step function velocity boundary. However, reflections at depths predicted by the refraction Moho are laminated, laterally discontinuous packages between 0.5 and 2 s thick, indicating a thin layered rather than block structure (Hale and Thompson, 1982). The base of the layered zone correlates in general with the position of the refraction Moho (Mooney and Brocher, 1987). The seismic expression of the Moho is variable in different tectonic provinces, indicating that the Moho may have had different origins or evolution (Hurich and Smithson, 1987). The Moho also appears relatively continuous and flat beneath zones of moving crustal blocks indicating that it may postdate deformation (Brown et al., 1987).

The Moho does not generally have any reflection signature on Archean profiles. An exception is the Minnesota profile. More often the expected position of the Moho is within a seismically transparent zone, which may indicate that the Moho in these areas is a gradual velocity increase, or a highly deformed boundary, or that signal to noise ratio in these terranes is low (Brewer and Oliver, 1990).

Limpopo line interpretation

The migrated reflection seismic line is shown in figure 6.18 (back pocket). The reflection line is shown to 12 s although the data were recorded to 13 s. This is due to software limitations in processing. Using an average crustal velocity of 6.5 km/s as determined from refraction studies, a 12 s time section translates to a 39 km depth section. The 212 km north-south profile begins in the Central Zone, crosses the Southern Marginal Zone and ends south of Pietersburg on the Kaapvaal Craton. Part of the CZ and the SMZ are obscured by Karoo Sequence sediments and volcanics within the Soutpansberg trough. An interpreted line drawing of the main events (events that are laterally coherent for 1 km or more) seen on the profile is shown in figure 6.19. Two migrated panels showing important features are reproduced in figures 6.20 and 6.21.

Most reflections are concentrated in the upper 6 s on the southern end of the profile. However, there is also a highly reflective south dipping wedge on the northern edge as well as a reflective block in the upper 4 s just south of this wedge.

The northern edge of the profile is dominated by a very reflective wedge defined by reflections A-A' and B-B' on figure 6.20, which starts at surface and ends at 7 s. The first few horizontal reflections are probably due to surface sediments. The edge of the block is defined by steep southerly dipping reflections dipping at 250 ms/km ($\sim 30°$) which truncate deeper horizontal to gently north dipping reflectors. There is no surface indication of the geology of this block.

Within the Central Zone is an unusually reflective block within the top 4 s (reflections C-C' in figure 6.20). It consists of 3 southerly dipping bands of reflections which flatten out around CMP 1400 to horizontal layers extending to CMP 2000. The reflections extend from surface to 3 s, cutting surface at about CMP 800. Above and below the continuous horizontal

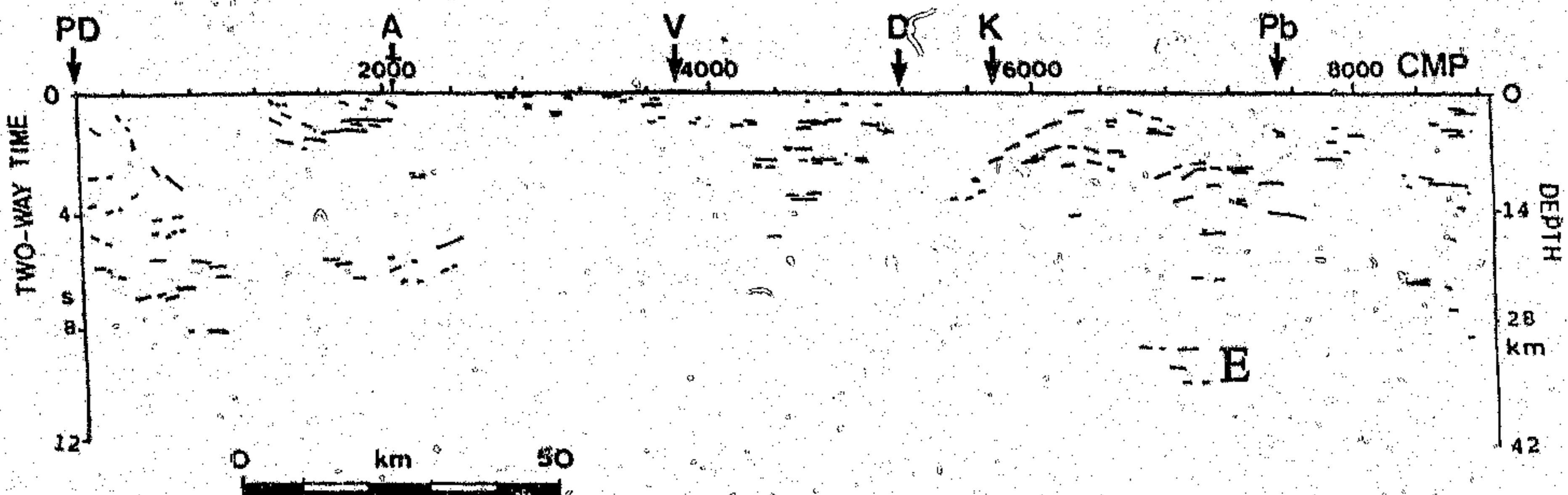

Figure 6.19 A line drawing of the migrated Limpopo seismic reflection profile showing the prominent reflections. PD - Pont Drift, A - Alldays, V - Vivo, D - Dendron, K - Kalkbank, Pb - Pietersburg.

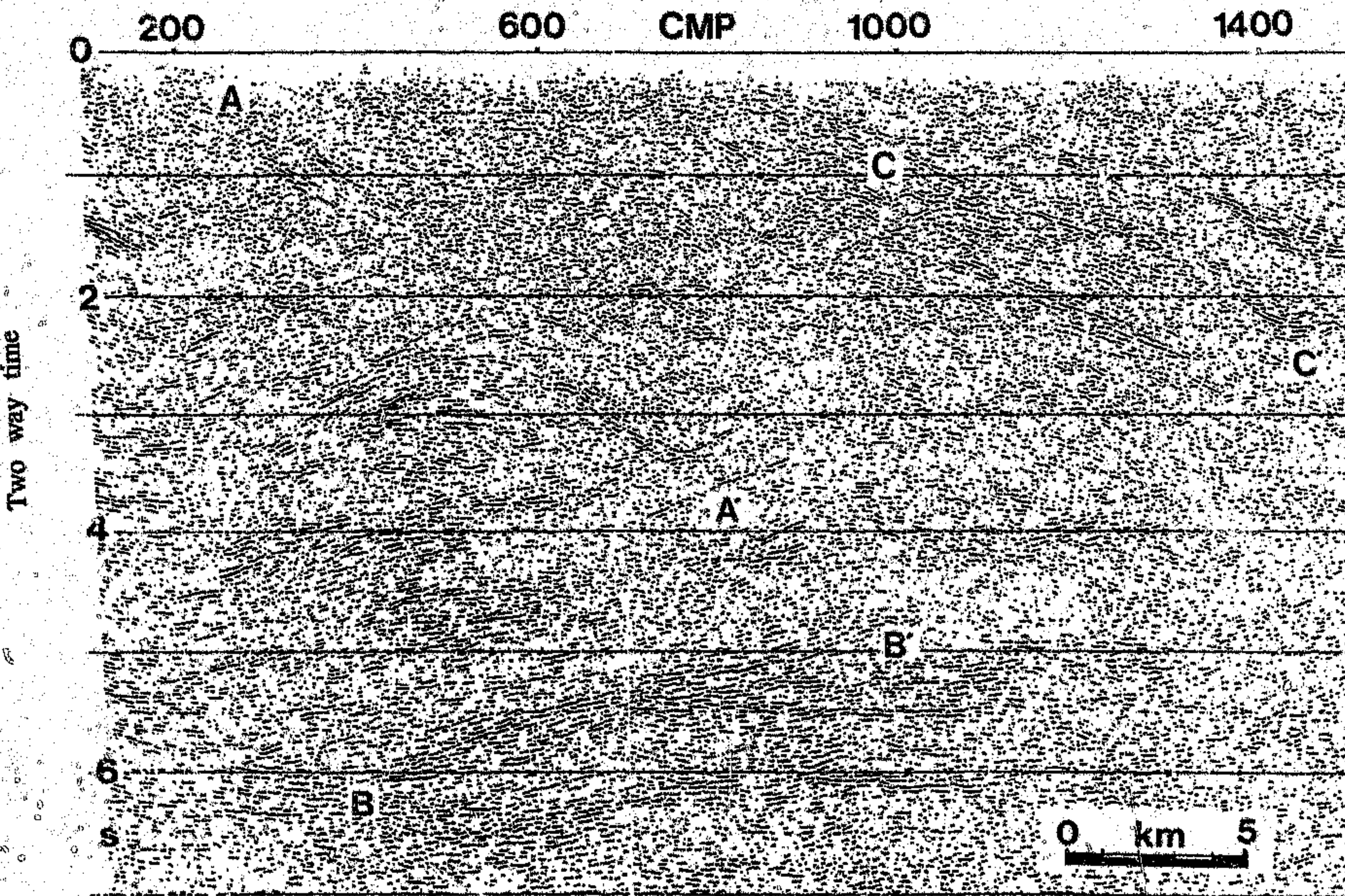

Figure 6.20 Migrated reflection seismic section, CMP 100-1500. Vertical scale is approximately the same as the horizontal scale for a crustal velocity of 6 km/s.

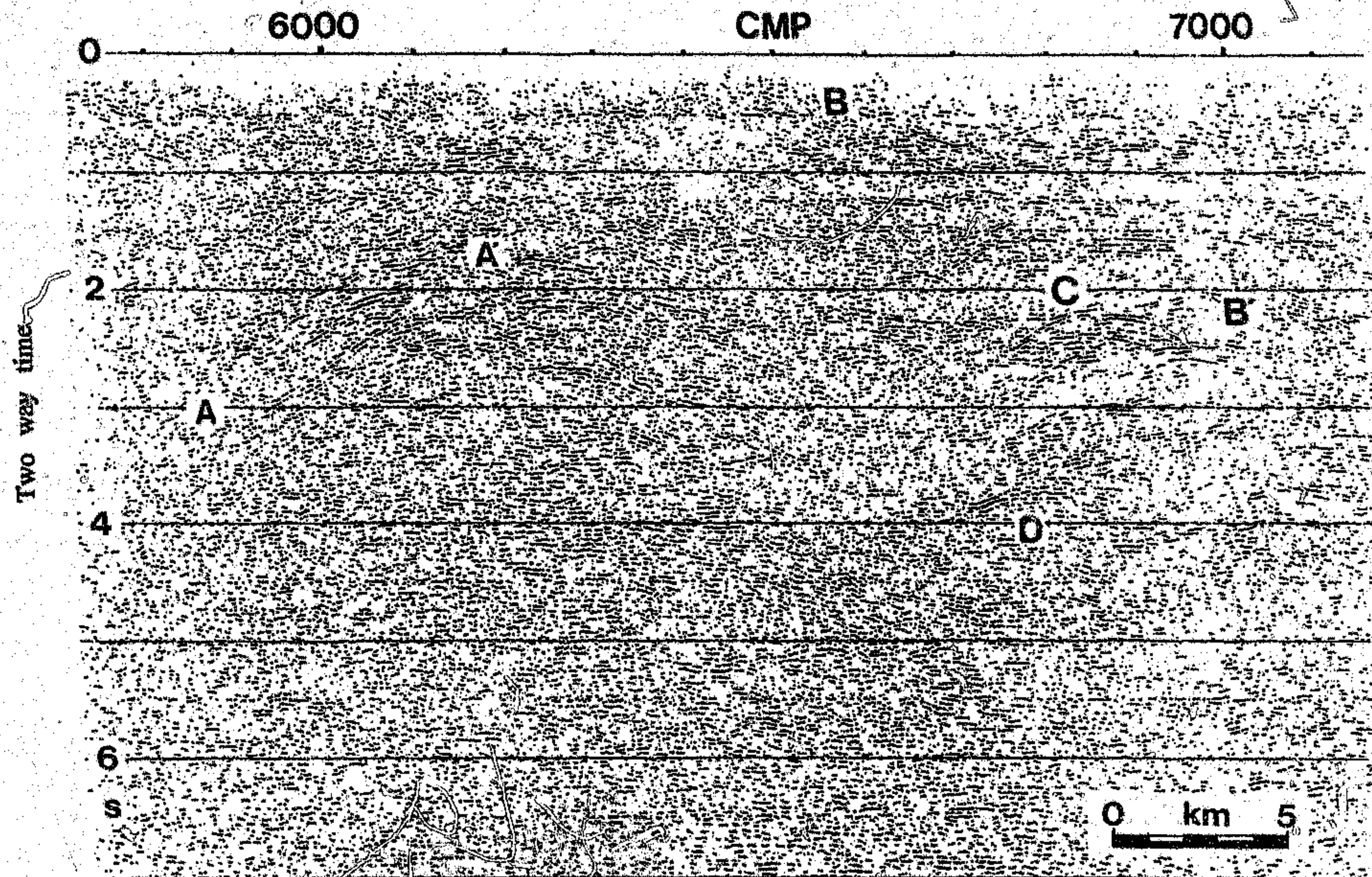

Figure 6.21 Migrated reflection seismic section, CMP 5700-7150. Vertical scale is approximately the same as the horizontal scale for a crustal velocity of 6 km/s.

reflections are shorter subhorizontal reflections. Elsewhere in the CZ the only reflections are in the Soutpansberg trough and a few upward curving reflections beneath reflections C-C'.

Sediments in the Karoo-Soutpansberg trough are evident as short horizontal reflections occurring at two way times less than 400 ms between CMP's 2600 and 3700. These reflections are not well imaged since processing was not optimum for shallow reflections as this was not the primary objective. The trough extends from CMP 2900 to CMP 3700 i.e. about 27 km wide. It has a depth extent of about 400 ms which is approximately 1.2 km. The sedimentary basin is truncated in the south by the Palala shear zone which is also the boundary of the CZ and SMZ. This fault zone has no seismic expression and its position can only be inferred from other truncated reflections. The northern boundary of the basin is a gently north dipping contact. Small faults can be recognised in the basement of the boundary (Stettler et al., in press).

Between Vivo and Dendron the SMZ is marked by several bands of short horizontal and dipping (both north and southward,) reflections concentrated above 3 s. Only isolated horizontal reflections occur below 3 s.

The probable seismic expression of the boundary between the KC and SMZ is marked by reflections A-A' (figure 6.21), the boundary dipping north from CMP 6500 at ~30° extending to 3 s. Reflections B-B' (figure 6.21) dip south at approximately 25° from CMP 6500 at surface extending to 2 s. Beneath B-B' are two dome like structures - C with its apex at 2.2 s and D, a wider dome with its apex at 3.5 s. These dipping reflections may form the compressional third zone on the generic section derived by Allmendinger et. al., 1987)

The southern part of the line, particularly south of Pietersburg, consists of numerous subhorizontal reflections from surface to 8 s with no apparent structure. Two groups of reflections, both gently dipping to the south, are found at 4 s and 8 s. These reflections occur within the KC indicating that the KC is characterised by many short horizontal reflections extending throughout the crust. Therefore the KC may be related to zone 1 on the generic section of Allmendinger et al. (1987)

There are few deep reflections which might correspond to Moho reflections. Reflections E in figure 6.19 between CMP's 6000 and 7100 occur at a depth 9 - 10.5 s which corresponds to a depth of between 32 and 37 km. The depth of the Moho on the KC is between 36 and 37 km as predicted by refraction and gravity work. Therefore these are possible Moho reflections. Most other reflections below 9 s are shorter than 2 km so cannot be considered to have significant lateral extent.

The three geological terranes traversed by the seismic line have distinct seismic signatures. The CZ is largely transparent except for a reflective block in the upper crust which may be undeformed crustal material. The SMZ and probable NMZ terranes are characterised by numerous short, horizontal to gently dipping reflections in the upper 6 s, except beneath the Soutpansberg trough. This lack of reflections may be due to the sediments absorbing all energy. This reflection pattern is in accordance with that described by Gibbs (1986) for granulite and gneiss terranes. The granite-greenstone terrane of the KC is the most reflective, with reflections visible down to 11 s. Large scale dome structures are visible at mid-crustal levels as well as sub-horizontal reflections in the upper 2 s which may be related to thin skinned tectonics. The terrane boundary between the KC and SMZ is seen as short northward dipping reflections, which is in accordance with other geophysical data. The Palala shear zone separating the CZ and SMZ is considered to be vertical and as such no seismic signature is expected. Therefore its position on the seismic section is inferred from the truncated reflections from the Soutpansberg trough. No continuous reflections at mid-crustal levels (3 - 5 s) connecting the south dipping NMZ/CZ boundary and the vertical SMZ/CZ boundary, which would indicate a decollement zone as postulated by McCourt and Vearncombe (1987), are apparent on the seismic section.

7. CONCLUSION

The Kaapvaal Craton (KC) is characterised by a uniformly reflective crust down to 8 s (~25 km). The reflections are fairly continuous and have an average length of between 1 and 5 km. There is evidence for thin skinned tectonics (shallow approximately horizontal reflections close to surface). The KC is largely in isostatic equilibrium which indicates a normal crustal thickness. This is verified by the refraction data where the Moho is found to occur between 36 and 38 km within the craton. There is insufficient evidence to indicate the presence of an abrupt upper/lower crustal interface. The absence of Moho reflections on the reflection profile may indicate poor data quality or it may also indicate a transitional Moho. Also the refraction data indicate that the Moho is transitional rather than a sharp velocity discontinuity. Electrical soundings (Van Zijl, 1978; De Beer et al., 1990) indicate that the uppermost layer (~10 km) of the KC is resistive which is characteristic of massive terranes with limited fracturing and deformation.

The boundary between the KC and Southern Marginal Zone (KC/SMZ) is defined on the reflection profile by curved northward dipping reflections beginning near surface 30 km north of Pietersburg and extending to 4 s (~12 km) at an angle of 35° to the horizontal. This is in agreement with the electrical work of De Beer et al. (1990) who were the first workers to propose that the KC/SMZ boundary dipped northwards with the KC rocks dipping beneath the rocks of the SMZ. The gravity profile can also be modelled using a north dipping contact between the SMZ and KC with the boundary intersecting the surface 20 km north of Pietersburg.

The Southern Marginal Zone (SMZ) is characterised by numerous short horizontal to gently dipping reflections in the upper 6 s. The reflections do not define any obvious structure. This is in agreement with the electrical data which shows the SMZ to have a low resistivity upper crust characteristic of fractured terranes indicating extensive deformation. The positive gravity anomaly over the SMZ is modelled using a 6-7 km thick layer of dense (2930 kg/m^3) granulites in the upper crust. De Beer and Stettler (in press) report on low magnetic susceptibilities in the SMZ which they attribute to magnetite-ilmenite solid solutions being formed during granulite grade metamorphism accompanied by a marked reduction in magnetic susceptibility.

No geophysical data set provides direct evidence as to the nature of the Southern Marginal Zone/Central Zone (SMZ/CZ) boundary. Gravity data indicates that it is most likely to be a near-vertical contact. This is verified by the reflection profile where reflections within the Soutpansberg trough are abruptly terminated in the vicinity of the SMZ/CZ boundary (8 km north of Vivo). The refraction data shows a 0.6 s slowdown 25 km north of the SMZ/CZ boundary. This may be due to either a sudden increase (~8 km) in the crustal thickness of the CZ or a low-velocity-layer (LVL) in the upper mantle. Since the gravity data is not easily modelled using a such a thick crust in the CZ, a LVL between 42 and 45 km and extending from beneath the KC into the Limpopo Belt is preferred.

The Central Zone (CZ) is largely seismically transparent except for a well defined block near Alldays consisting of 3 parallel dipping reflections which extend from near surface to about 3 s where they flatten out. It is also characterised by a low resistivity upper crust, consistent with the interpretation of it being a fractured terrane. However, the electrical data also indicates a block of high resistivity material characteristic of massive terranes. De Beer and Stettler (in press) suggest that these may be crustal remnants of a previous cratonic terrane not affected by the thrusting and shearing during the last Limpopo deformation event. The regional Free-air gravity field over the CZ is lower than that over the KC. This is in part due to the lower elevation over the CZ, but is also explained using a slightly thicker (1-3 km) crust beneath the CZ. The refraction data are also best modelled using a thicker (5 km) crust beneath the CZ.

The <u>Central Zone/Northern Marginal Zone (CZ/NMZ) boundary</u> is seen on the reflection profile as a south dipping wedge of reflections extending to 7 s at an angle of 35° to the horizontal. The NMZ is also characterised by numerous horizontal to gently dipping reflectors. The depth to the Moho is 35 km beneath the NMZ (Stuart and Zengeni, 1987) increasing to about 40 km beneath the ZC. The boundary between the ZC and NMZ is a south dipping thrust zone (Gwavava et al., in prep.).

REFERENCES

Allmendinger, R. W., Nelson, K. D., Potter, C. J., Barazangi, M., Brown, L. D. and Oliver, J. D., (1987). Deep seismic reflection characteristics of the continental crust. Geology, 15: 304-310.

Anhaeusser, C.R., Mason, R., Viljoen, M.J. and Viljoen, R.P., (1969). A reappraissal of some aspects of Precambrian shield geology. Geol. Soc. Amer. Bull., 80: 2175-2200.

Barnett, C. T., (1976). Theoretical modelling of the magnetic and gravitational fields of an arbitrarily shaped three-dimensional body. Geophysics, 41: 1353-1364.

Barton, J. M., Jr., (1983a). Pb-isotopic evidence for the age of the Messina Layered Intrusion, Central Zone, Limpopo Mobile Belt. Spec. Publ. Geol. Soc. S. Afr., 8: 39-41.

Barton, J. M., Jr, (1983b). Our understanding of the Limpopo belt - A summary with proposals for future research. Spec. Publ. Geol. Soc. S. Afr., 8: 191-203.

Barton, J. M., Jr. and Key, R. M., (1981). The tectonic development of the Limpopo Mobile Belt, and the evolution of the Archaean cratons of southern Africa. In: A. Kroener (Editor), Precambrian Plate Tectonics. Elsevier, Amsterdam: 185-212.

Barton, J. M., Jr., Du Toit, M.C., Van Reenen D. D. and Ryan, B., (1983a). Geochronologic studies in the Southern Marginal Zone of the Limpopo Mobile Belt, Southern Africa. Spec. Publ. Geol. S. Afr., 8: 55-64.

Barton, J. M., Jr., Ryan, B. and Fripp, R. E. P., (1983b). Rb-Sr and U-Th-Pb isotopic studies of the Sand River gneisses, Central Zone, Limpopo mobile belt. Spec. Publ. Geol. Soc. S. Afr., 8: 9-18.

Barton, J. M. Jr., (1990). The Limpopo belt: A historical perspective. In: Roering, C., Barton, J. M. Jr. and Van Reenen, D. D., (Eds.), The Limpopo belt - A field workshop on granulites and deep crustal tectonics. Johannesburg: 1-4.

Bloch, S., Hales, A. L. and Landisman, M., (1969). Velocities in the crust and upper mantle of southern Africa from multi-mode surface wave dispersion. Bull. Seism. Soc. Am., 59: 1599-1629.

Blundell, D. J., (1990). Seismic images of continental lithosphere. Journal Geol. Soc. London., 147: 895-913.

Blundell, D. J. and Raynaud, B., (1986). Modelling of lower crustal reflections observed on BIRPS profiles. In: M. Barazangi and L. Brown (Editors), Geodynamics Series, 13, American Geophysical Union, Washington: 287-296.

Bott, M. H. P., (1970). The Interior of the Earth, Edward Arnold, London.

Brewer, J. A. and Oliver, J. E., (1980). Seismic reflection studies of deep crustal structure. Ann. Rev. Earth Planet. Sci. 8: 205-230.

Briggs, I. C., (1974). Machine contouring using minimum curvature. Geophysics, 39: 39-48.

Christensen, N. I., (1989). Reflectivity and seismic properties of the deep continental crust. Journ. Geoph. Res., 94: 17793-17804.

Clowes, R. M., Ellis, R. M., Hajnal, Z. and Jones, I. F., (1983). Seismic reflections from subducting lithosphere? Nature, 303: 668-670.

Coward, M. P. and Fairhead, J. P., (1980). Gravity and structural evidence for the deep structure of the Limpopo belt, Southern Africa. Tectonophysics, 68: 31-43.

Coward, M. P. and Daly, M. C., (1984). Crustal lineaments and shear zones in Africa: Their relationship to plate movements. Precambrian Res., 24: 27-45.

Cox, K. G., Johnson, R. L., Monkman, C. J., Stillman, C. J., Vail, J. R. and Wood, D. N., (1965). The geology of the Nuanetsi Igneous Province. Phil. Trans. Geol. Soc. Lond., A257: 71-218.

De Beer, J. H., Le Roux, C. L., Hanstein, T. and Strack, K. M., (1991). DC resistivity and LOTEM model for the deep str[illegible] of the northern edge of the Kaapvaal craton, South Africa. Ph[illegible] arth Planet. Int., 66: 51-61.

De Beer, J. H. and Stettler, E. H., (1988). Geophysical characteristics of the southern African continental crust. Journal of Petrology, Special Lithosphere Issue: 163-184.

De Beer, J. H. and Stettler, E. H., (in press). The deep structure of the Limpopo belt. Precambrian Res.

De Wit, M. and Van Schalkwyk, J., (1990). The Limpopo belt. A 1990 Perspective - Geology and petrography. In: Van Reenen, D. D. and Roering, C., (Eds.), The Limpopo belt - A field workshop on granulites and deep crustal tectonics. Johannesburg: 7-17.

Durrheim, R.J., 1989. A seismic investigation of the Kaapvaal Craton. Ph.D. thesis (unpubl.), Witwatersrand University, Johannesburg, 171 pp.

Du Toit, M. C. and Van Reenen, D. D. (1977). The southern margin of the Limpopo mobile belt, northern Transvaal, with special reference to metamorphism and structure. In: Ermanovics, I. F., Key, R. M. and McEwan, G., (Eds.)., The proceedings of a seminar pertaining to the Limpopo Mobile Belt. Bull. Geol. Surv. Botswana, 12: 83-97.

Du Toit, M. C., Van Reenen, D. D. and Roering, C., (1983). Some aspects of the geology, structure and metamorphism of the Southern Marginal Zone of the Limpopo metamorphic complex. Spec. Publ. Geol. Soc. S. Afr., 8: 121-142.

Emenike, E. A., (1986). Gravity signature of the Limpopo-Kaapvaal fossil plate boundary in southern Africa. Tectonophysics, 128: 127-137.

Fripp, R. E. P., (1983). The Precambrian geology of an area around the Sand River near Messina, central zone, Limpopo mobile belt. Geol. Soc. S. Afr. Spec. Publ., 8: 89-102.

Gane, P. G., Atkins, A. R., Sellschop, J. P. F. and Seligman, P., (1956). Crustal structure in the Transvaal, Bull. Seism. Soc. Am., 46: 293-316.

Gibb, R. A. and Thomas, M. D., (1976). Gravity signature of fossil plate boundaries in the Canadian Shield. Nature, 262: 199-200.

Gibbs, A. K., (1986). Seismic reflection profiles of Precambrian crust: A qualitative assessment. In: M. Barazangi and L. Brown (Editors), Geodynamics Series, 14, American Geophysical Union, Washington: 95-104.

Gibbs, A. K., Payne, B., Setzer, T., Brown, L. D., Oliver, J. D. and Kaufman, S., (1984). Seismic-reflection study of the Precambrian crust of central Minnesota. Bull. Geol. Soc. Am., 95: 280-294.

Gibson, B. S. and Levander, A. R., (1990). Apparent layering in common-midpoint stacked images of two-dimensionally heterogeneous targets. Geophysics, 55: 1466-1477.

Goleby, B. R., Kennet, B. L. N., Wright, C., Shaw, R. D. and Lambeck, K., (1990). Seismic reflection profiling in the Proterozoic Arunta Block, central Australia: processing for testing models of tectonic evolution. Tectonophysics, 173: 257-268.

Grant, F. S., (1984a). Aeromagnetics, geology and ore environments, I. Magnetitee in igneous, sedimentary and metamorphic rocks: an overview. Geoexploration, 23: 303-333.

Grant, F.S., (1984b). Aeromagnetics, geology and ore environments, II. Magnetite and ore environments. Geoexploration, 23: 335-362.

Green, R. W. and Bloch, S., (1969). Recent developments in seismic investigations of crustal and upper mantle structures in South Africa. Geol. Soc. S. A. Spec. Publ. 2: 477-484.

Green, A., Milkereit, B., Percival, J., Davidson, A., Parrish, R., Cook, F., Geis, W., Cannon, W., Hutchinson, D., West, G. and Clowes, R., (1990). Origin of deep crustal reflections: seismic profiling across the high-grade metamorphic terranes in Canada. Tectonophysics, 173: 627-638.

Gwavava, O., Swain, C. J., Podmore, F. and Fairhead, J.D., (in prep.) Evidence of crustal thinning beneath the Limpopo Belt and Lebombo monocline of southern Africa based on regional gravity studies and implications for the reconstruction of Gondwana.

Hale, L. D. and Thompson, A. G., (1982). The seismic reflection character of the continental Mohorovicic discontinuity. Journ. Geoph. Res., 87: 4625-4635.

Hansen, K. M., Roy-Chowdhury, K. and Phinney, R. A., (1988). The sign ...r for seismic event detection. Geophysics, 53: 1024-1033.

Harris, N. B. W., Hawkesworth , C. J., Van Calsteren, P. and McDermott, F., (1987). Evolution of continental crust in southern Africa. Earth. Planet. Sci. Lett., 83: 85-93.

Hatcher, R. D., (1986). Interpretation of seismic reflection data in complexly deformed terranes: a geologists perspective. In: M. Barazangi and L. Brown (Editors), Geodynamics Series, 14, American Geophysical Union, Washington: 9-12.

Hawkesworth C. J., Moorbath S. and O'Nions, R. D., (1975). Age relationships between greenstone belts and "granites" in the Rhodesian Archaean craton. Earth. Planet. Sci. Lett., 25: 251-262.

Hickman, M. H., (1978). Isotopic evidence for crustal reworking in the Rhodesian Archean craton, southern Africa. Geology., 6: 214-216.

Hurich, C. A. and Smithson, S. B., (1987). Compositional variation and the origin of deep crustal reflections. Earth and Planet. Sci. Lett., 85: 416-426.

Jackson, S. L., Sutcliff, R. H., Ludden, J. N., Hubert, C., Green, A. G., Milkereit, B., Mayrand, L., West, G.F. and Verpaelst, P., (1990). Southern Abitibi greenstone belt: Archean crustal structure from seismic-reflection profiles. Geology, 18: 1086-1090.

Jarchow, C. M. and Thompson, G. A., (1989). The nature of the Mohorovicic discontinuity. Ann. Rev. Earth Planet. Sci., 17: 475-506.

Klemperer, S. L. and the BIRPS group, (1987). Reflectivity of the crystalline crust: hypotheses and tests. Geophys. J. R. astr. Soc., 89: 217-222.

Kleywegt, R. J., (1988). Gravity signature of the Limpopo-Kaapvaal fossil plate boundary in southern Africa - Discussion. Tectonophysics, 145: 349-350.

Latham, T. S., Best, J., Chaimov, T., Oliver, J., Brown, L. and Kaufman, S., (1988). COCORP profiles from the Montana plains: the Archean cratonic crust and a lower crustal anomaly beneath the Williston basin. Geology, 16: 1073-1076.

Light, M. P. R., (1982). The Limpopo mobile belt: a result of continental collision. Tectonics, 1: 325-342.

MacGregor, A. M., (1953). Precambrian formations of tropical southern Africa. Int. Geol. Cong. Algiers. (1952)., 20: 39-50.

Mane, M. J., Geerthsen, K. and Pitts, B. E., (1991). Gravity data reduction and interpretation: A new approach. SAGA 2nd Technical Meeting, Johannesburg: 127-130.

Mason, R. (1973). The Limpopo mobile belt - southern Africa. Phil. Trans. Geol. Soc. Lond., A273: 463-485.

Matthews, D. H. and Cheadle, M. J., (1986). Deep reflections from the Caledonides and Variscides west of Britain and comparison with the Himalayas. In: Reflection Seismology: a global perspective, M. Barazangi and L. Brown (Editors), Geodynamics Series, 13, American

Geophysical Union, Washington: 5-20.

McCourt, S., and Vearncombe, J. R., (1987). Shear zones bounding the central zone of the Limpopo mobile belt, southern Africa. J. Struct. Geol., 9: 127-137.

Meissner, R., (1986). The Continental Crust: A geophysical approach. International Geophysics Series, 34, Academic Press Inc. 426pp.

Mooney, W. F. D. and Brocher, T. M., (1987). Coincident seismic reflection/refraction studies of the continental lithosphere: a global review. Geophys. J. R. astr. Soc. 89: 1-6.

Robertson, I. D. M. and Du Toit, M. C., (1981). Mobile belts: A. The Limpopo belt. In: Hunter, D.R., Ed., The Precambrian of the Southern Hemisphere. Elsevier, Amsterdam: 641-671.

Roering, C. and Smit, C. A., (1990). The Limpopo belt: A 1990 perspective - The regional structural framework. In: Van Reenen, D. D. and Roering, C., (Eds.), The Limpopo belt - A field workshop on granulites and deep crustal tectonics. Johannesburg: 31-36.

SACS (South African Committee for Stratigraphy). (1980). Stratigraphy of South Africa. Part I. Lithostratigraphy of the Republic of South Africa, South West Africa/Namibia, and the Republics of Bophuthatswana, Transkei and Venda. Geol. Surv. S. Afr. Handbook., 8: 690 pp.

Sierra Geophysics, Inc., (1988). SierraSeis User manual. rev. 1.

Seismograph Service (England) Limited. Course notes for Seismic Data Processing - An overview.

Smit, P. J., Hal[illegible] A. and Gough, D. I., (1962). The grav[illegible] survey of the Republic of South Africa. Handbook Geol. Surv. S. Afr., 3: 484pp.

Smithson, S. B., Brewer, J. A., Kaufman, S., Oliver, J. E. and Zawislak, R. L., (1980). Complex Archean lower crustal structure revealed by COCORP crustal reflection profiling in the Wind River Range, Wyoming. Earth Planet. Sci. Lett., 46: 295-305.

Spence, G. D. E., Whittall, K. P. and Clowes, R. M., (1984). Practical synthetic seismograms for laterally varying media calculated by assymptotic ray theory. Bull. Seism. Soc. Am., 74: 1209-1223.

Stettler, E. H., De Beer, J. H. and Blom, M. P., (1989). Crustal domains in the northern Kaapvaal craton as defined by magnetic lineaments. Precambrian Res., 45: 263-276.

Stettler, E. H., De Beer, J. H., Aldrich, S., Du Plessis, Roer[illegible] C., Van Reenen, D. D., Geerthsen, K., Barton, J. M., Jr., Smit, A. and Brandl, G., (in press). A reflection seismic profile across the Limpopo metamorphic belt on the Kaapvaal craton. Geology.

Stolt, R. H., (1978). Migration by Fourier transform. Geophysics, 42: 23-48.

Stuart, G. W. and Zengeni, T. G., (1987). Seismic crustal structure of the Limpopo mobile belt, Zimbabwe, Tectonophysics, 144: 323-335.

Tankard, A. J., Jackson, M. P. A., Erikkson, K. A., Hobday, D. K., Hunter, D. R. and Minter, W. E. L., (1982). Crustal Evolution of Southern Africa: 3.8 Billion Years of Earth History. Springer - Verlag, New York, 523 pp.

Van Biljon, W. J. and Legg, J. H., (Eds.), (1983). The Limpopo Belt. Geol. Soc. S. Afr. Spec. Publ., 8.

Van Reenen, D. D., Barton, J. M. Jr., Roering, C., Smit, C. A. and Van Schalkwyk, J. F., (1987). Deep crustal response to continental collision: The Limpopo belt of southern Africa. Geology., 15: 11-14.

Van Reenen, D. D., Roering, C., Brandl, G., Smit, C. A. and Barton, J. M. Jr., (1990). The granulite-facies rocks of the Limpopo belt, southern Africa. In; Vielzeuf, D. and Vidal, P., (Eds.), Granulites and Crustal Evolution. Kluwer Academic Publishers, Netherlands: 257-289.

Van Reenen, D. D. and Roering, C., (Eds.), (1990). The Limpopo Belt - A field workshop on granulites and deep crustal tectonics. Johannesburg.

Van Zijl, J. S. V., (1978). The relationship between the deep electrical structure of the tectonic provinces in southern Africa. Part 1. Results obtained by Schlumberger soundings, Trans. geol. Soc. S. Afr., 81: 129-142.

Warner, M., (1987). Migration - why doesn't it work for deep continental data? Geophys. J. R astr. Soc., 89: 21-26.

Watkeys, M. K., (1983). Brief explanatory notes on the provisional geological map of the Limpopo belt and environs. Geol. Soc. S. Afr. Spec. Publ., 8: 5-8.

Watkeys, M. K. and Armstrong, R. A., (1985). The importance of being alkaline - deformed late-Archean lamprophyric dykes, central zone, Limpopo belt. Trans. Geol. Soc. S. Afr., 88: 195-206.

Yilmaz, O., (1987). Seismic data processing. Soc. Expl. Geophys., Tulsa: 526 pp.

Yilmaz, O. and Chambers, R., (1984). Migration velocity analysis by wave field extrapolation. Geophysics, 49: 1664-1674.

STACKING VELOCITIES

CMP	TIME	VELOCITY	CMP	TIME	VELOCITY
145	0	4600	250	0	4400
	300	4800		350	4600
	625	5000		500	4950
	750	5400		700	5700
	1000	5600		1300	5800
	1500	5600		1850	6100
	2000	5900		3650	6500
	4150	6500		5750	6900
	12000	7500		12000	7500
410	0	5400	485	0	5100
	400	5600		300	5300
	700	5750		480	5650
	980	5900		750	5700
	1300	6050		1100	6200
	2200	6400		1250	6300
	4550	6800		1600	6600
	12000	7500		2250	6900
				2950	7000
				12000	7500
830	0	5100	960	0	5500
	270	5300		250	5800
	400	5400		300	5900
	500	5600		500	5950
	850	5800		650	6200

CMP	TIME	VELOCITY
	1500	6100
	1800	6300
	2200	6600
	3300	7000
	12000	7500
	800	6400
	1500	6650
	2000	7000
	12000	7500
1135	0	5400
	200	5600
	300	5800
	475	6100
	750	6300
	1200	6600
	2025	6850
	3700	7200
	12000	7500
1210	0	5300
	200	5500
	350	5700
	500	5800
	600	6150
	900	6250
	1500	6350
	1750	6600
	2775	6800
	12000	7500
1360	0	6300
	225	5500
	450	5800
	510	5950
	750	6100
	1200	6500
	1975	6700
	2700	7000
	12000	7500
1505	0	5000
	250	5200
	480	5550
	650	5800
	850	6000
	1150	6400
	1375	6700
	2000	6900
	2350	7100
	3720	7300
	12000	7500

CMP	TIME	VELOCITY	CMP	TIME	VELOCITY
1625	0	5300	1885	0	4900
	200	5500		200	5100
	300	5800		450	5900
	650	6250		725	6100
	825	6400		1000	6400
	1725	6650		1250	6500
	2025	6900		1575	6700
	3200	7100		2375	7000
	12000	7500		3700	7300
				12000	7500
2000	0	5500	2470	0	5000
	260	5700		250	5200
	750	6400		350	5500
	1100	6600		500	5700
	1750	6800		625	6200
	2750	7000		900	6400
	12000	7500		1400	6800
				2000	7000
				3550	7300
				12000	7500
2605	0	5100	2800	0	4800
	250	5300		275	5000
	450	5500		500	5400
	550	5900		750	5600
	850	6050		980	5900
	1500	6650		1750	6500
	3150	7100		2150	6700
	4500	7300		3500	6900
	12000	7500		3950	7300
				12000	7500

CMP	TIME	VELOCITY	CMP	TIME	VELOCITY
2890	0	4900	2965	0	4900
	250	5100		240	5100
	375	5450		480	5650
	650	5800		800	6000
	1300	6000		1150	6300
	1500	6200		1450	6600
	1750	6500		2250	6700
	2850	7000		4450	7100
	4050	7200		12000	7500
	12000	7500			
3030	0	4600	3150	0	4800
	250	4800		240	5000
	400	5150		450	5300
	500	5400		510	5400
	800	5550		625	5700
	1000	6000		800	6200
	1200	6200		1500	6500
	2050	6600		3750	7200
	3350	7100		12000	7500
	12000	7500			
3240	0	4800	3435	0	4500
	250	5000		250	4700
	300	5200		325	4800
	600	5800		500	5200
	900	6100		625	5600
	2000	6500		750	5950
	2950	7000		1600	6300

CMP	TIME	VELOCITY	CMP	TIME	VELOCITY
	4200	7100		2200	6600
	12000	7500		2850	6900
				4500	7100
				12000	7500
3620	0	4500	3740	0	4600
	200	4700		200	4800
	275	4800		250	4900
	750	5400		425	5200
	1000	5700		780	5500
	1500	6200		1150	5800
	2200	6500		2325	[illegible]
	2575	6800		2570	6600
	5020	7000		3330	6800
	12000	7500		3875	6900
				12000	7500
4055	0	5100	4255	0	5200
	210	5400		220	5450
	250	5700		380	5700
	430	6000		450	6000
	600	6200		780	6400
	900	6400		1075	6600
	1120	6550		1520	6700
	1380	6700		1920	6850
	2880	6900		2950	7100
	3680	7100		3900	7200
	12000	7500		12000	7500

CMP	TIME	VELOCITY	CMP	TIME	VELOCITY
4590	0	4800	5260	0	4800
	250	5100		430	5200
	300	5300		500	5300
	380	5550		760	5700
	530	5700		940	6000
	680	5900		1150	6300
	750	6400		1430	6400
	1420	6900		1600	6500
	2210	7000		2760	6900
	3550	7300		12000	7500
	12000	7500			
5585	0	5000	6705	0	5200
	250	5300		200	5600
	300	5600		300	5900
	500	5700		380	6400
	700	5800		470	6600
	780	6100		600	6700
	1100	6400		800	6800
	1500	6600		1300	6900
	2430	7000		2350	7050
	3110	7200		3230	7100
	12000	7500		12000	7500
7200	0	4800	8110	0	5300
	250	5100		400	5800
	350	5300		550	6100
	490	5700		700	6200
	675	6000		800	6600
	800	6300		1200	6800
	1125	6500		2050	7000

CMP	TIME	VELOCITY	CMP	TIME	VELOCITY
	2675	6900		3110	7200
	12000	7500		12000	7500
8505	0	5300	8650	0	4900
	300	5600		160	5100
	350	6000		280	5600
	600	6150		480	5900
	900	6300		600	6300
	950	6500		1000	6400
	1450	6850		1310	6600
	2000	7000		1960	6700
	12000	7500		3330	7200
				12000	7500

INITIAL MUTE

CMP	OFFSET	TIME	CMP	OFFSET	TIME
630	175	0	2700	175	0
	225	0		225	0
	525	80		725	200
	1325	250		1125	250
	1725	500		1525	375
	2525	600		1725	500
				2125	650
				2525	700
3330	175	0	6600	175	0
	225	0		225	0
	925	200		925	200
	1325	300		1525	450
	1725	450		2525	700
	1925	650			
	2525	800			

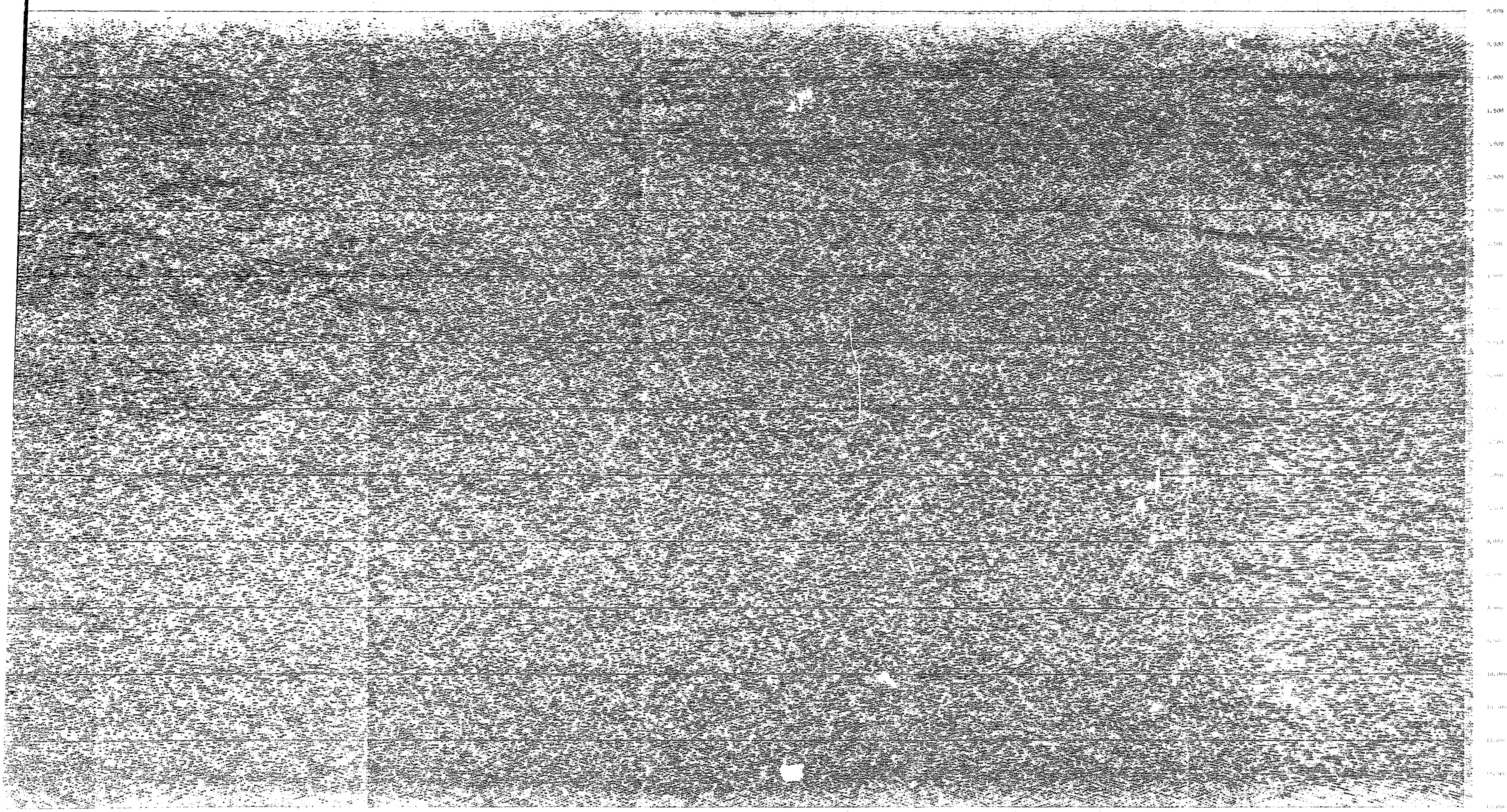

GENMIN GEOPHYSICS
DATA PROCESSING CENTRE

PONTDRIFT-PIETERSBURG
GOVERNMENT LINE
FINAL STACK
F.K. MIGRATION
USING 80% SMOOTHED
STACKING VELOCITIES
BANDPASS FILTER
15-65 HZ AT 1.0 SEC
15-60 HZ AT 2.0 SEC
15-50 HZ AT 4.0 SEC
TAB
WINDOW 1000 MSEC. 60%
EXPONENTIAL GAIN
POWER 2.5

SCALE TR
15 TRACES/CM AND 5 CM/SEC


0.000
0.500
1.000
1.500
2.000
2.500
4.000

[illegible]

750